nagra
National Cooperative for
the Disposal of Radioactive Waste

TECHNICAL REPORT 91-02E

Grimsel Test Site

Ventilationtest – In-situ-Experiment for Determination of Permeability in Crystalline Rock

November 1993

H. Kull, W. Brewitz, K. Klarr

GSF – Research Centre for Environmental Sciences,
Munich, Federal Republic of Germany

GRIMSEL TEST SITE/SWITZERLAND
A JOINT RESEARCH PROGRAM BY

- NAGRA - National Cooperative for the Disposal of Radioactive Waste, Wettingen, Switzerland
- BGR - Federal Institute for Geoscience and Natural Resources, Hannover, Federal Republic of Germany
- GSF - Research Centre for Environmental Sciences, Munich, Federal Republic of Germany

Hardstrasse 73, CH-5430 Wettingen/Switzerland, Telephone +41-56-37 11 11

nagra National Cooperative for the Disposal of Radioactive Waste

TECHNICAL REPORT 91-02E

Grimsel Test Site

Ventilationtest – In-situ-Experiment for Determination of Permeability in Crystalline Rock

November 1993

H. Kull, W. Brewitz, K. Klarr

GSF – Research Centre for Environmental Sciences, Munich, Federal Republic of Germany

GRIMSEL TEST SITE/SWITZERLAND
A JOINT RESEARCH PROGRAM BY

- NAGRA - National Cooperative for the Disposal of Radioactive Waste, Wettingen, Switzerland
- BGR - Federal Institute for Geoscience and Natural Resources, Hannover, Federal Republic of Germany
- GSF - Research Centre for Environmental Sciences, Munich, Federal Republic of Germany

Hardstrasse 73, CH-5430 Wettingen/Switzerland, Telephone +41-56-37 11 11

FOREWORD

Concepts for the disposal of radioactive waste in geological formations place significant emphasis on acquiring extensive knowledge of the proposed host rock and the surrounding strata. For this reason, Nagra has, since May 1984, been operating the **Grimsel Test Site (GTS)** which is located at a depth of 450 m in the crystalline rock of the Aar Massif of the Central Swiss Alps. The general objectives of the research being carried out in this underground laboratory include

- the build-up of know-how in planning, performing and interpreting field experiments in various scientific and technical disciplines and

- the acquisition of practical experience in the development of investigation methodologies, measuring techniques and test equipment which will be of use during actual repository site explorations.

The GTS is operated by Nagra and, on the basis of a German-Swiss cooperative agreement, various experiments are carried out by Nagra, the "Bundesanstalt für Geowissenschaften und Rohstoffe, Hannover" (BGR) and the "Forschungszentrum für Umwelt und Gesundheit, München" (GSF). The Grimsel projects of both GSF and BGR are supported by the German Federal Ministry for Research and Technology (BMFT). NTB 85-46 (German version NTB 86-47) provides an overview of the German-Swiss investigation programme. In a special issue of the Nagra Bulletin 1988 (German version "Nagra informiert 1+2/1988"), the status of the programme up to 1988 is described.

VORWORT

Bei Konzepten, welche die Endlagerung radioaktiver Abfälle in geologischen Formationen vorsehen, ist die Kenntnis des Wirtgesteins und der angrenzenden Gesteinsschichten von grundlegender Bedeutung. Die Nagra betreibt deshalb seit Mai 1984 das **Felslabor Grimsel (FLG)** in 450 m Tiefe im Kristallin des Aarmassivs. Die generelle Zielsetzung für die Arbeiten in diesem System von Versuchsstollen umfaßt

- den Aufbau von Know-how in der Planung, Ausführung und Interpretation von Untergrundversuchen in verschiedenen wissenschaftlichen und technischen Fachgebieten, und

- den Erwerb praktischer Erfahrung in der Entwicklung und der Anwendung von Untersuchungsmethoden, Meßverfahren und Meßgeräten, die für die Erkundung von potentiellen Endlagerstandorten in Frage kommen.

Im Felslabor der Nagra werden, auf der Basis eines deutsch-schweizerischen Zusammenarbeitsvertrages, verschiedene Versuche von den beiden deutschen Partnern Bundesanstalt für Geowissenschaften und Rohstoffe, Hannover (BGR) und Forschungszentrum für Umwelt und Gesundheit GmbH, München (GSF) durchgeführt. Das Deutsche Bundesministerium für Forschung und Technologie (BMFT) fördert die Arbeiten der BGR und der GSF im FLG. Der NTB 85-47 (englische Version NTB 85-46) enthält eine Übersicht des FLG und die Zusammenfassung der Untersuchungsprogramme mit Status August 1985. In der Ausgabe 1+2/1988 des Heftes "Nagra informiert" bzw. der englischen Spezialausgabe "Nagra Bulletin 1988" ist der Stand der Arbeiten anfangs 1988 beschrieben.

AVANT-PROPOS

Lors d'études de concepts de stockage de déchets radioactifs dans des formations géologiques, on attache une grande importance à l'acquisition d'informations étendues sur la roche d'accueil et les formations rocheuses environnantes. C'est pour cette raison que la Cédra exploite depuis mai 1984 son **laboratoire souterrain du Grimsel (LSG)** situé à 450 m de profondeur dans le cristallin du massif de l'Aar, situé au milieu des alpes centrales. Les principaux objectifs des recherches effectuées dans ce réseau de galeries comprennent:

- l'acquisition de savoir-faire dans diverses disciplines techniques et scientifiques en ce qui concerne la conception, la réalisation et l'interpretation d'expériences in situ, ainsi que

- l'accumulation d'expériences pratiques dans la mise au point et l'application de méthodes d'in-vestigation, de techniques et d'appareillages de mesure, qui pourraient être utilisés lors de l'exploration de sites potentiels de dépôts finals.

Le LSG est exploité par la Cédra et diverses expériences y sont réalisées par celle-ci et deux institutions allemandes: la"Bundesanstalt für Geowissenschaften und Rohstoffe, Hannover" (BGR) et le "Forschungszentrum für Umwelt und Gesundheit GmbH, München" (GSF) dans le cadre d'un traité de collaboration germano-suisse. Les projets poursuivis au Grimsel par la BGR et le GSF sont financés par le Ministère fédéral allemand de la recherche et de la technologie (BMFT). Les rapports NTB 85-46 (version anglaise) et NTB 85-47 (version allemande) présentent un aperçu du laboratoire souterrain et un résumé des programmes de recherches avec état au mois d'août 1985. L'état d'avancement de ce programme en 1988 est présenté dans la publication "Cédra informe 1+2/1988" (version française) et "Nagra informiert 1+2/1988" (version allemande), ainsi que dans une édition spéciale en anglais (Nagra Bulletin 1988).

Le présent rapport a été élaboré dans le cadre des collaboration mentionnés. Les auteurs ont présenté leurs vues et conclusions personnelles. Celles-ci ne doivent pas forcément correspondre à celles de Nagra ou ses partenaires participants.

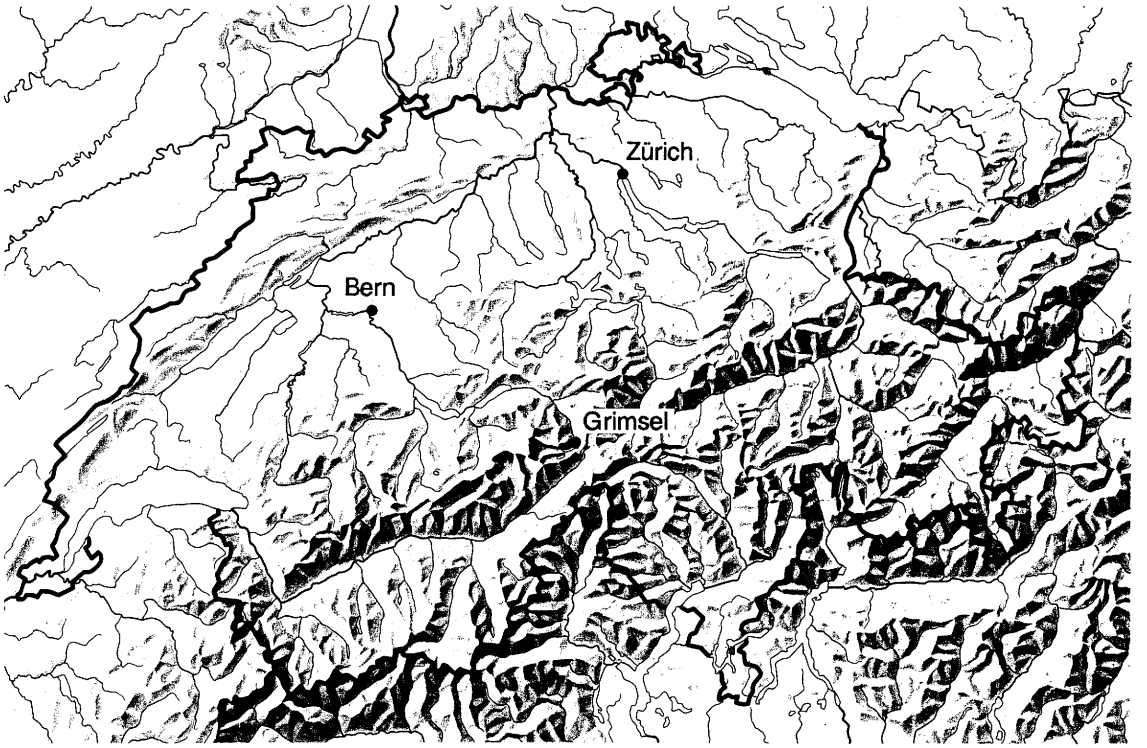

Location of Nagra's underground test facility at the Grimsel Pass in the Central Alps (Bernese Alps) of Switzerland (approximate scale 1 cm = 25 km).

Geographische Lage des Nagra Felslabors am Grimselpass (Berner Oberland) in den schweizerischen Zentralalpen (Massstab: 1 cm = ca. 25 km)

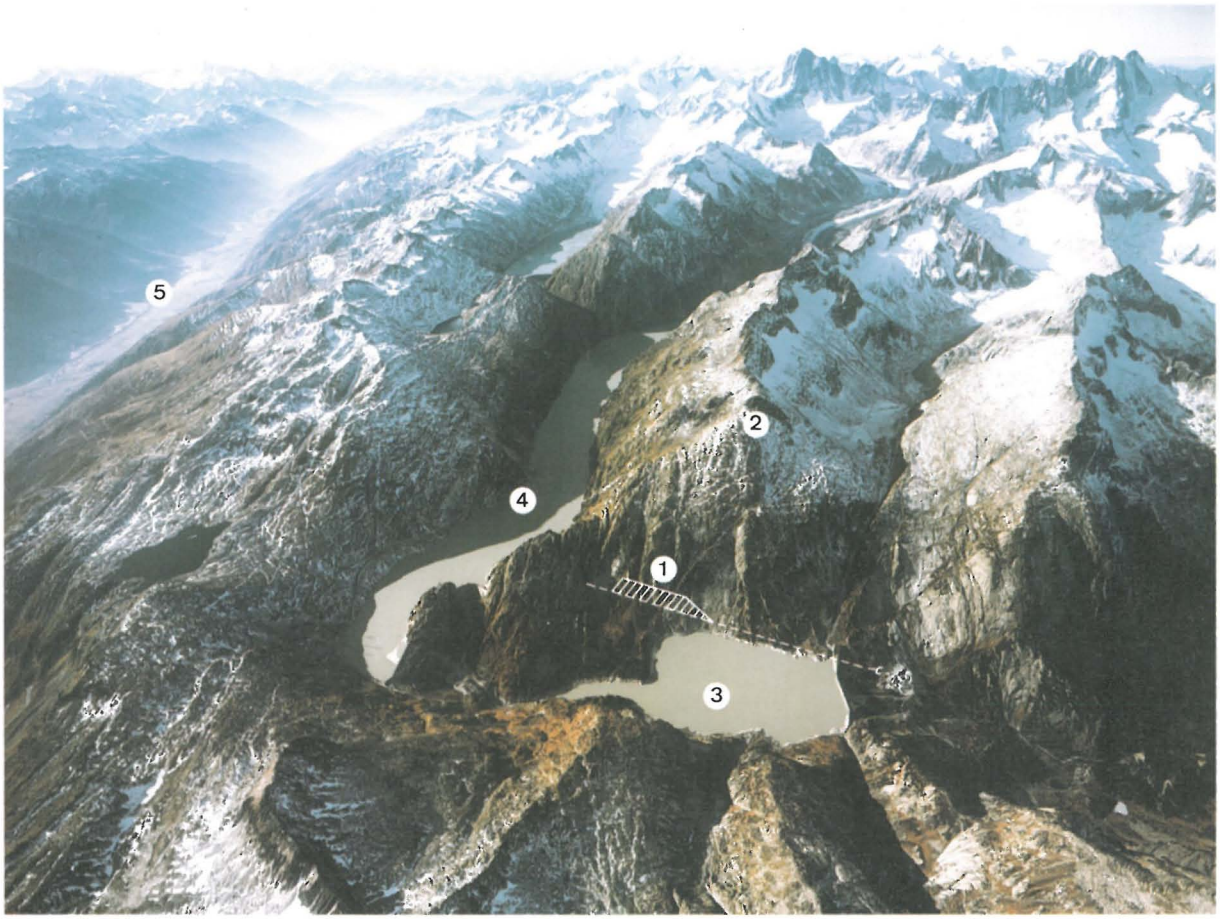

GRIMSEL-GEBIET

Blick nach Westen

1 Felslabor
2 Juchlistock
3 Räterichsbodensee
4 Grimselsee
5 Rhonetal

GRIMSEL AREA

View looking West

1 Test Site
2 Juchlistock
3 Lake Raeterichsboden
4 Lake Grimsel
5 Rhone Valley

FLG FELSLABOR GRIMSEL
GTS *GRIMSEL TEST SITE*

Situation

0 — 100 m

- Zugangsstollen/*Access tunnel*
- Fräsvortrieb/*by tunnel boring machine*
- Sprengvortrieb/*excavated by blasting*
- Zentraler Aaregranit ZAGR / *Central Aaregranite CAGR*
- Biotitreicher ZAGR / *CAGR with high content of biotite*
- Grimsel-Granodiorit / *Grimsel-Granodiorite*
- Scherzone/*Shear zone*
- Lamprophyr/*Lamprophyre*
- Wasserzutritt/*Water inflow*
- SB — Sondierbohrung/*Exploratory borehole*
- US — US Bohrung/*US borehole*
- ZB — Zentraler Bereich/*Central facilities*
- AU — Auflockerung/*Excavation effects*
- BK — Bohrlochkranz/*Fracture system flow*
- EM — El.magn. HF-Messungen/*-measurements*
- FRI — Kluftzone/*Fracture zone investigation*
- GS — Gebirgsspannungen/*Rock stresses*
- HPA — Hydr. Parameter/*Hydr. parameters*
- MI — Migration/*Migration*
- MOD — Hydrodyn. Modellierung/*H. modeling*
- NM — Neigungsmesser/*Tiltmeters*
- UR — Untertageradar/*Underground radar*
- US — Seismik/*Underground seismic testing*
- VE — Ventilationstest/*Ventilation test*
- WT — Wärmeversuch/*Heat test*

A — A Schnitt/*Section*

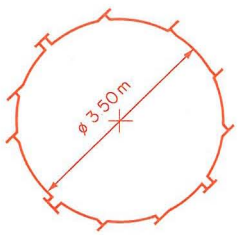

6/88

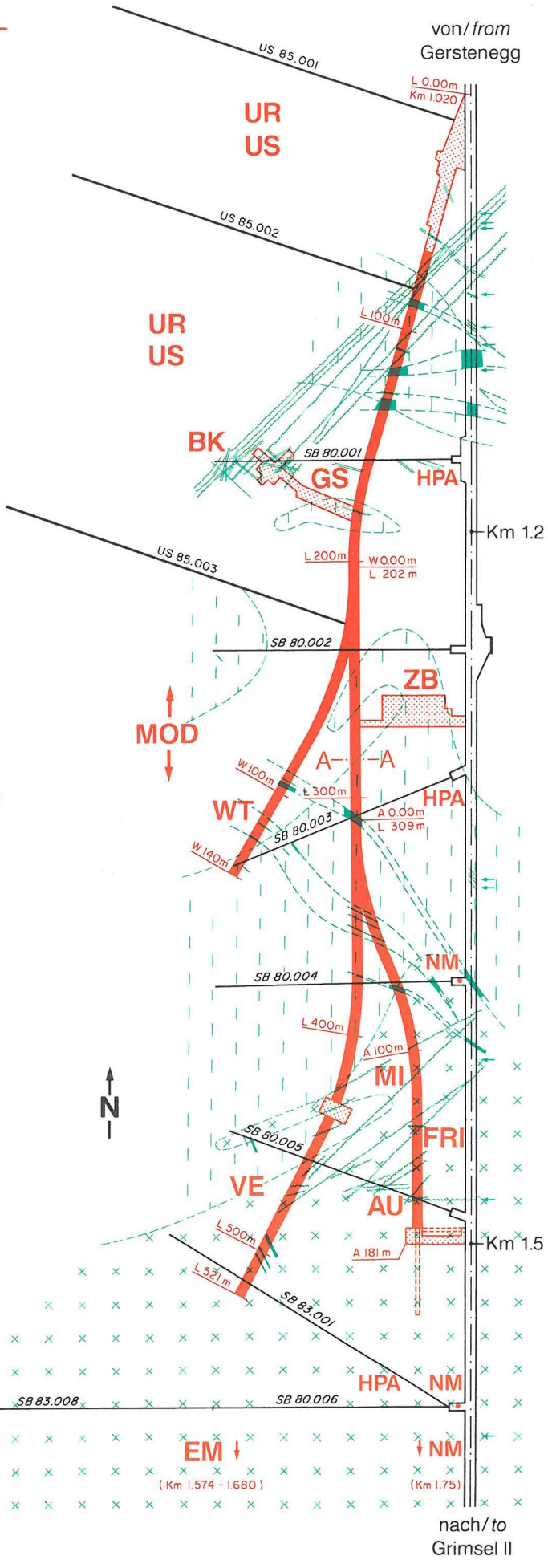

SUMMARY

The ventilation test is an in situ test aimed at determining the mean permeability - or macropermeability - of a hydrogeologically representative underground rock volume with relatively low water inflow rates.

Measurements are made of the natural rate of water inflow and hydraulic head distribution in the near vicinity of a defined section of the drift, taking care not to interfere with the flow conditions in the adjoining rock by drilling numerous exploratory boreholes. The parameters required for the hydraulic evaluation of the rock section under investigation are determined by means of structural geological mapping of the drift surface - taking into consideration the exploratory boreholes in the remaining drift system.

In order to define the large-scale permeability of the crystalline rock, a test drift 70 m long at the Grimsel Test Site was separated into two measuring chambers and water inflow was measured under alternating ventilation and climatic conditions.

The hydraulic gradient, which is also required for permeability calculations, was obtained through pressure measurements in two observation boreholes located parallel to the drift.

With the aid of borehole tests and petrophysical laboratory investigations, further procedures were employed in order to determine the permeability, the aim being to verify the results from the ventilation test.

In addition, the hydraulic flow field was analysed by numerical modelling based on the measured data obtained .

This report describes the tests performed from 1985 to 1990 (phases 1 and 2) and the corresponding test procedures. On the basis of the measured values obtained in situ, a site-specific flow model is being developed for the jointed crystalline rock in the ventilation test area of the Grimsel Test Site.

ZUSAMMENFASSUNG

Der Ventilationstest ist ein In-situ-Versuch zur Bestimmung der mittleren Durchlässigkeit -Makropermeabilität- eines hydrogeologisch repräsentativen Gebirgsbereiches unter Tage mit relativ geringen Wasserzuflußraten.

Meßtechnisch erfaßt werden der natürliche Wasserzufluß und die Druckverteilung in der näheren Umgebung eines abgeschotteten Stollenabschnittes, ohne daß dabei die Strömungsverhältnisse im angrenzenden Gebirge durch Erkundungsbohrungen unzulässig beeinträchtigt werden. Durch die strukturgeologische Kartierung der Stollenoberfläche werden für die hydraulische Bewertung des zu untersuchenden Gebirgsbereiches notwendige Parameter ermittelt.

Im Felslabor GRIMSEL wurde zur Bestimmung der Gebirgsdurchlässigkeit des Kristallins ein 70 m langer Teststollen mit zwei Meßkammern eingerichtet und der Wasserzufluß unter verschiedenen Belüftungs- bzw. Klimazuständen gemessen.

Der ebenfalls zur Durchlässigkeitsberechnung notwendige hydraulische Gradient wurde durch Druckmessungen in zwei stollenparallelen Beobachtungsbohrungen bestimmt.

Durch Bohrlochtests und petrophysikalische Laboruntersuchungen wurden weitere Verfahren zur Bestimmung von Durchlässigkeitsbeiwerten für die Absicherung des Ventilationstestergebnisses eingesetzt.

Darüber hinaus wurde auf der Basis der vorliegenden Meßdaten das hydraulische Strömungsfeld durch eine numerische Modellierung analysiert.

Der vorliegende Bericht beschreibt die in den Jahren 1985 bis 1990 (Phase 1 und 2) durchgeführten Versuche und eingesetzten Testverfahren. Auf der Basis der in situ bestimmten Meßwerte wird ein standortspezifisches Fließmodell für das geklüftete Kristallingebirge entwickelt.

RESUME

Le test de ventilation est un essai in situ visant à déterminer la perméabilité moyenne - macroperméabilité - d'une section de roche souterraine, représentative au niveau de l'hydrogéologie et présentant un afflux relativement faible.

On mesure le débit d'eau naturel et la répartition de la pression dans le champ proche d'une section isolée de galerie, en veillant à ce que les forages de reconnaissance ne perturbent pas les conditions d'écoulement prévalant dans la roche avoisinante. Les paramètres nécessaires à l'évaluation hydraulique de la section rocheuse a étudier sont obtenus par la cartographie géologique (géologie structurale) de la surface de la galerie.

Pour définir la perméabilité à grande échelle du cristallin, on a construit dans le laboratoire souterrain du GRIMSEL une galerie de 70 mètres de long, comprenant deux chambres de mesure, et mesuré l'afflux d'eau dans différentes conditions climatiques et de ventilation.

La gradient hydraulique, nécessaire aussi pour calculer la perméabilité de la roche, a été obtenu en mesurant la pression dans deux forages d'observation parallèles à la galerie.

Des tests de forage et des analyses pétrophysiques en laboratoire ont permis de recourir à d'autres méthodes pour déterminer les coefficients de perméabilité, l'objectif consistant à confirmer les résultats du test de ventilation.

En outre, on a analysé le champ d'écoulement hydraulique par modélisation numérique, sur la base des données de mesure obtenues.

Ce rapport décrit les test réalisés de 1985 à 1990 (phases 1 et 2) et les méthodes correspondantes. Sur la base des valeurs mesurées obtenues sur le terrain, on a mis au point un modèle d'écoulement spécifique au site pour le massif cristallin saillé.

TABLE OF CONTENTS

LIST OF FIGURES

LIST OF TABLES

1. INTRODUCTION

The ventilation test at the GRIMSEL Test Site in Switzerland is the further refinement of a hydraulic test with the same basic concept which has already been performed at the STRIPA mine in Sweden and the KONRAD mine in Germany. A common feature of the rock at these three different test locations is its low permeability and associated low water flow (WILSON et al., 1981; BREWITZ et al., 1984; BRASSER, 1986; BRASSER & KULL, 1988b).

The ventilation test method was used at the three locations mentioned above because it was impossible to measure the low water influxes into the tunnel system using conventional techniques. The aim was to investigate key rock parameters in connection with numerical modelling of the hydraulic regime for the large area of rock in question.

In subsurface facilities, some of the inflowing formation water is removed by ventilation and is thus withdrawn from the water balance for the overall system. However, as the water balance forms the basis for calculating and evaluating the rock permeability, the amounts of water removed by ventilation also require to be determined.

The ventilation technique allows such extremely small amounts of moisture to be collected and measured for selected areas of rock. Water inflow measurements are accompanied by measurements of formation water pressure in the near-drift zone and the hydraulic gradient is then obtained from these data. The rock permeability can then be derived from these results.

The results of the investigations have confirmed that the data from laboratory experiments and borehole tests have only a limited application to large-scale hydraulic conditions.

2. AIM OF THE VENTILATION TEST

The scientific objective of the ventilation test performed at the Grimsel Test Site was to determine the mean permeability of tight, slightly fractured crystalline rock using a simple measuring technique. The area of application is underground cavities and voids, particularly tunnel systems with simple geometries, where the hydraulic regime in the near-field has to be characterised.

The effect of an underground cavity on the long-term evolution of hydraulic pressure and water fluxes in the surrounding rock is investigated. The test also considers the influence of ventilation on the temperature distribution in the near-vicinity of the drift and on the formation water pressure.

Because of the low water flow in the sparsely fractured zones of the crystalline rock, it was necessary to develop a technique which was capable of measuring the small volumes of formation water flowing into the drift.

The main objectives of the ventilation test were to improve measuring techniques and procedures and to further develop methods for numerical analysis.

This includes the actual ventilation technique, the equipment used for measuring the water flow into the tunnel, determination of hydraulic pressures in the rock and identification of zones which, compared with the rest of the rock formation, supply a relatively large volume of water to the drift. A no-contact technique, which involves measuring temperatures at the drift surface, was used to distinguish structures which are hydraulically more active from zones which are hydrogeologically homogeneous and hydraulically less significant.

The ventilation test concept has two components - the mean permeability of the crystalline rock is determined analytically, using rock parameters obtained during experiments and numerical modelling is used to analyse the hydraulic flow regime in the near vicinity of the drift.

The data obtained during the ventilation test and the experience gained in relation to the technical practicalities of performing such experiments will ultimately form the basis for similar ventilation tests to be applied in underground characterisation of potential repository host rocks.

3. THE GEOLOGY OF THE TEST LOCATION

The Grimsel Test Site is situated in the Juchlistock mountain range, which is in the area of Switzerland known as the Berner Oberland.

The Juchlistock range belongs to the Aar Massif, a largely autochthonous crystalline massif some 120 km long and 20-25 km wide which strikes SW-NE (KEUSEN et al., 1989; LABHART, 1977). Nagra's Grimsel Test Site, which has been in operation since 1983, is located in the Central Aare Granite or, as the rock in this part of the massif is termed, the Grimsel Crystalline. The Test Site is accessible via the tunnel system of the Oberhasli power plant which was constructed at the beginning of this century.

3.1 Selection of the test location

The present location of the ventilation test was decided prior to construction of the Grimsel Test Site in 1983. Selection of the location was made on the basis of geological investigations carried out in the exploratory boreholes drilled between 1980 and 1983 from the main access tunnel into the western section of the Juchlistock which had not been disturbed by underground construction activities.

The site selected was in a zone of rock opened up by exploratory boreholes SB 80.005 and SB 83.001. The drift excavated for the ventilation test is located in the southern part of the Test Site (see the overview plan of the GTS at the beginning of the report).

This part of the Test Site is located in one of the hydraulically less permeable areas of the Grimsel Crystalline and thus corresponds to the characteristic hydraulic regime found in the majority of this rock massif; the conditions are also similar to those which would be expected for a repository hosted in granitic rock.

Pronounced fracture systems with high water flow rates and high hydraulic pressures, such as are found in the Strahlchälen (Fig. 1) in the northern part of the Test Site, are absent in the ventilation test drift. The water-bearing structures in the test zone are restricted to isolated fractures, contact surfaces between lamprophyre dykes and matrix blocks and, finally, a shear zone. Shear zones of this type penetrate the entire Juchlistock and separate the compact rock zones from one another (KEUSEN et al., 1989).

Water flow from these compact rock zones is relatively low and, with the exception of a few locations, ventilation during the tunnel construction phase had the effect of drying out the rock surface.

Any external influence on the hydraulic regime of the ventilation test drift is minimised by its being located at a considerable distance from other test locations and drifts.

The distribution of water-bearing structures and estimated water inflow volumes formed the basis for dividing the 70 m-long test drift into two sections, namely a forward chamber (L450-L480 m) and a rear chamber (L480-L521 m)(cf. Fig. 3).

In the forward chamber, the geology is dominated by matrix zones and by the presence of the highly textured shear zone mentioned previously.

In the rear chamber, the single fractures and lamprophyres which are typical for the Grimsel Crystalline can be identified in addition to the matrix zones.

3.2 Geology of the test zone

The test zone consists mainly of granodioritic gneisses (Grimsel Granodiorite). On a macroscopic scale, a distinction can be drawn between the Grimsel Granodiorite (GrGr) and the Central Aare Granite (ZAGr) which is exposed to the north of the test drift; this is based on the higher proportions of dark minerals, the coarse-grained fabric and the pronounced parallel texture of the Grimsel Granodiorite.

The habit of the gneisses is determined by the mineral parageneses microcline / orthoclase, albite, muscovite / biotite and quartz. Microcrystalline shear zones, fissures and fractures frequently occur in the feldspar and quartz crystals; together with the grain boundary surfaces, these determine the microfabric and hence the matrix permeability of the rock.

The cleavage of the granodioritic gneisses generally strikes north-east/south-west and dips steeply to the south-east. Several ductile shear zones of varying thickness strike parallel to the cleavage. At the Test Site, water outflow points can frequently be observed within the shear zones.

In the forward test chamber, an approximately 10 m-thick shear zone is exposed between tunnel metres L465 - L475 m. In the rear section of the drift there are several small shear zones in the cm to dm range (e.g. at L498 m). On a macroscopic scale, these shear zones are characterised by pronounced banding and by an increased biotite content. Microscopically they show intense mylonitization at fabric surfaces. The granodioritic matrix is recrystallised in the shear zones.

The occurrence of brittle deformations (fractures) is higher within the ductile shear zones (IROUSCHEK & BOSSART, 1989). One reason for this accumulation of brittle deformations could be that the blocks of the Grimsel Massif, which are separated by the mylonitized shear zones, have moved in different directions (FLACH & NOELL, 1989).

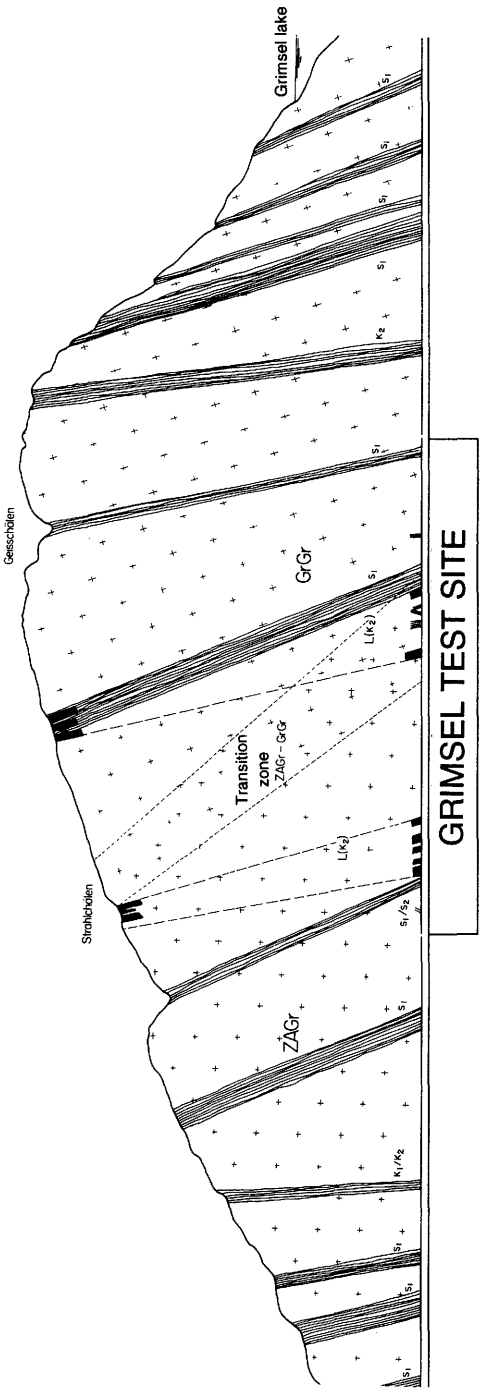

Fig. 1: North-south section through the Juchlistock showing the hydraulically active structures in the area of the Test Site (after KEUSEN et al., 1989).

The orientation of the fractures in the shear zone is more or less parallel to the cleavage surfaces. Flat-lying tension joints (extension fractures) can be seen in the test drift at L481 m and L490 m.

The gneisses are penetrated sporadically by north-west-striking, subvertical lamprophyre dykes (Fig. 2). Variants of the lamprophyres at the Test Site include kersantite dykes and, less frequently, spessartite dykes; these are characterised by a marked foliation and preferred orientation of stressed mineral aggregates. Aplite dykes also occur at the Test Site, but are not exposed in the region of the test drift.

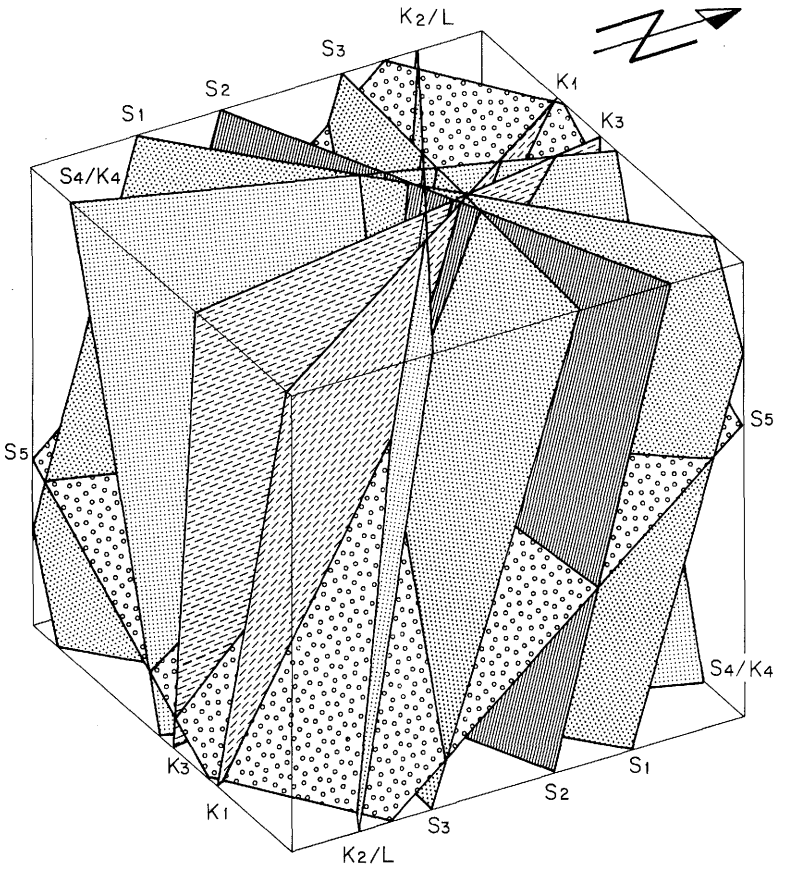

Fig. 2: Block diagram showing the most important shear and fracture structures of the Grimsel Massif (from KEUSEN et al., 1989).

The lamprophyre dykes in the test zone are exposed at L461 m, L494 m and L502 m. In the contact zone with the gneisses, the lamprophyres are sheared and often overprinted at the edges by a marked brittle deformation. The lower

competence of the lamprophyres, as compared with the gneisses, is expressed very clearly in the "cuspate-lobate" folds at the gneiss/lamprophyre contacts, in so far as these folds have not been overprinted by subsequent formation of fault gouge horizons (BOSSART & MARTEL, 1990).

The strike direction and thickness of the lamprophyres is not constant in the vicinity of ductile shear zones. Changes in orientation and thickness occur over short distances, both above ground and within the shear zone in the forward section of the ventilation test drift.

The ductile and brittle structures of the Grimsel Crystalline can be assigned to different time phases with varying temperature and pressure conditions. The following Table gives the most important steps in the genesis of these structures.

Table 1: Times at which the ductile and brittle deformation structures of the Grimsel Crystalline were formed (after KEUSEN et al., 1989).

Age of solidification of granodiorites	Variscan (approx. 320-280 Ma)
Intrusion of lamprophyres	approx. 250-230 Ma
Peak of alpine metamorphism	400 °C / 250-300 MPa
Formation of ductile structures: - cleavage and mineral stretching lineation of the granodiorite - shear zones and mylonitization - deformation of lamprohyres (cuspate-lobate folds) - formation of tension joints	Miocene approx. 20-5 Ma
Formation of brittle structures - consolidation and hydrothermal infilling of tension joints - fracture formation in existing ductile shear zone - formation of fault gouges and tectonic microbreccias in the fractures	Pliocene, Pleistocene approx. 5-0 Ma

3.3 Hydraulically active structures in the test area

The ventilation test drift can be divided into two hydrogeologically distinct sections with different geological characteristics:

1) **Massive granodiorite:**
   Ductile and brittle deformations occur only sporadically and the drift surface is dry with the exception of a few small damp zones. Other wet zones are restricted to contacts between granodiorite and lamprophyres and isolated points within the lamprophyre dykes.

2) **Parallel-textured shear zones:**
   Ductile and brittle deformations occur frequently and the surface of the drift is generally wet. Where the fractures are exposed, drops of water emerge from the rock, either as single points or in lines. The lamprophyres are wet through.

The most significant flow paths in the shear zone of the ventilation test drift are the so-called "fault gouges". "Fault gouges" are fractures in the ductile shear zones which are filled with fine fault breccia. They are constantly regenerated through recurring tectonic rock movements (BOSSART & MAZUREK, 1990). In the regenerated fractures, angular clasts from the shear zone are suspended in a highly porous, mica-rich groundmass. "The fault" gouges are interconnected parallel to the cleavage and their thickness varies widely on a millimetre scale. Perpendicular to the cleavage, the connections between the "fault gouges" are somewhat restricted.

The lamprophyres in the ventilation test shear zone do not function as flow barriers. In zones of high ductile deformation (shear zones), their thickness varies in the centimetre to decimetre range and their lateral extent is restricted. Even over a distance of a few metres it is no longer possible to make a clear identification of these lamprophyres.

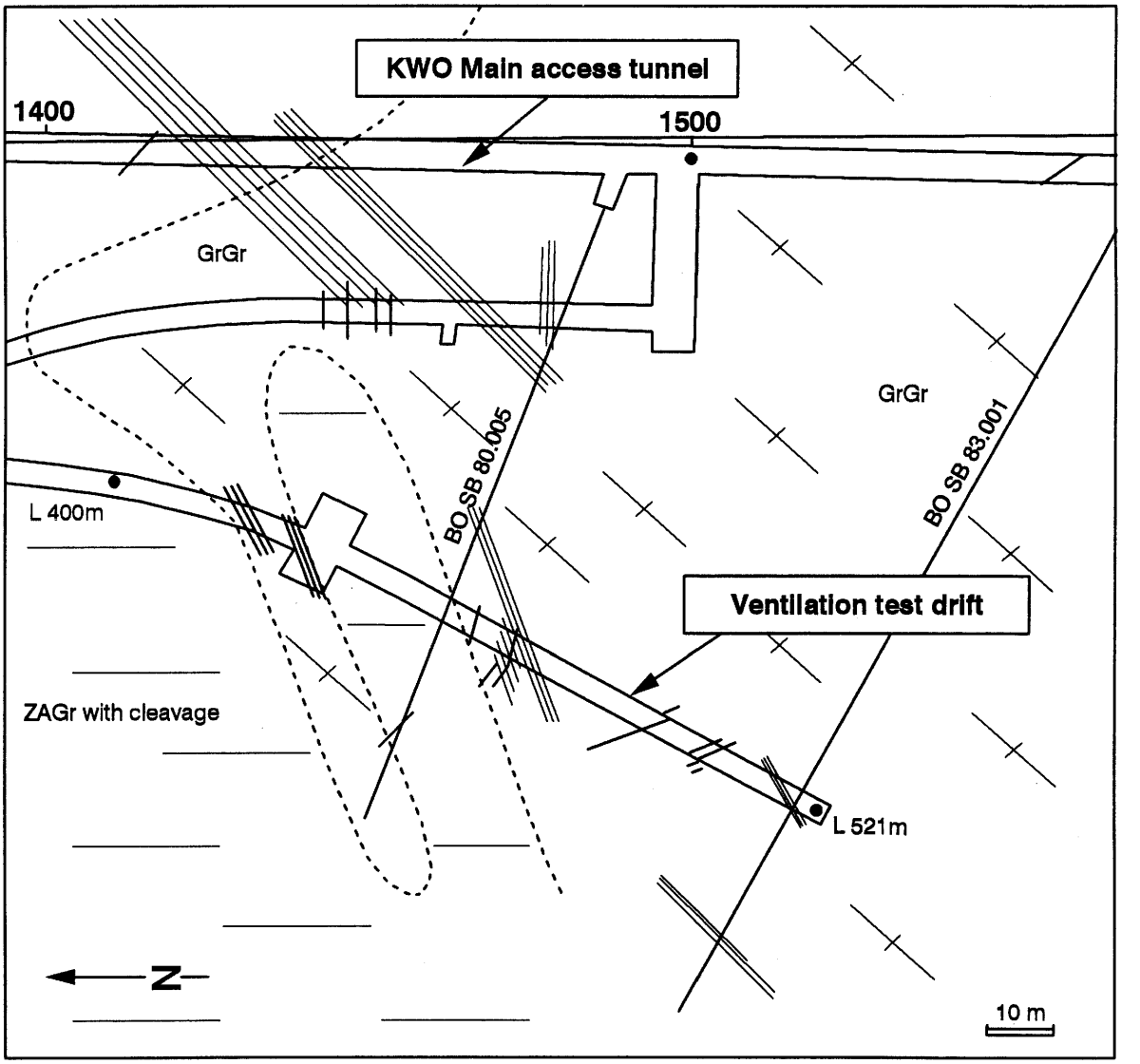

Fig. 3: Geological structures in the area of the ventilation test drift at the Grimsel Test Site. Indication of lamprophyres and shear zones.

The formation water pressures in the region of the Test Site are influenced by the overlying rock formations and the tunnels, which act as pressure sinks, as well as by local-scale structures. Pressures are generally lower in the vicinity of tunnels. On the other hand, six years after construction of the tunnel systems, hydrostatic pressures of 4 MPa (= 400 m water column) are still being measured in the area of a pronounced fracture system in borehole SB 80.001.

In the ventilation test area, the formation water pressure at the final depth of borehole SB 83.001 (Fig. 3) was still over 3 MPa.

The alkaline formation water (pH < 10) has a low mineralisation level. The electrical conductivities vary between 50 and 120 µS/cm. The annual temperature of the formation water fluctuates between 10 and 13°C.

Given the increased water flow in the shear zones as compared with the granodioritic matrix, the shear zones can be classified along with the discontinuity systems S1/S2 and S3 of the Grimsel Crystalline as being hydrogeologically particularly active features (cf. Table 2 and Fig. 2 (from KEUSEN et al., 1989)). As is the case for the cleavage plane, the shear zones in the Grimsel Crystalline dip subvertically. The significance of the shear zones in terms of influence on the regional flow regime is determined by their spatial dimensions and their structural geology. Water flow within the shear zones is associated with individual fracture and shear surfaces. The matrix sections of the shear zones have similar hydraulic properties to the matrix sections of the slightly structured granodioritic gneisses.

Based on mineral distribution and orientation, it can be assumed that the granodioritic matrix sections which are parallel to the cleavage plane (subvertical) have a higher permeability than those perpendicular to the cleavage plane (horizontal).

According to petrofabric analyses in the region (CHOUKROUNE & GAPAIS, 1983), a distinction can be drawn in the shear

zones between the S2 discontinuities, representing the main cleavage plane with a SSW-NNE strike direction, and the S1 and S3 discontinuities (Fig. 2).

In the ventilation test drift, the discontinuity system of a water-bearing shear zone is exposed between tunnel metres L465 and L475 (Fig. 4). Investigations of the structural geology of cores from observation boreholes BOVE 84.011 and 84.018, BOVE 88.001 to 88.004 and exploratory borehole SB 80.005 confirmed the spatial dimensions of the shear zone up to several tens of metres away from the drift. Correlation of the shear zone with corresponding structures in the main access tunnel indicates that the shear zone probably extends laterally for more than 100 m. The key structural data for the shear zone in the ventilation test drift and for the discontinuity systems S1/S2 and S3 (KEUSEN, 1989) are presented in Table 2.

Table 2: Orientation and thickness of the shear zone in the ventilation test drift as compared with the orientation of the discontinuity system S1, S2 and S3 (after KEUSEN et al., 1989).

System	Strike azimuth	angle of dip	Thickness
Shear zone	160° ± 15°	70° ± 10°	8 - 14 m
S1	142°	77°	-
S2	157°	75°	-
S3	183°	65°	-

The local shear and cleavage planes in the shear zones generally have the same orientation as the regional discontinuity systems S1/S2 and S3. However, their lateral extent in the test zone can only be traced over a distance of a few metres, which means that the hydraulic activity of an individual structure can effectively be determined only on a local scale.

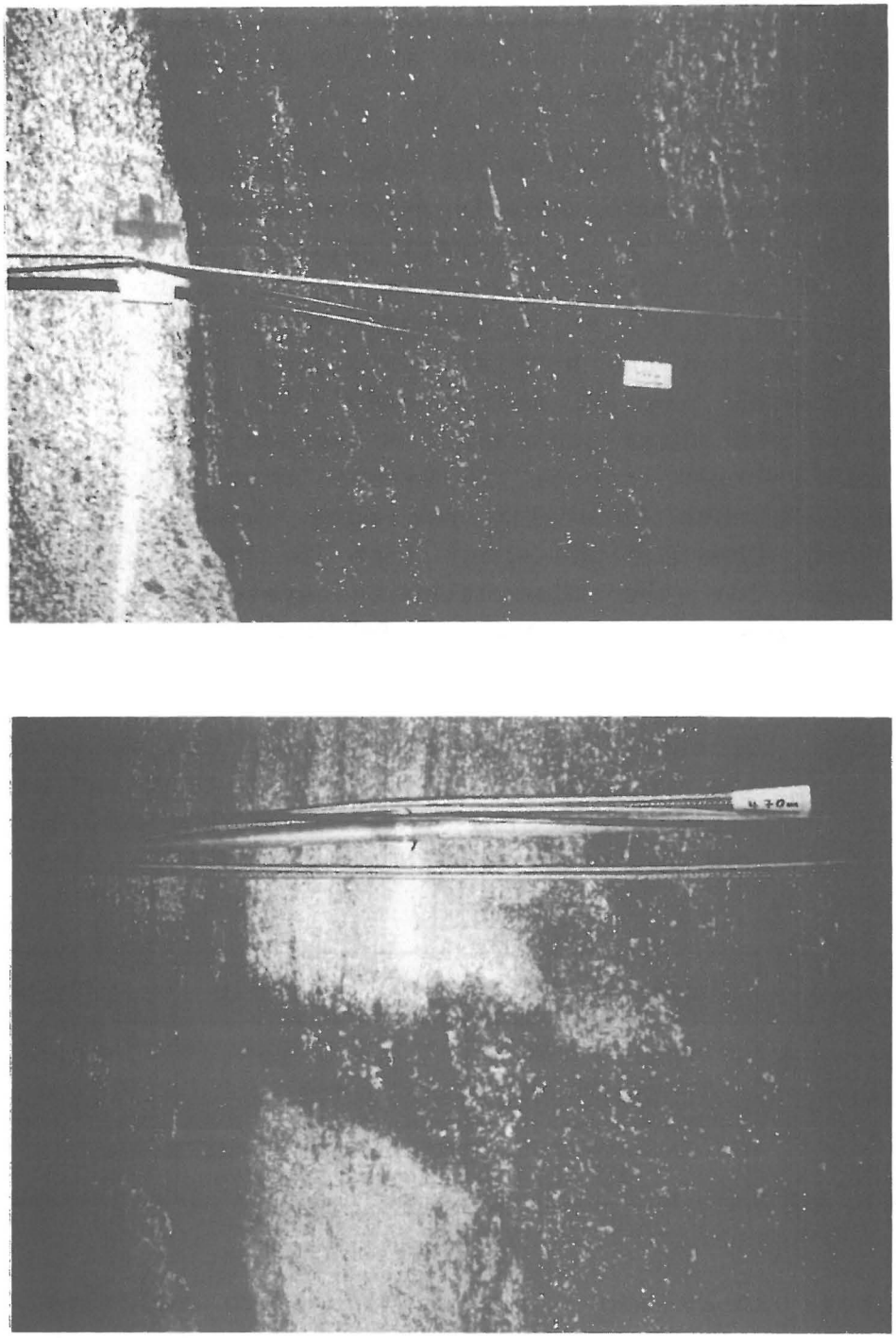

Fig. 4: Water inflow points in the ventilation test drift. The top picture shows the transition zone between undisturbed granodiorite and the shear zone at L465 m. The bottom picture shows wet areas within the shear zone.

3.4 Macropermeability and flow modelling

The mean permeability of the rock surrounding the ventilation drift can be determined by means of hydraulic modelling based on the results of in situ measurements. The average permeability is a description of the sum of vertical and horizontal flow components in a stratified, natural groundwater aquifer. In this report, the term macropermeability is introduced to indicate the average permeability of a fractured rock mass; this always relates to the whole rock volume being considered, and not to individual hydraulically active horizons or structures.

The fractured crystalline rock is assumed to be hydraulically homogeneous and the macropermeability determined from model calculations is dependent in each case on the flow model on which the calculations are based.

In a **fracture water model**, the macropermeability is determined in the first instance by the hydraulic activity and the yield of individual fractures. These two parameters are, in turn, dependent on the frequency, degree of penetration, orientation and aperture of the fractures being considered. The transmissivity and storativity of the rock matrix, which is considered to be a low-porosity medium, are generally ignored.

In a **dual porosity and permeability model**, both the fractures and the rock mass are considered as porous media. This means that the fracture component is described in a similar way to the matrix using a transmissivity value and a storage coefficient. In this model the rock formation is characterised by two homogeneous zones of differing permeability, for which the macropermeability is determined.

If an **equivalent porous flow model** is used, the fractures are assumed to be distributed homogeneously in the rock. A distinction is no longer drawn between the fracture and matrix permeability. The macropermeability of large volume of rock characterised in this way relates exclusively to a porous, homogeneous medium.

A homogeneous medium in this connection is a representative area of rock in which small-scale variations have no influence on large-scale hydraulic properties. In this respect it is unimportant whether these variations are of a petrographic or hydraulic nature.

3.5 Hydrogeological model concepts

In hydrogeological terms, the Grimsel Crystalline of the Juchlistock can be considered as a water-saturated aquifer with a free surface. The height of the water table is determined by the volume of precipitation, atmospheric pressure and the topography of the rock massif.

The land surface of the Juchlistock is introduced in the regional hydrogeological model as an external flow boundary on the one hand and as a pressure boundary on the other. Near-surface water, which infiltrates preferentially via brittle deformation structures (fractures and shear zones), is dispersed through a fine network of fractures in the rock and saturates all the pores of the rock matrix. The equipotential lines follow the topography (VOBORNY et al., 1991).

As depth increases, there is a transition from water movement which is determined largely by discontinuity systems to surficial flow which is dependent on the permeability of the rock matrix. The driving force for water movement is the height of the water table, which is determined by morphology.

The flow-field in the near vicinity of the Test Site is determined by the presence of the tunnel system; the tunnels act as pressure sinks which drain the rock formation. The trend of the equipotential lines in this area is determined on the one hand by the location of the tunnels and, on the other hand, by the permeability of the different hydraulic structures encountered. Flow of water stored in the rock matrix into the tunnels occurs preferentially through higher-permeability structures, namely interlinked

fractures and shear zones with numerous brittle deformations.

The rock matrix of the Grimsel Crystalline, which is considered to be an equivalent porous medium, forms matrix blocks which are separated by the permeability systems of the shear zones (cf. chapter 3.4). The influence of other structures on the flow regime in such a matrix block, for example isolated lamprophyre dykes or fracture systems with a low degree of separation, is only relevant for modelling purposes if these structures are actually encountered by a tunnel.

4. VENTILATION TEST PROCEDURE FOR DETERMINING ROCK PERMEABILITY

In underground tunnel and drift systems, the formation water flowing from the rock is removed to some extent by ventilation. In areas of rock with no notable water flow, a drift atmosphere which is undersaturated with water vapour often results in a situation where the small quantities of moisture coming from the rock are neither visible nor measurable either qualitatively or quantitatively. This makes it difficult to assess the actual water inflow rates, and hence the rock permeability, in a relatively dry tunnel system. If the rock in question is fairly impermeable, as is the case for the Grimsel Granodiorite, it can be assumed that the small volumes of water flowing out of the matrix will evaporate at the tunnel wall. Direct measurement of water volumes is only possible in fractured zones or in mechanically stressed areas of rock with notable water flow. However, in order to obtain an accurate estimate of the average rock permeability, it is necessary to have information both on freely inflowing volumes of water and on volumes evaporating off from only slightly wet matrix sections.

4.1 Test concept

The basic aim of the ventilation test is to determine the amounts of moisture absorbed by circulating air in largely homogeneous sections of rock. The balancing between moisture input and extraction is best performed in individual zones which are isolated from the rest of the tunnel system. If this is combined with measurements of hydraulic head distribution in the rock in the near vicinity of the tunnel, it is then possible to calculate the rock permeability according to methods proposed, for example, by THIEM (1870).

The basic prerequisites for carrying out the ventilation test are defined climatic conditions in the separate drift

sections which are not affected by external climatic fluctuations. To ensure that this was the case, constant volumes of air with a known humidity and temperature were pumped into the measuring sections via a closed circulation system.

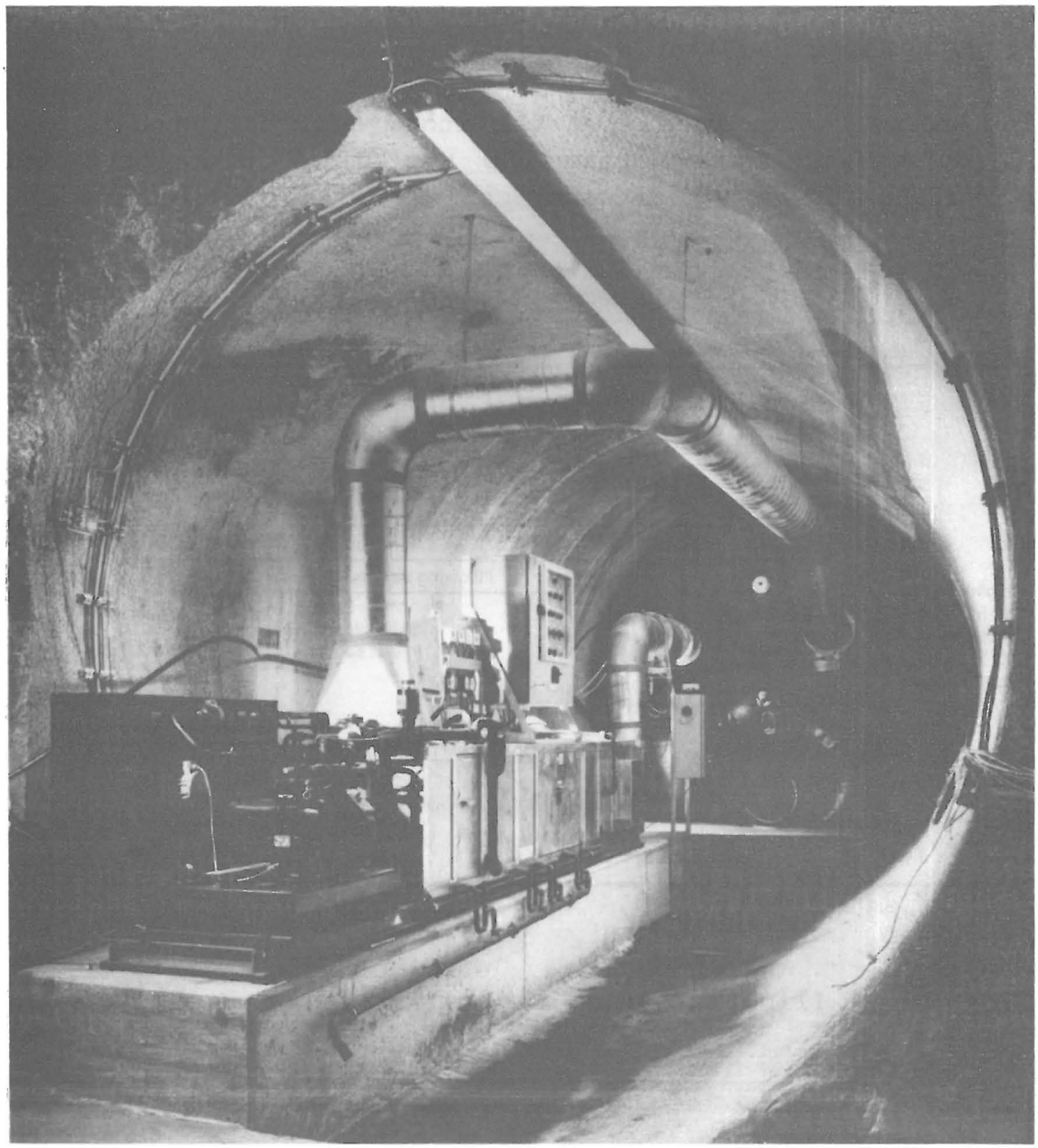

Fig. 5: Access to the ventilation test drift showing the air-circulation system and the mining cushion in the background.

The moisture entering the drift from the rock is absorbed by the circulating air and condenses in the cooling trap of the ventilation plant. The resulting volumes of water are then measured (Fig. 6).

In parallel with these measurements, the hydraulic head distribution in the rock is measured in observation boreholes running parallel and perpendicular to the test drift.

The water inflow rate from the individual drip points can be determined by covering the wet areas with foil and measuring the amount of water collected.

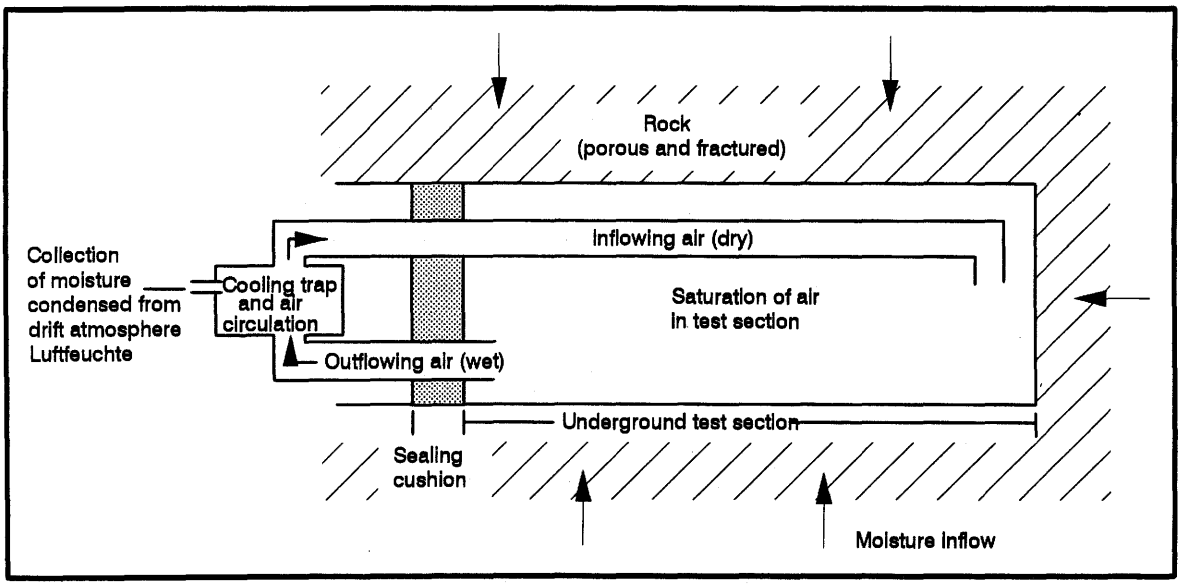

Fig. 6: Illustration of the ventilation test principle.

4.2 Dimensions of the test location

The test drift, which is located in the southern section of the Test Site, is 75 m long and was drilled using a full-face tunnelling machine. The drift cross-section is more or less circular with a diameter of 3.5 m, giving a cross-sectional surface area of 9.6 m^2. The total volume of the idealised cylinder is 722 m^3. The drift surface and cylinder mantle surface amount to approx. 825 m^2. Two rubber mining cushions are used to divide the test drift into two sections. The ventilation test drift is sealed off from the remainder of the tunnel system at tunnel metres 446.5 to 450 m and between the two measuring chambers at 477 to 480.5 m. The forward chamber is 27 m long (volume 260 m^3, surface area 297 m^2) and the rear chamber 40 m long (volume 368 m^3, surface area 440 m^2).

Depending on the topography, the rock overburden to ground surface is approx. 400 m. Other tunnel systems are located at distances of 40 m (migration drift) and 75 m (main access tunnel). There are no tunnels to the west of the ventilation test site. An extended cavern was blasted at the entrance to the test drift for the purpose of housing the technical instrumentation (ventilation apparatus, data acquisition systems, etc.).

The two parallel observation boreholes located to the west of the drift are at distances of approximately 3.5 m and 5.25 m from the drift axis. Two exploratory boreholes drilled from the main access tunnel pass through the roof zone of the test drift at a distance of approx. 2 m. Four additional boreholes between 29 and 55 m long penetrate the shear zone in the floor and roof of the drift (Fig. 7).

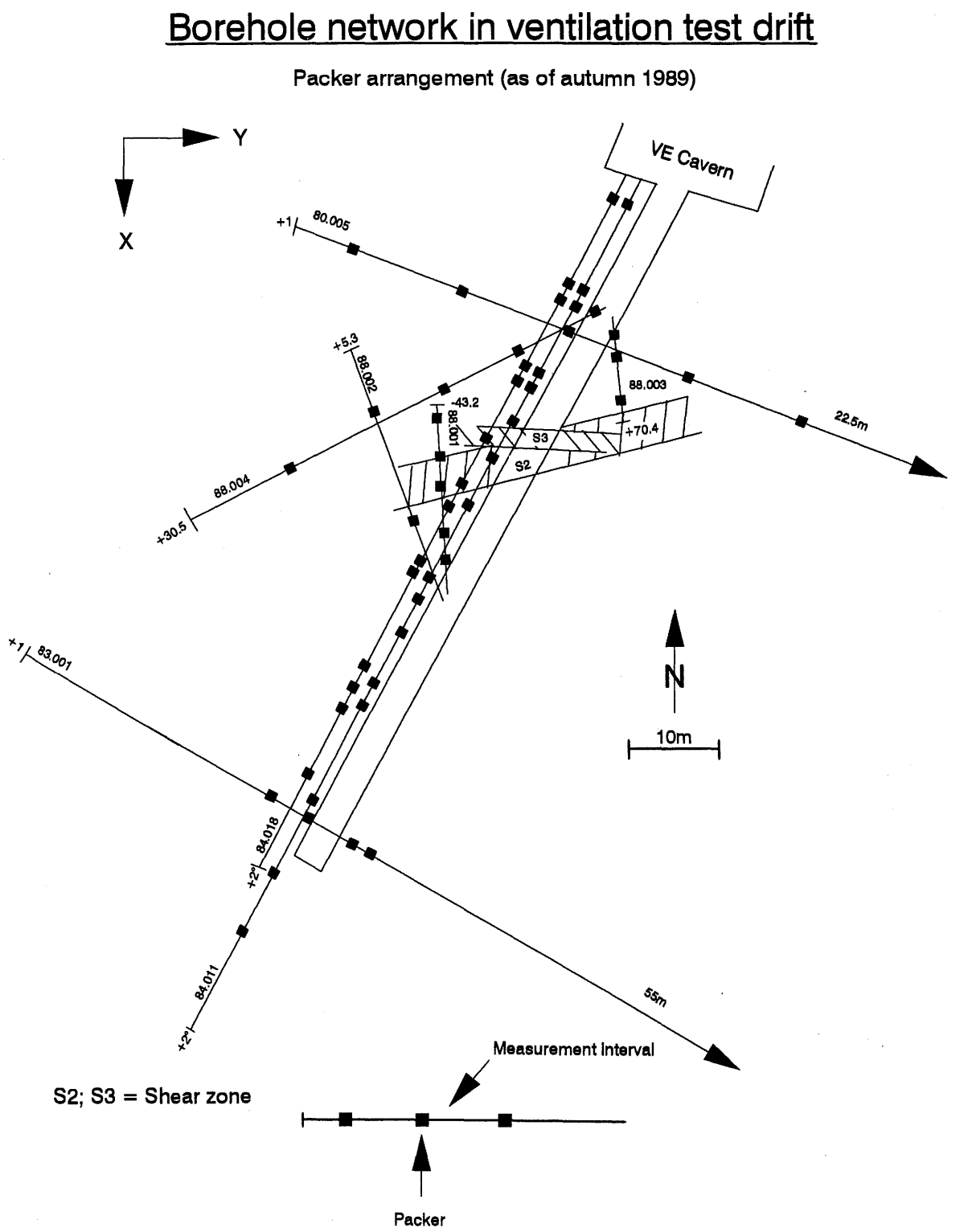

Fig. 7: Location plan of the measurement boreholes and the shear zone.

4.3 Technical configuration of the test

4.3.1 Ventilation equipment

The ventilation of the two measuring chambers is via a closed system with an air-conditioning unit and circulating air pump (Fig. 8). Irrespective of climatic fluctuations in the remainder of the Test Site, this system regulates the volume, humidity and temperature of the air entering a measuring chamber.

The air flux is generated by a circulating air ventilator in the air-conditioning unit. The speed-regulated ventilator extracts the air from the measuring chamber via a pipe system and pumps conditioned air back into the chamber through ventilation pipes. With a maximum volume flux of 2200 m^3/h, the volume of air in a chamber can be exchanged up to eight times per hour.

The air extracted from the measuring chamber is condensed in the cooling trap of the air-conditioning unit. The cooling trap consists of a direct evaporator and a mist collector. The collected air is cooled to +10 to +1°C in the direct evaporator, which is connected to a heat-exchange system via a coolant circulating unit. The cooling power is maximum 12.4 kW. Depending on the relative humidity and the temperature of the incoming air, the dew point is reached as a result of cooling and the humidity in the air condenses out. The condensate accumulates in the mist collector and is then led off to a water volume measurement system.

The cooled air is then heated up again (+10 to +50 °C) using a multiphase electro-heat register and a reheating device which, like the direct evaporator, is linked to the heat-exchange system. The reheating device and the heat register have a heating power of 14 and 16 kW respectively.

The necessary dehumidification and heating capacity of the air-conditioning unit is controlled via an automated

desired/actual value adjustment of relative humidity and air temperature.

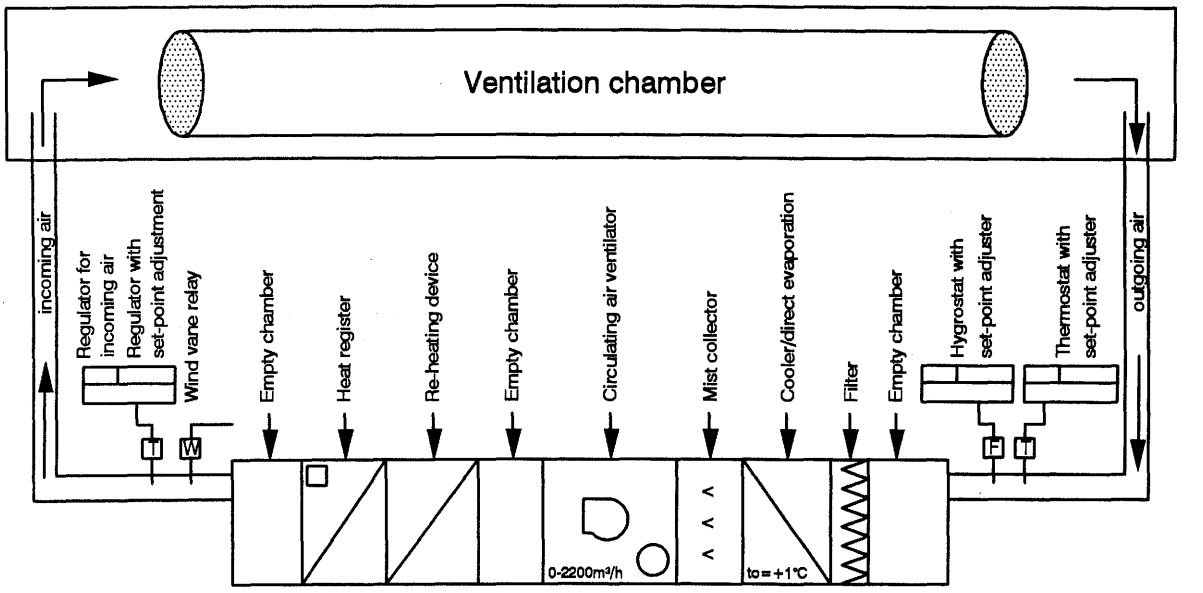

Fig. 8: Technical components of the air-conditioning unit.

4.3.2 Recording measured values

The system for recording measured values and storing data is shown in Fig. 9. In the test drift, measurements are made of air temperature, humidity and circulating air velocity, as well as of volumes of water influx in the measurement intervals of the observation boreholes (cf. measurement location overview in Fig. 10), hydraulic pressure and rock temperatures. The measured data are recorded continuously in the form of analogue voltage signals, with an hourly sampling rate. The data are secured and stored on magnetic tape in the form of binary raw data files using a central data acquisition facility.

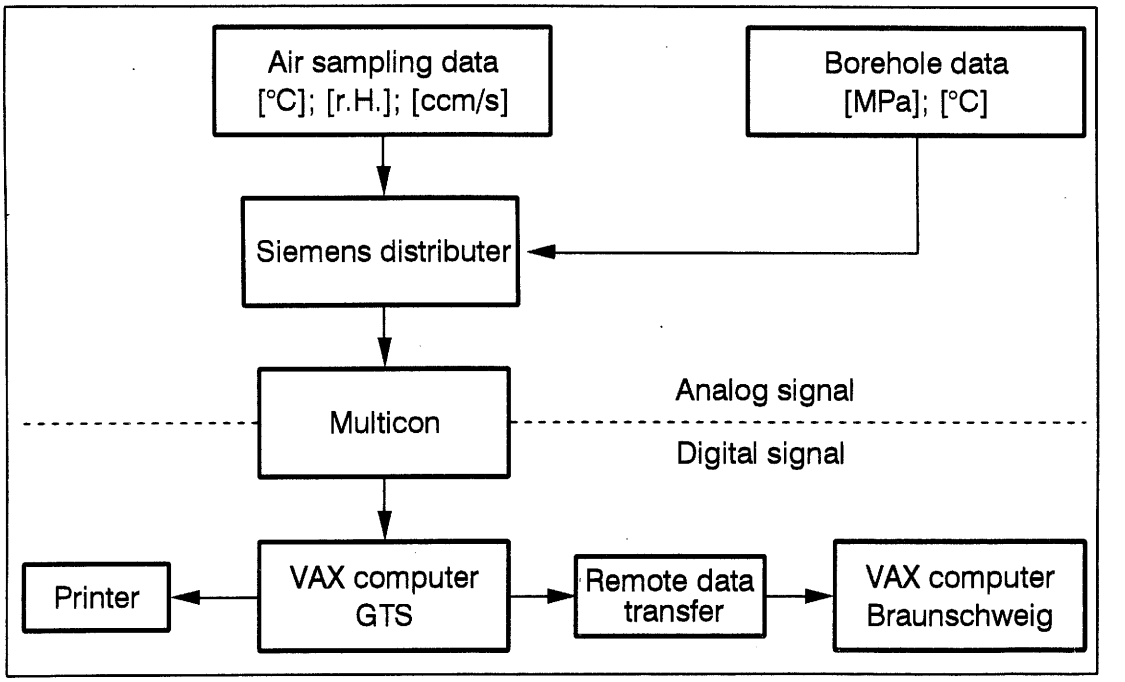

Fig. 9: Configuration of the measured value acquisition systems for the ventilation test.

Water volumes

The volume of water which condenses out in the air-conditioning unit is measured using an electronically controlled water volume measurement apparatus. The introduction and removal of condensed water, the taring of the measurement system (which functions according to the weighing principle) and the instantaneous error flag indicating a system malfunction are all controlled electronically. Measurement of the volume of condensed water is also performed at hourly intervals. The measuring range of the purpose-built apparatus is between 0.1 and 2.5 l/h, and having to handle smaller and greater water volumes frequently resulted in system collapse. The water not removed from the measuring chambers using the ventilation system is collected in sumps, pumped away using a submersible pump and led to the water volume measurement system via hoses. Measurement of this pumped volume of water is carried out according to the liquid flow principle via calibrated impeller-water meters or via rocking container systems where the containers have

specified volumes of 100 and 350 ml. The volume of water pumped out at a particular stage of the test is read manually. The rocking container system proved very reliable in long-term operations.

Temperature and relative humidity

Integrated sensors (Vaisala HMP 14A and HMP 123Y) were used to measure the relative humidity and temperature of the air. Measurements were performed in the inlet and outlet unit of the ventilation system and in the centre of the measurement chamber at axis level. The measuring range of the thermocouples (PT-100) is between -20 and +80°C, with an accuracy of ± 0.3°C. The measurement of relative humidity is done using a capacitive thin film sensor (type HUMICAP). The accuracy of the sensors, which are calibrated for the range 0 to 100%, is ± 3% relative humidity.

The rock temperature in the boreholes is also measured using PT-100 resistance thermometers, although the technical specifications are somewhat different. A four-wire installation system was used because of the length of the cables. For the measuring range 0 to 30°C, the accuracy given by the manufacturer is ± 0.5% of the measured value.

Air circulation rate

The air circulation rate in the system was measured using anemometers supplied by the company WOELKE (type MA 1/2 F3-004). The measuring range can be adjusted between 0 and 12 m/s.

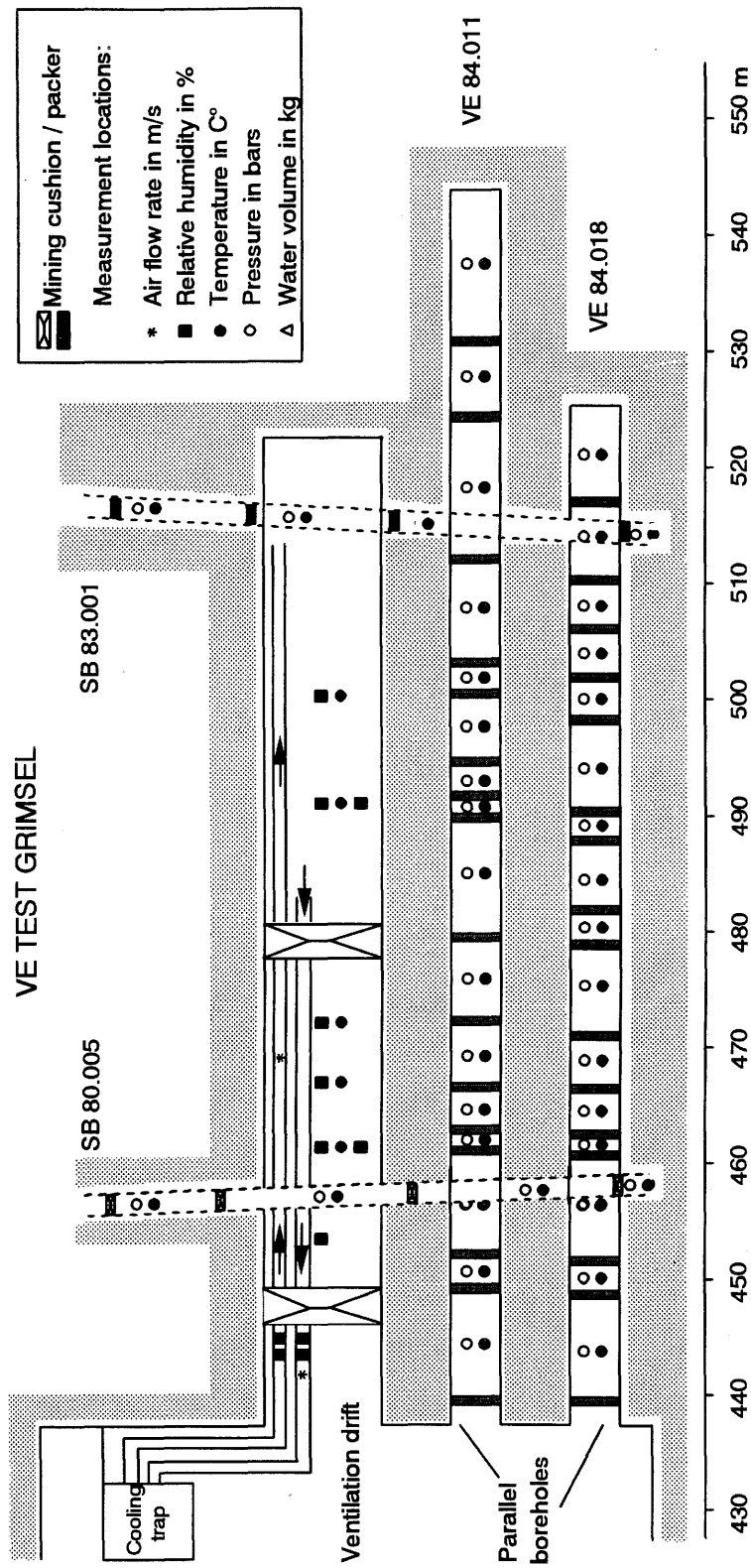

Fig. 10: Schematic representation of measurement location configuration in the ventilation test drift and in the boreholes.

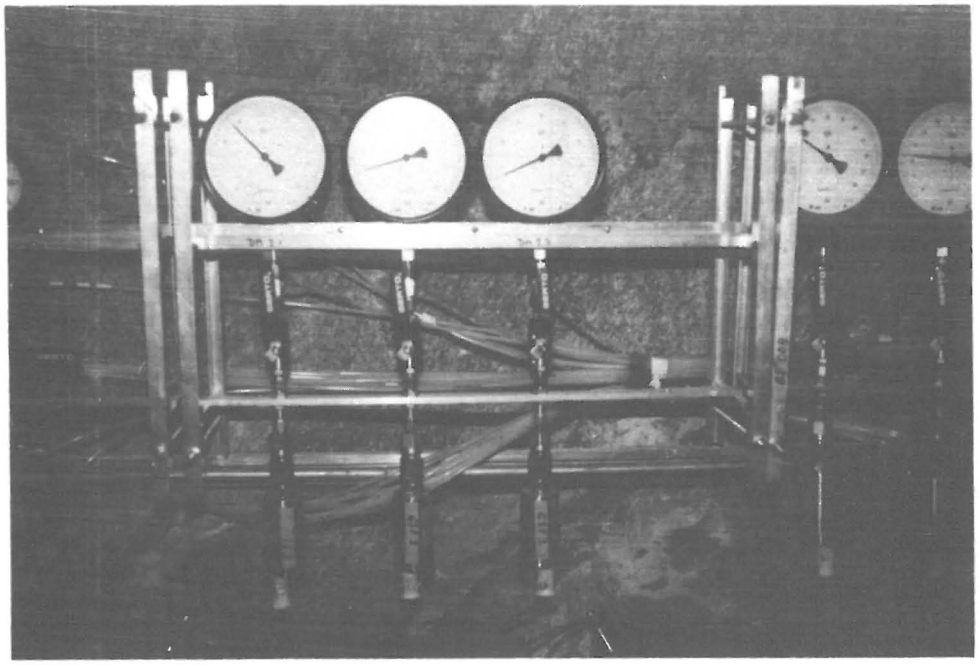

Fig. 11a: Visual check of pressure data using precison manometers.

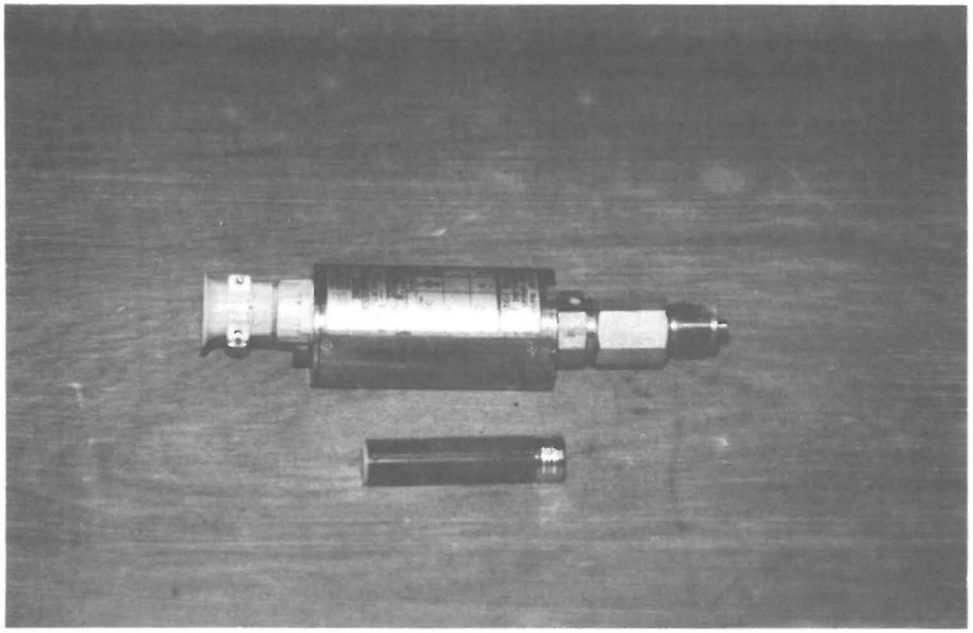

Fig. 11b: Piezo-resistive pressure transducers for measuring formation water pressures.

Formation waterpressure

The hydraulic formation water pressures were measured in intervals of the different boreholes. Measurements were carried out using piezo-resistive pressure measurement transducers (type Labom E 2311) which were installed in the ventilation test chamber (Fig. 11). The operating principle of the transducers is based on a temperature-compensated overpressure measurement. The measuring range of the equipment is between 0 and 2 MPa and 0 and 4 MPa and corresponds to an analogue voltage signal of 0 to 5 volts. The maximum error of the linearised signal of the transducers is < 0.5% of the measuring range end-value. The zero point of the transducers is equivalent to the air pressure at the Test Site. The Test Site is at an altitude of approx. 1700 metres above sea-level. Fluctuations in air pressure were not taken into account in measurements made during the tests. During measurement phases, the borehole intervals were completely saturated with water.

Configuration of the measured data registration system

The system for registering measured data from the ventilation test consists of the sensors (data transmitters) of the MULTICON data acquisition facility, a MICRO-VAX computer with a magnetic tape recording facility and a printer (Fig. 9). The MICRO-VAX computer, which is located in the central facility of the GTS, is also linked to the data acquisition systems for the GSF heater and tiltmeter experiments (BREWITZ & PAHL, 1986). 192 MULTICON channels were available for the ventilation test sensors. The incoming measured values, in the form of analogue voltage signals of 0 to 5 volts, are registered by the MULTICON data acquisition facility (16-bit resolution) and converted into a 14-bit digital signal. The digital values are recorded in an hourly cycle, transmitted to the MICRO-VAX and stored on hard disk and magnetic tape in binary format as raw data files. A dot printer (PHILIPS) was used for special measurements with smaller cycles. The hourly raw data files

were transmitted using a remote data transfer system (DATEX P) from the MICRO-VAX at the GTS to the central computer (VAX) at the "Institut für Tieflagerung" in Braunschweig. At the GTS, a printer could be used to output the binary raw data in tabular form. Analysis and presentation of the measured data in a time diagram was done using the central computer (mainframe) in Braunschweig.

The key technical components of the experiment, such as the air-conditioning unit, compressed air supply for the mining cushions and the water volume measurement system, were connected to the GTS alarm system. Every malfunction or perturbation in the test drift was communicated via this system to the central facility at the Test Site; steps could thus be taken immediately to remedy the situation.

4.3.3 Plastic sheeting within the shear zone

In order to characterise individual open water inflow points within the shear zone, damp areas on the drift surface in the forward chamber were covered with plastic sheeting. The volumes of formation water accumulating under the plastic foil at these locations was measured using rocking containers with a mechanical pulse counter (cf. chapter 4.3.2). To ensure that fluctuations in the drift climate did not affect water influx, the edges of the sheeting were stuck to the cleaned drift surface using a sealant (GOODRICH) specifically designed for use on granitic rock. Sealing the sheeting to the rock proved problematic in the contact zones between lamprophyre dykes and the granodiorite gneiss, as well as in areas of fractured rock. The water which was not collected in the plastic sheeting was collected in two sumps at L465 and L470 m and led to the water volume measuring system. Between tunnel metres L465 and L473, a total of 4 zones with an area of approx. 35 m^2 were covered with foil (see BOSSART & HUFSCHMIED, 1989); this represents about 30% of the tectonic shear zone which is exposed at the drift surface.

4.3.4 Instrumentation and equipment for the packer tests

Hydraulic investigations (hydrotests) were carried out in the boreholes BOVE 88.002, 88.003, 88.004 and BOSB 80.005, which were equipped for this purpose with pneumatic multi-packer systems (HEINIGER, 1989). The location and instrumentation of the tested boreholes is shown in Fig. 7.

The hydraulic pressures in the test intervals of the boreholes were measured using piezo-resistive overpressure sensors in the boreholes and relative pressure sensors in the ventilation test drift. The latter are connected to the individual measuring intervals via pressure pipes. The measuring range of the sensors is between 0 and 2.5 and 0 and 6.0 MPa respectively, and the accuracy is better than 0.25% of the measuring range end-value. Precision manometers were also installed for in situ observations.

Injection of water into the test intervals is done using separate pipes. A rotary pump was used for injection tests in areas with low formation water pressures (< 1.7 MPa) and a relatively high transmissivity ($T > 10^{-9}$ m^2/s). Flow rate was measured using mass flow meters (type MICRO MOTION D 6 and D 25).

A pressure vessel with an integrated weighing cell was used for measuring flow in areas of rock with lower transmissivities ($T < 10^{-9}$ m^2/s) (Fig. 12). The injection pressure required in the pressure vessel is produced using nitrogen gas bottles and the water weighed in the weighing cell is introduced via pipes to the test interval.

An HPLC laboratory pump (type Shimadzu HPLC-5) was used for constant flow tests with high formation water pressures (> 1.7 MPa) and low flow rates (< 10 ml/min).
Continuous acquisition and storage of data from the pressure and flow measurements is done separately from the registration of other ventilation test data using a data-logger (type THERMODAC 32 and PC AT 03).

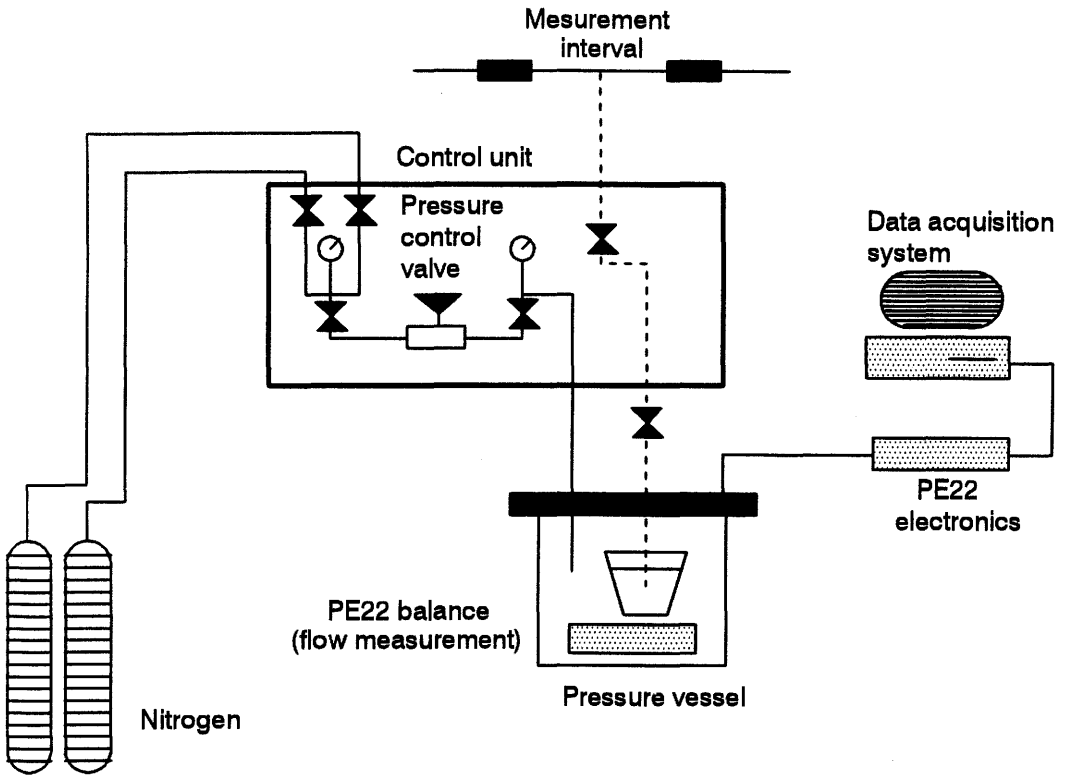

Fig. 12: Hydrotest configuration (HEINIGER, 1989).

4.4 Test procedure

The water influxes into the ventilation drift were determined separately for the forward and rear measuring chambers. By varying air temperature and relative humidity in the chambers, it was possible to investigate the extent to which water influx and pressure distribution in the measurement boreholes depend on the drift climate.

The water influxes were measured for mean air temperatures of 13, 17 and 22°C, relative humidities of 65, 50 and 30% (Figs. 13/14) and an air volume flux between 1500 and 2100 m^3/h. Each temperature step corresponded to a ventilation phase with a duration of several months. In the saturation phase before and after ventilation of a chamber, measurement of outflowing water dripping openly from the rock was performed solely via the pump sumps.

Following ventilation, the water inflow rate from the vicinity of the shear zone in the forward measuring chamber was measured using plastic sheeting with an air temperature of 15°C and a relative humidity between 70 and 100%.

During the ventilation experiments, the pressure and temperature in the immediate vicinity of the test drift were measured in observation boreholes BOVE 84.011 and BOVE 84.018. The boreholes, which run parallel to the drift at distances of 1.75 and 3.5 m, are divided into 32 measurement intervals. Individual intervals in the observation boreholes and additional holes (SB 80.005; SB 83.001 and BOVE 88.001 to 88.004) are up to 35 m away from the drift (cf. Fig. 7). The pressure measurements conducted in these intervals were used to determine the extent of the pressure sink in the vicinity of the ventilation test drift and to determine the corresponding pressure gradients.

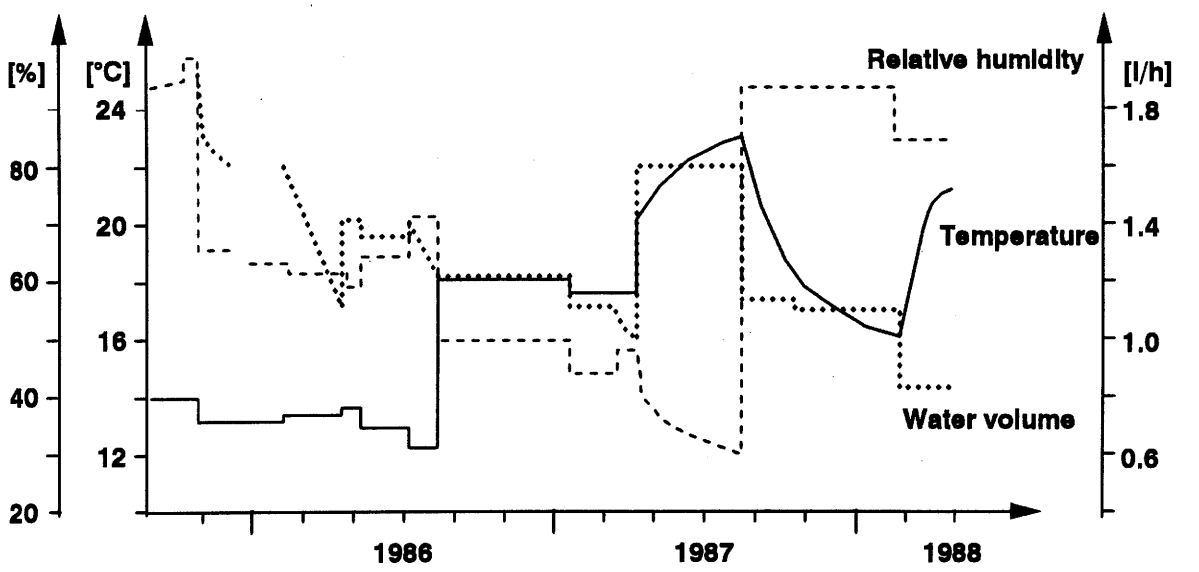

Fig. 13: Water inflow and ventilation test phases in the forward chamber.

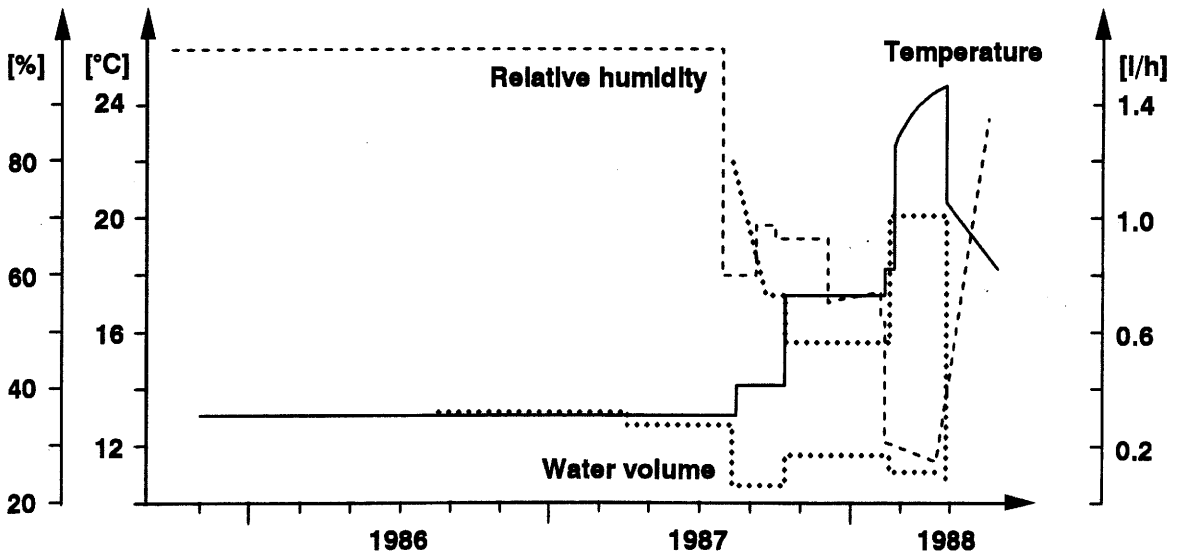

Fig. 14: Water inflow and ventilation test phases in the rear chamber.

4.5 Test results

4.5.1 Water balance

The water inflow rates to the drift (cf. Figs. 13/14) determined during the ventilation and saturation phases are presented in Table 3 for the forward and rear measuring chambers and for the shear zone.

Table 3: Overview of the water inflow rates for both measuring chambers during the ventilation test phases.

Ventilation phases			forward chamber		Rear chamber
Phase	Temperature	Humidity	Shear zone	Matrix	Matrix + Lamprophyre
No.	°C	% r.h.	Flow rate in l / h		Flow rate in l / h
1.forward	13	65	1.4 ± 0.25		
2.forward	18	50	1.2		
3.forward	21	35	1.6		
	18	< 100	1.1	< 0.25*	
	12.5	< 100			0.3
1.rear	13	65			0.9
2.rear	17	60			0.6
3.rear	23	30			0.7
surface-related flow rate			flow rate in ml/(s·m^2)		flow rate in ml/(s·m^2)
forward and rear chambers			$1.25 \cdot 10^{-3}$		$0.35 \cdot 10^{-3}$
Shear zones and matrix			$3 \cdot 10^{-3}$	$< 0.3 \cdot 10^{-3}$	

* extrapolated

The water balance for the forward chamber during ventilation phase 1 (T_L = 13°C; RH = 70 - 60%) shows a mean water influx of 1.4 l/h (T_L = air temperature in °C; RH = relative humidity). During ventilation phase 2 (T_L = 18°C; RH = 50 - 45%), the water inflow rate drops to approx. 1.2 l/h. During phase 3 (T_L = 20 - 22°C; RH = 40 - 30%), the entire drift surface in the forward chamber dried out, with the exception of the area at L465 m. The inflow rate stabilised at 1.6 l/h. During the subsequent saturation phase (rise in relative humidity in the chamber to 100%), an inflow rate of approx. 1.1 l/h was measured.

Related to the whole drift surface area of the forward chamber (297 m^2), the water inflow rate was $1.25 \cdot 10^{-3}$ $ml/(s \cdot m^2)$.

A similar trend was identified during ventilation of the rear chamber. During the saturation phase prior to ventilation, a more or less constant water influx of 0.3 l/h was measured over a period of one year. During ventilation phase 1 (T_L = 13°C; RH = 60 - 70%), the mean water influx was 0.9 l/h; this dropped to 0.6 l/h during phase 2 (T_L = 17°C; RH = 68 - 58%). During phase 3 (T_L = 22 - 24°C; relative humidity = 30%), the inflow rate, corrected down by 0.3 l/h, was 1.0 l/h. The 0.3 l/h component came from the forward chamber and is the result of a comparison of water inflow rates in the test drift during ventilation of the rear chamber (cf. Figs. 13 and 14).

Calculated for the whole drift surface area of 440 m^2, the water inflow rate was $0.35 \cdot 10^{-3}$ $ml/(s \cdot m^2)$.

Subsequent to the saturation phase in the forward chamber, a water inflow rate of between 0.8 and 1.3 l/h was determined for the sections of the shear zone which were covered with plastic sheeting (Fig. 15). The mean water influx during the 85-day test period was 1.1 l/h. The linear regression lines for total water influx from the shear zone showed a slightly increasing tendency during the observation period. The largest water flow was in the region of foil 4 (L464.5 to L465.5 m), with approx. 0.6 l/h.

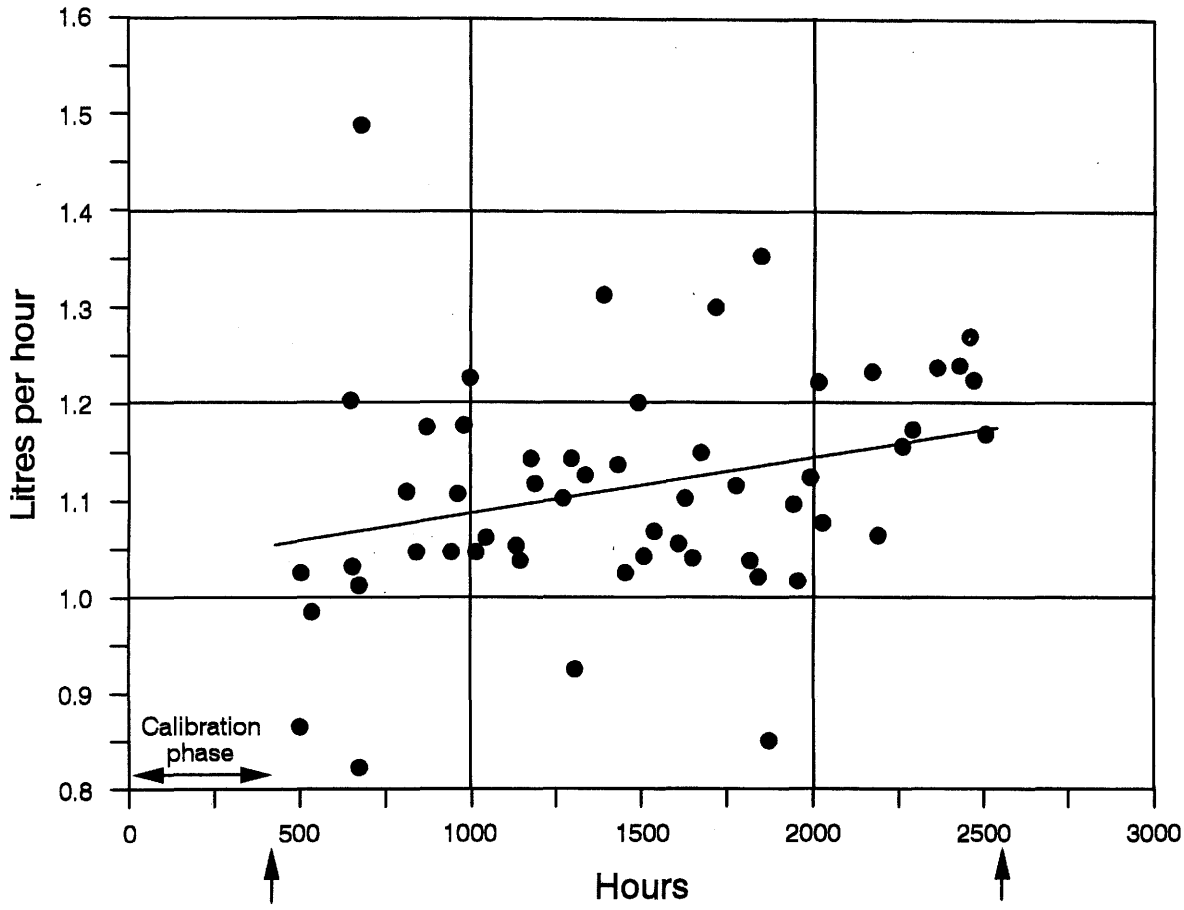

Fig. 15: Water inflow from the shear zone during the period from July to November 1988 (from BOSSART & HUFSCHMIED, 1989).

Related to the drift surface area which is taken up by the shear zone (approx. 100 m^2), the mean water inflow rate of 1.1 l/h corresponds to an average flow rate of $3 \cdot 10^{-3}$ $ml/(s \cdot m^2)$.

In the forward chamber, the ventilation process has the effect of extracting an additional 0.45 l/h from the matrix; this was confirmed by a comparison of measured water flow rates from the ventilation and saturation phases and from collection using plastic sheeting. Extraction of this additional volume of water from the rock can be explained by evaporation processes at the drift surface rather than by pressure-related flow.

4.5.2 Pressure distribution and evolution

The pressure distribution in the borehole measurement intervals close to the drift is very random (Fig. 16). In the intervals which are only 1.75 m away from the drift, the pressures measured varied between 0 and 587 kPA. The intervals without detectable pressure build-up, where the mean porewater pressure is equal to the atmospheric pressure, are linked with the ventilation drift via open fractures. The area of the shear zone (L465 to L475 corresponding to P 10 to P 12) is characterised by a relatively high pressure of up to 2 bars.

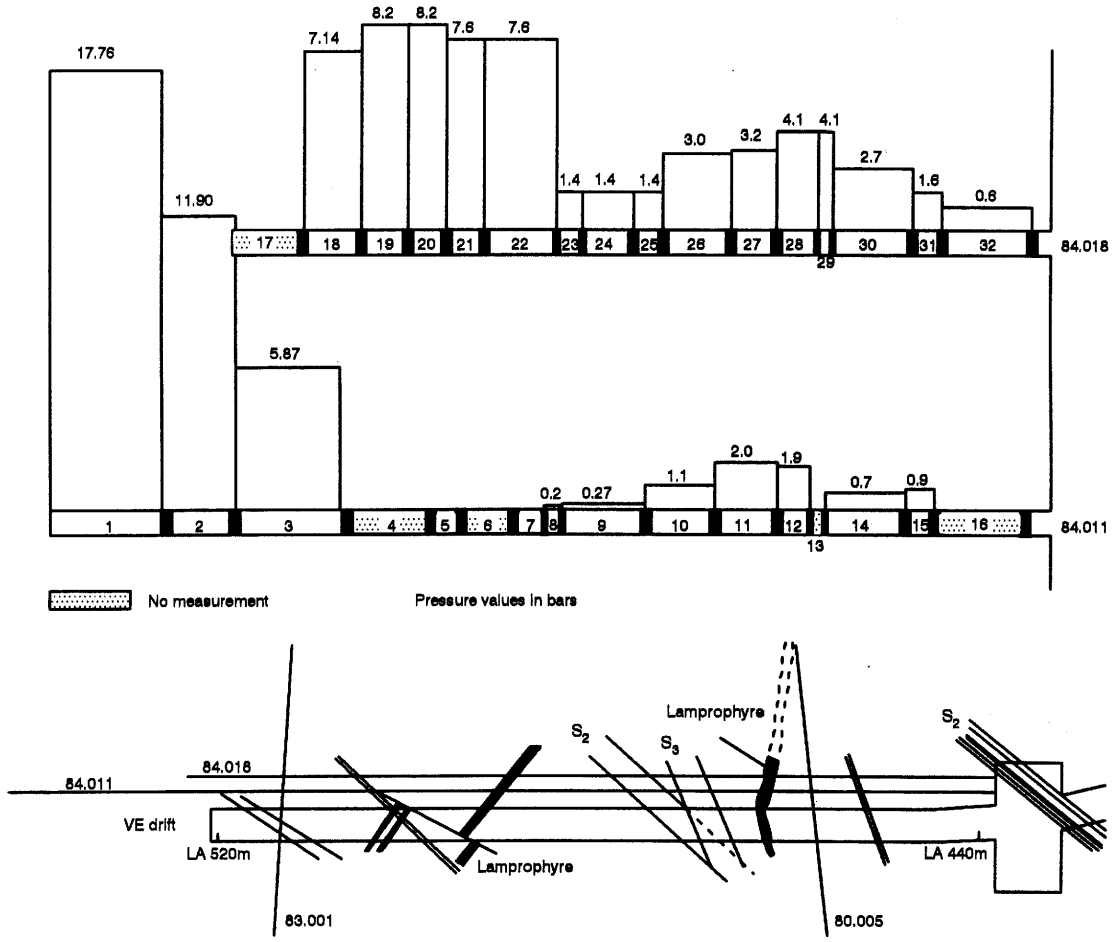

Fig. 16: Pressure distribution [bar] in the parallel boreholes 84.011 (P1-16) and 84.018 (P17-32) from March 1988 (single measured values)/(* May 1987).

In the intervals which are 3.5 m away from the drift, the mean porewater pressures are between 60 and 820 kPA. In this case also, the area of the shear zone (P 26 to P 29) is distinguished from its surroundings by a relatively high pressure value of up to 400 kPa. Other structural elements such as lamprophyre dykes have no detectable influence on the pressure distribution in the vicinity of the drift.

In the measuring intervals at a greater distance from the drift (10 to 35 m), the mean porewater pressure rises from 1.2 MPa to around 3.0 MPa (Fig. 17). However, the formation water pressure of 4.0 MPa expected for a depth of approx. 400 m was not reached.

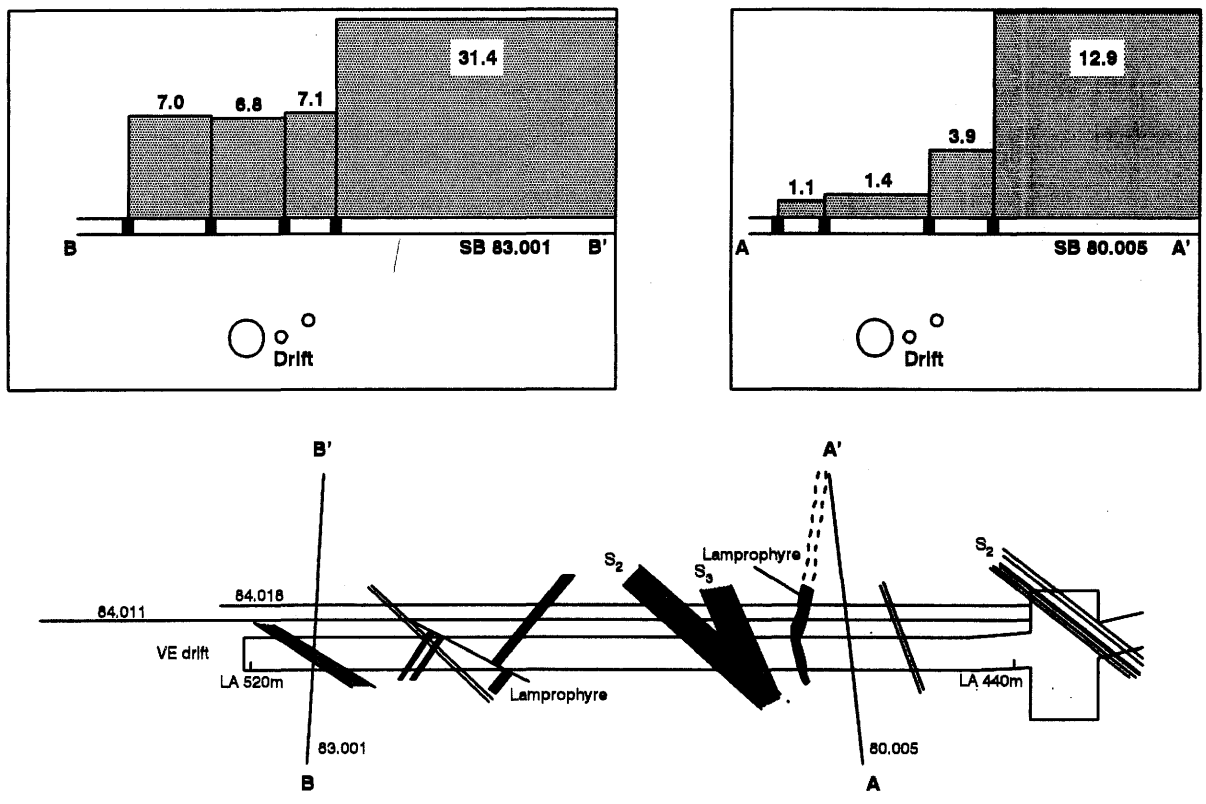

Fig. 17: Pressure distribution [bar] in the boreholes 80.005 and 83.001 (single measured values from March 1988).

Up to a distance of around 5 m from the drift, the rise in water pressure in the rock is influenced considerable by

single structures (Fig. 18). As distance from the VE drift increases, the pressure values also rise. However, the pressure sink around the VE drift extends beyond the measuring range of 35 m.

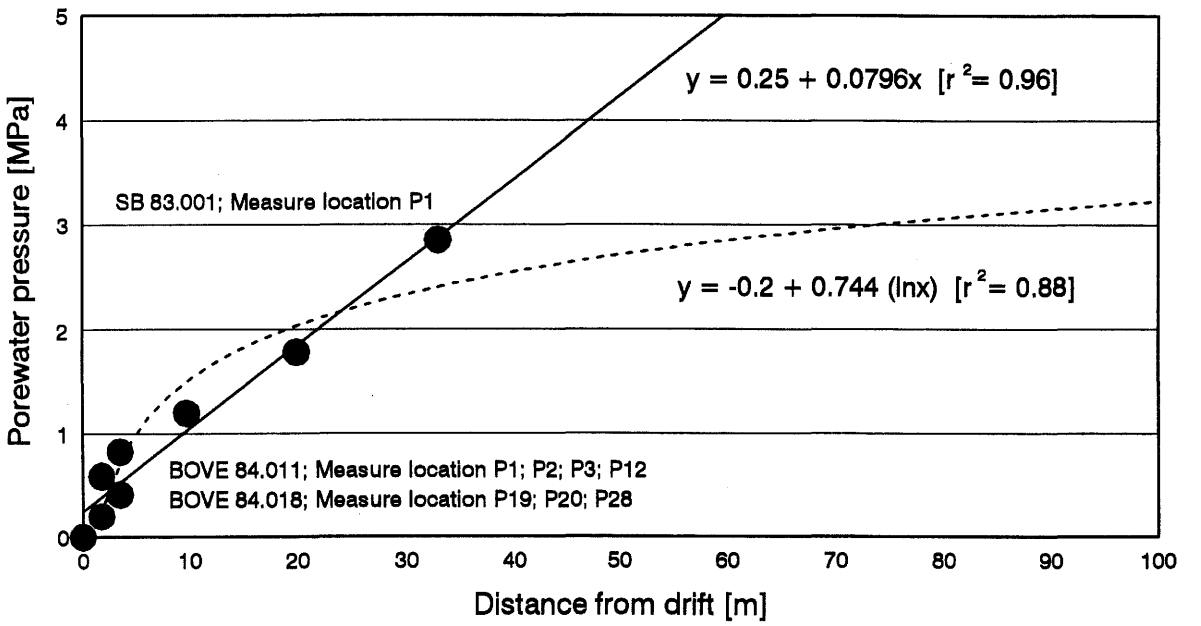

Fig. 18: Pressure distribution in the near vicinity of the drift.

The effective pressure gradient in the sink has an average value of 80 kPa/m (Fig. 19). For the area of the shear zone in the drift vicinity, the pressure gradient is 110 kPa/m. As is the case for the mean porewater pressure, the hydraulic gradient in the drift vicinity is also influenced by so-called skin effects (e.g. relaxation of the matrix structure, fissures and fractures and non-saturated zones).

The skin effect describes the surficial hydraulic damage to the rock as a result of tunnel excavation and drilling. A distinction is drawn between positive (lowering of the permeability) and negative (increase in permeability) skin effects.

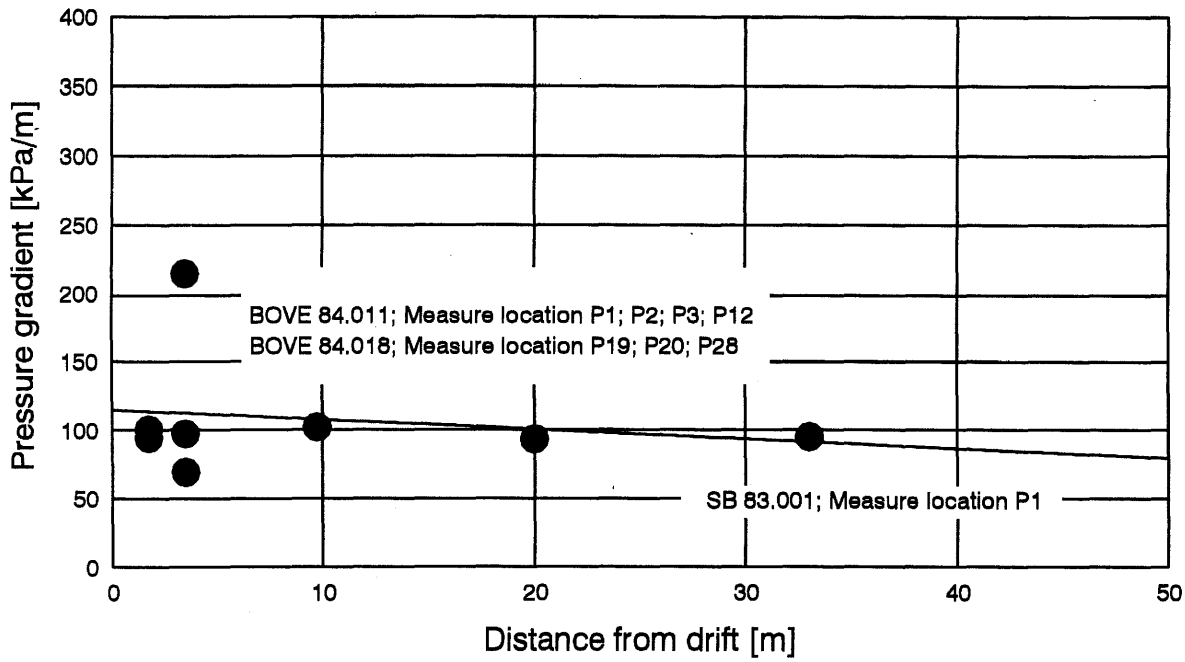

Fig. 19: Derivation of the effective pressure gradient from selected measuring locations.

Fig. 20 shows the hydraulic potentials measured in the intervals of boreholes BOVE 88.002 to 88.004 and SB 80.005 following completion of the ventilation tests. The relatively low potentials in borehole 88.003 can be explained by the fact that the measuring intervals are intersected by a fracture network; this network is linked to the second interval in borehole 80.005 and possibly opens into the neighbouring migration drift. The other potentials measured correspond to the level of pressure drawdown around the ventilation drift.

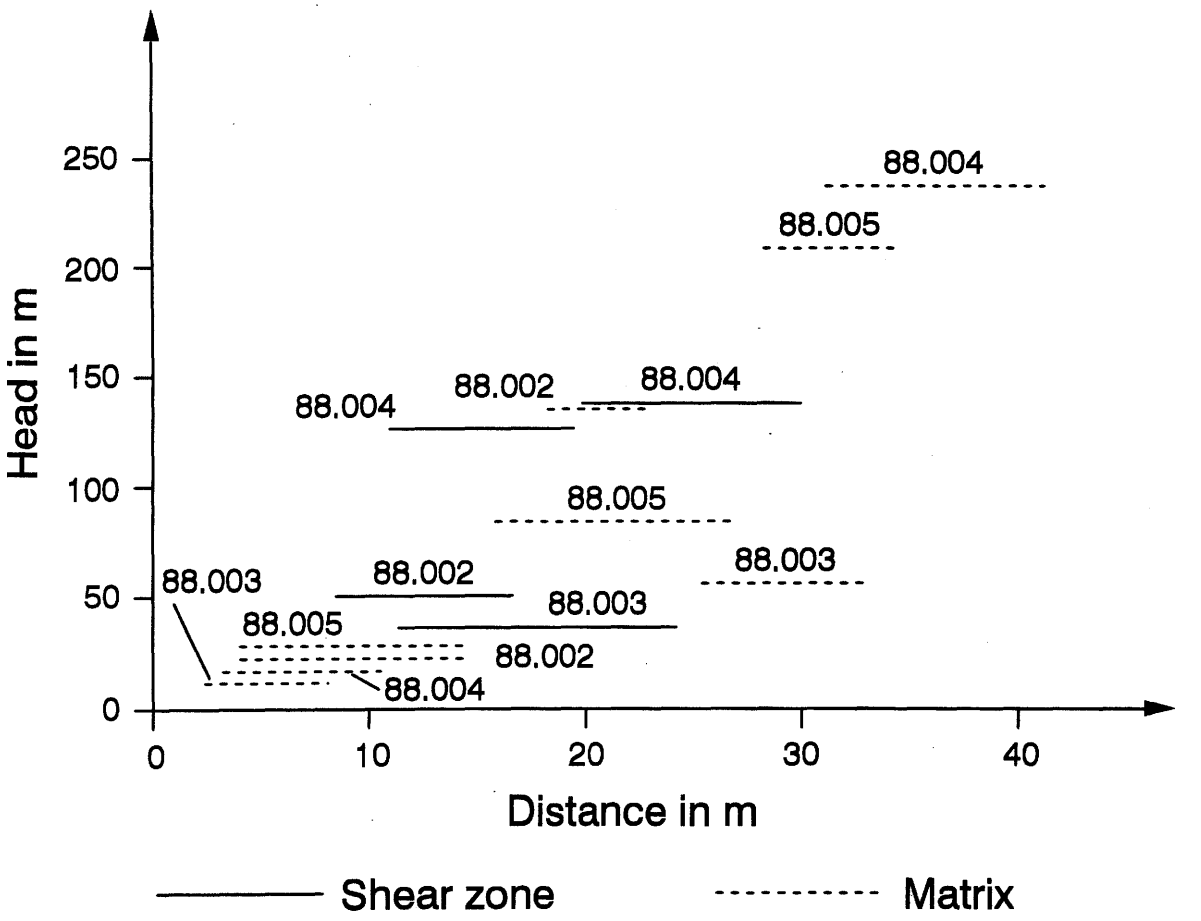

Fig. 20: Hydraulic potentials (m water column) in the shear zone and matrix. Derived from the formation water pressures measured in boreholes BOVE 88.002, 88.003, 88.004 and 80.005.

During the test period, from 1986 to 1988, the mean porewater pressures in the borehole measurement intervals remained more or less stationary. The duration of pressure build-up required to reach quasi-stationary pressure conditions was up to several months for individual measurement intervals (Fig. 21).

At the beginning of ventilation phases 2 and 3 in the forward chamber, a direct influence of ventilation on the mean porewater pressure as a result of a temperature increase in the incoming air was detected in section 12 of borehole 84.011 (cf. Fig. 21). A similar effect, but with a time

shift, was also observed in section 28 of borehole 84.018. Following temperature equalisation in the rock, both pressures dropped again to the original level.

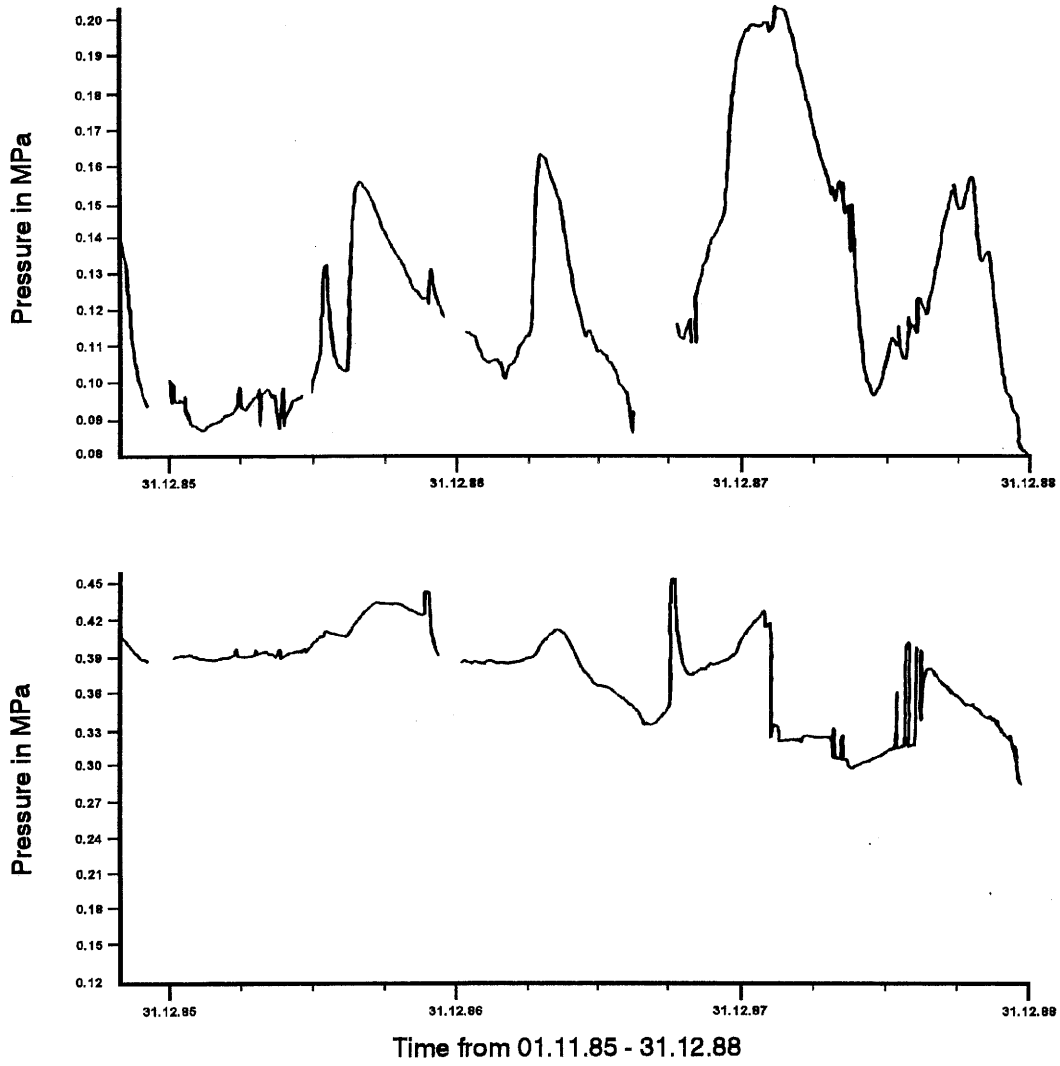

Fig. 21: Pore water pressures in the measuring intervals 12 (BOVE 84.011) and 28 (BOVE 84.018).

4.5.3 Temperature evolution

Owing to the increase in air temperature during ventilation of the forward chamber, the rock temperature at a distance of 1.75 m from the drift rose from approx. 12°C to 17°C. At a distance of 3.5 m from the drift, the rock temperature rose by 3°C. During the entire test period, the temperature in the area of the shear zone was always 0.5 to 1°C lower than that of the surrounding granodioritic matrix zones.

4.5.4 Summary of test results

The test results give the following picture of the hydrogeological regime in the region of the ventilation test drift:

- water inflow in the forward chamber is approx. 1.1 l/h without ventilation and approx. 1.6 l/h with ventilation
- water inflow from the area of the shear zone is approx. 1.1 l/h
- water inflow in the rear chamber is approx. 0.35 l/h without ventilation and approx. 0.7 l/h with ventilation
- a water inflow rate of 0.2 to $1.0 \cdot 10^{-3}$ ml/(s•m^2) for the matrix zone and $3.0 \cdot 10^{-3}$ ml/(s•m^2) for the shear zone can be derived from the water balance
- rock moisture is also mobilised by the ventilation process
- the pressure sink formed around the ventilation test drift exceeds the measured range of 35 m

- the pressure distribution in the near-drift zone and in the vicinity of other boreholes and tunnels is disturbed

- a gradient of 80 kPa/m for the pressure sink can be derived from the pressure rise curve, which is assumed to be linear for early data

- ventilation of the test drift has only a temporary effect on the porewater pressure in near-drift areas

- the initial temperature in the rock in the vicinity of the test drift was approx. 12°C

- following ventilation (air temperature > 22°C) the rock temperature rose to 17°C (1.75 m) and 15°C (3.5 m) respectively.

4.6 Analytical determination of macropermeability

The mean rock permeability, defined in the following as macropermeability, is a mean value derived from individual permeabilities which describes the hydraulic flow characteristics of a large volume of rock. With an estimated radius of influence of 50 m around the test drift, the volume of rock included in the ventilation test is approximately 100,000 m^3. Compared with this, the volume of the test field in borehole measurements is usually only a few cubic metres. The dimensions of drillcores, which are generally used in the laboratory to determine permeability values, are therefore often only a few cubic centimetres.

In so far as they do not determine the overall hydraulic regime, local structural features and direction-dependent water movements can generally be ignored in a volume of rock this size.

Analytical determination of macropermeability and specification of hydraulic boundary conditions proceeded on the

basis of the long-term observations during the ventilation test. These were complemented by petrophysical studies of selected, non-fractured rock samples carried out in the laboratory.

The methods used for interpretation of DARCY flow, which are well-known from hydrological applications (see chapter 4.6.2), were used in the evaluation process. The hydraulic characteristics of the microfractured, large-scale rock body were taken as being equivalent to the flow properties of a porous medium.

4.6.1 Hydraulic boundary conditions

Excavation of drifts and tunnels alters the hydraulic potential and, consequently, the flow-field in a water-saturated rock formation. Depending on the location of a drift underground, and the hydraulic properties of the surrounding rock, the flow conditions are initially non-stationary; later, once equilibrium has been reached, the conditions are quasi-stationary.

Water movement (filter velocity v = m/s) in the altered flow-field can be assumed to be proportional to the hydraulic gradient (grad h).

In DARCY's Law (1856), the linear relationship between the hydraulic gradient and the filter velocity is described using a proportionality factor - the hydraulic conductivity (K)

$$v = K \cdot \text{grad } h.$$

Important prerequisites for DARCY flow are largely **homogeneous** and **isotropic flow conditions** and **laminar water flow** - both related to the entire tunnel length ("filter section") - in the area of rock being considered. With some reservations, these prerequisites can considered as being

fulfilled for the ventilation test area, which is taken as being equivalent to a representative elementary volume (rev). Reservations apply to the isotropy (influence of the shear zone, cf. chapter 3.3), the near-drift zone and the influence of individual inhomogeneities such as lamprophyre dykes.

If the dynamic viscosity and the specific weight of the water, as well as the geometry of the pore space structure, are taken into account, the hydraulic conductivity can be converted into a corresponding **specific permeability** and a **mean permeability** (macropermeability). The hydraulic conductivity is indicated with K or k_f are identical. The hydraulic conductivity can also be derived from the **transmissivity** (T) and the thickness of the groundwater aquifer, i.e. the length of the test interval (m).

$$K = T/m$$

The permeability (k) is calculated as follows:

$$k = K \cdot \mu_W / \gamma_W$$

$$\gamma_W = \rho \cdot g$$

k	= permeability,	m^2
K	= hydraulic conductivity (K_f),	$m\ s^{-1}$
T	= transmissivity,	$m^2\ s^{-1}$
m	= thickness of the aquifer,	m
μ_W	= dynamic viscosity of water,	Pa·s
γ_W	= specific weight of water,	$Pa\ m^{-1}$
ρ_W	= density of water,	$Kg\ m^{-3}$
g	= earth acceleration,	$m\ s^{-2}$

The symbols and units for calculating the rock permeability, and their designation at normal temperatures (approx. 20°C) and low ionic strength (mineralisation < 500 ppm), are given in Table 4.

Table 4: Units used for the permeability of slightly mineralised water at 20°C.

Symbol	Designation	Unit
k = K·dynamic viscosity/ specific weight	Permeability	m^2
K = Filter velocity hydraulic gradient	hydraulic conductivity	m/s
T = K·thickness of aquifer	Transmissivity	m^2/s

(1 Darcy ≈ 10^{-12} m^2 ≈ 10^{-5} m/s)

It should be mentioned in this context that, when calculating the macropermeability in the region of the ventilation test, the **pressure gradient** rather than the **hydraulic gradient** was used in the equations.

$$\text{grad } h_{\text{hydraul.}} = dh/dl$$

$$\text{grad } p_{\text{Druck}} = dp/dl$$

dh	= hydraulic head,	m
dp	= measured pressure difference,	Pa
dl	= flow distance,	m

A further boundary condition is the **law of mass conservation** (continuity principle) which should be taken into consideration when calculating water movement in an equivalent porous (fractured) medium.

In the case of non-stationary flow conditions, the volume of water extracted from the effective pore space of a

geometrically defined volume element per unit of time is not immediately replaced. The apparent emptying of the effective pore space of an elastic rock (rigid grain skeleton and fractures) causes a change in pressure distribution in the volume element. When calculating stationary flow states, the petrophysical parameters of the effective pore space and the storage coefficient can generally be ignored.

The storage coefficient S in a water-saturated aquifer is defined as:

$$S = \Phi_{eff.} \cdot m \cdot \gamma \cdot [C_w + (C_{gest.} / \Phi_{eff.})]$$

$$S_{stationär} = konstant$$

$$S_s = S / m$$

S	= storage coefficient,	-
S_S	= specific storage coefficient,	m^{-1}
m	= thickness of aquifer,	m
γ	= specific weight ($\rho \cdot g$),	$Pa\ m^{-1}$
C_{gest}	= compressibility of grain skeleton,	Pa^{-1}
C_w	= compressibility of water,	Pa^{-1}
$\Phi_{eff.}$	= effective porosity,	-

In the case of stationary or quasi-stationary flow conditions, the amount of water extracted is introduced directly back to the volume element from "outside". The mass balance in the volume element itself is equalised. During the quasi-equilibrium flow state, the pressure distribution in the volume element does not change.

It is assumed from now on that the flow conditions in the defined volume element correspond to the flow conditions in the area of influence of a pressure sink. Geometrically speaking, the boundary of the pressure sink in the case of the ventilation test is the "outer" boundary which separates the hydraulic zone of influence of the test drift (characterised by change in porewater pressure) from the rock which has not been subject to hydraulic change (inner boundary of the pressure continuum). The influence of periodically recurring pressure fluctuations (e.g. earth tides, changes in atmospheric pressure; FLACH & NOELL, 1989) on

the flow conditions can generally be ignored in the case of long-term observations.

Within the pressure sink, the influence exerted by the pressure- and temperature-dependent elastic properties of the fluid and solid phase (**actual conditions**) on the pressure evolution in the water-saturated rock is small since both phases are relatively incompressible and there is no gas phase. In the zone of the pressure continuum, the decompression of the water and/or the compression (deformation) of the effective pore space balances out the removed water volume. In the area of the pressure continuum, it is guaranteed that the mass balance will be equalised by water being supplied from the ground surface ("free water table"). In this case, the water flow is dependent on the influence of gravity (infiltration rate through gravity flow; VOBORNY et al., 1991).

Table 5: Boundary conditions for the interpretation of water movement in the vicinity of the ventilation test drift.

Aquifer type	confined aquifer, water-saturated
Rock zone	rev (representativ elementary volume) - homogeneous - isotropic
Flow conditions	Darcy flow (laminar, equivalent-porous)
Flow state	Steady-state and quasi-stationary (flow rate, pressure, temperature and composition of water and rock = constant)
Driving force	- pressure gradient (pressure sink) - gravity (pressure continuum)
Extent of pressure sink	- << extent of aquifer and of pessure continuum - radial to test drift - influence of other sinks ignored
Boundary conditions for pressure sink	Pressure boundary condition
Boundary condition for pressure continuum	- flow boundary condition - atmospheric pressure - "free" water level - water supply from ground surface
Compressibility of water at 12.5 °C	approx. $4.7 \cdot 10^{-10}$ 1/Pa
Compressibility of crystalline rock	approx. $2 \cdot 10^{-11}$ 1/Pa

4.6.2 Evaluation procedure

The analytical calculation of groundwater flow is based on the **validity of Darcy flow and mass conservation.**

The relevant initial equation for describing non-stationary water movement through a volume element is a transport equation of the partial differential equation type. In a spatial cartesian coordinate system, it takes the general form (after DE MARSILY, 1986; LANGGUTH & VOIGT, 1980).

$$\frac{\partial^2 h}{\partial x^2} + \frac{\partial^2 h}{\partial y^2} + \frac{\partial^2 h}{\partial z^2} = \frac{S_s}{K} \cdot \frac{\partial h}{\partial t}$$

x,y,z	= cartesian coordinates,	m
h	= metres water column,	m
S_s	= specific storage coefficient,	m^{-1}
K	= hydraulic conductivity,	$m\ s^{-1}$
t	= time,	s

For the case of two-dimensional water flow being considered, transformation into a rotationally symmetric (radial) coordinate system results in the following equation

$$\frac{\partial^2 h}{\partial r^2} + \frac{1}{r} \cdot \frac{\partial h}{\partial r} = \frac{S}{T} \cdot \frac{\partial h}{\partial t}$$

r	= distance between measuring points,	m
S	= storage coefficient,	-
T	= transmissivity,	$m^2\ s^{-1}$

This is known as a fundamental or diffusivity equation, which can be used to derive the well-known equations for analytical calculation of groundwater flow for stationary

and non-stationary conditions (e.g. the well formula of THIEM, 1870; THEIS, 1935; COOPER & JACOB, 1946; JACOB & LOHMAN, 1952).

For stationary flow conditions, i.e. no temporal change in the mass balance in the volume element, the product of the right-hand side of the differential equation is equal to zero (LAPLACE equation).

$$\frac{\partial^2 h}{\partial x^2} + \frac{\partial^2 h}{\partial y^2} + \frac{\partial^2 h}{\partial z^2} = 0$$

or

$$\frac{d^2 h}{dr^2} + \frac{1}{r} \cdot \frac{dh}{dr} = 0$$

The well function of THEIS (1935) for non-stationary flow conditions and the so-called well formula of THIEM (1870) for stationary flow conditions are derived from the diffusivity equation. Both describe radial flow in the proximity of a well or a borehole.

The well formula of THIEM (1870) was used to calculate the **mean rock permeability (macropermeability) for the ventilation test.**

$$K \cdot m = q \,/\, 2\,\pi \cdot \ln (R2/R1) \,/\, (h2-h1)$$

q	= flow rate,	$m^3\ s^{-1}$
R	= distance of pressure measurement from test drift,	m
h	= hydraulic pressure in m water column,	m
m	= length/thickness of test zone,	m
K	= hydraulic conductivity,	$m\ s^{-1}$

This applies for quasi-stationary flow conditions in a confined aquifer and is effectively identical to the calculation method for the straight-line procedure (method II of the radial distance-drawdown procedure) of COOPER & JACOB (1946) which is used for non-stationary flow conditions in a confined aquifer.

Calculations for both non-stationary and stationary flow conditions were included when determining mean permeability from hydraulic **borehole measurements**. The hydrotest and evaluation procedures are outlined in Table 6.

Table 6: Hydrotest and evaluation procedures for hydraulic borehole investigations.

Test procedure	Flow boundary conditions	Evaluation
a) Pulse Test Pressure increase/decrease	non-stationary	- type-curve-matching
b) Constant Head (QCH) Injection test	non-stationary	- straight-line procedure (JACOB & LOHMAN, 1952)
	stationary	- straight-line procedure (DUPUIT, 1863; THIEM, 1906; MOYE, 1967)
c) Constant Flow (QCF) Injection test	non-stationary	- straight-line procedure (COOPER & JACOB, 1946)
	stationary	- straight-line procedure (DUPUIT, 1863; THIEM, 1906; MOYE, 1967)
d) Pressure build up (PR)	transient/ non-stationary	- (HORNER, 1951)

When evaluating constant head injection tests (QCH) according to JACOB & LOHMAN (1952), time is plotted semilogarithmically against the quotient of pressure difference and flow rate. The gradient of the straight-line section of curve, "semilog straight line", is inversely proportional to the transmissivity. "Skin and boundary effects" are ignored in this approach.

In the constant flow tests (QCF), the flow rate is kept constant and the change in pressure is measured as a function of time. For non-stationary flow boundary conditions, these tests were evaluated using the approach of COOPER & JACOB (1946).

For stationary flow boundary conditions, the constant head and constant flow tests were evaluated using the methods of THIEM (1906), DUPUIT (1863) and MOYE (1967). However, experience has shown that, over the relatively short experimental durations of several hours, stationary flow conditions were not actually reached in the measurement interval.

The pressure recovery (PR) test period (not influenced by secondary effects) which follows the QCH and QCF tests was evaluated using the method of HORNER (1951).

The hydraulic communication between matrix and shear zone areas was determined during long-term injection tests (interference tests). The pressure response in selected test intervals in the proximity of an injection borehole was measured.

The pulse tests which were carried out did not provide any meaningful results. They were not taken into consideration when determining the mean rock permeability.

For water, the DARCY equation represents the theoretical basis for **evaluating permeability studies carried out on drillcore samples** in the laboratory. For investigations performed using gas as the flowing phase, the extended equation for compressible phases applies.

$$k_{gas} = \frac{2\, q\, \mu\, L\, p_0}{A\,(p_1^2 - p_2^2)}$$

k_{gas}	= gas permeability,	m^2
q	= flow rate,	$m^3\ s^{-1}$
μ	= viscosity,	$Pa \cdot s$
L	= core length,	m
A	= core cross-section,	m^2
p_0	= atmospheric pressure,	Pa
p_1	= injection pressure,	Pa
p_2	= pressure at core end,	Pa

Slip flow effects are accounted for by the KLINKENBERG correction.

$$k = \frac{k_{gas}}{1 + b\ /\ p}$$

k	= corrected gas permeability,	m^2
b	= Klinkenberg constant,	Pa
p	= mean pressure,	Pa

The effective porosity, which is a measure of the hydraulically active pore space of the rock, is also given.

$$\Phi_{eff.} = \frac{V_{por}}{V_{tot}}$$

$\Phi_{eff.}$	= effective porosity,	$m^3\ m^{-3}$
V_{por}	= volume of effective pore space,	m^3
V_{tot}	= total volume,	m^3

4.6.3 Results of the in situ permeability calculations

Calculation of the transmissivity and the associated hydraulic conductivities for the region of the ventilation test drift was based on the pressure gradient between measurement intervals P12 (BOVE 84.011) and P28 (BOVE 84.018) from the shear zone area (L465 to L478 m) and a measured water flow rate in the drift of 1.6 l/h. Fig. 22 shows the correlation between the hydraulic conductivity and the length of the hydraulically active test intervals.

The transmissivity of a disk of rock with a uniform thickness of one metre (transmissivity equal to permeability) is thus less than $2 \cdot 10^{-9}$ m^2/s, corresponding to $2 \cdot 10^{-16}$ m^2.

If structural geological features, such as shear zones and lamprophyres are ignored, then a mean rock permeability (macropermeability) of less than $8 \cdot 10^{-18}$ m^2 results for the total length of the forward measuring chamber of 27 m.

If a 10 m-thick shear zone is taken into account as the hydraulically dominant structure with a flow rate of 1.1 l/h, the shear zone has a permeability of less than $2 \cdot 10^{-17}$ m^2. With a flow rate of 0.4 l/h, the permeability of the matrix zones in the forward chamber is below $3 \cdot 10^{-18}$ m^2.

With measured flow rates of 0.35 and 0.7 l/h, the mean rock permeability (macropermeability) of the rear chamber is around 10^{-18} m^2.

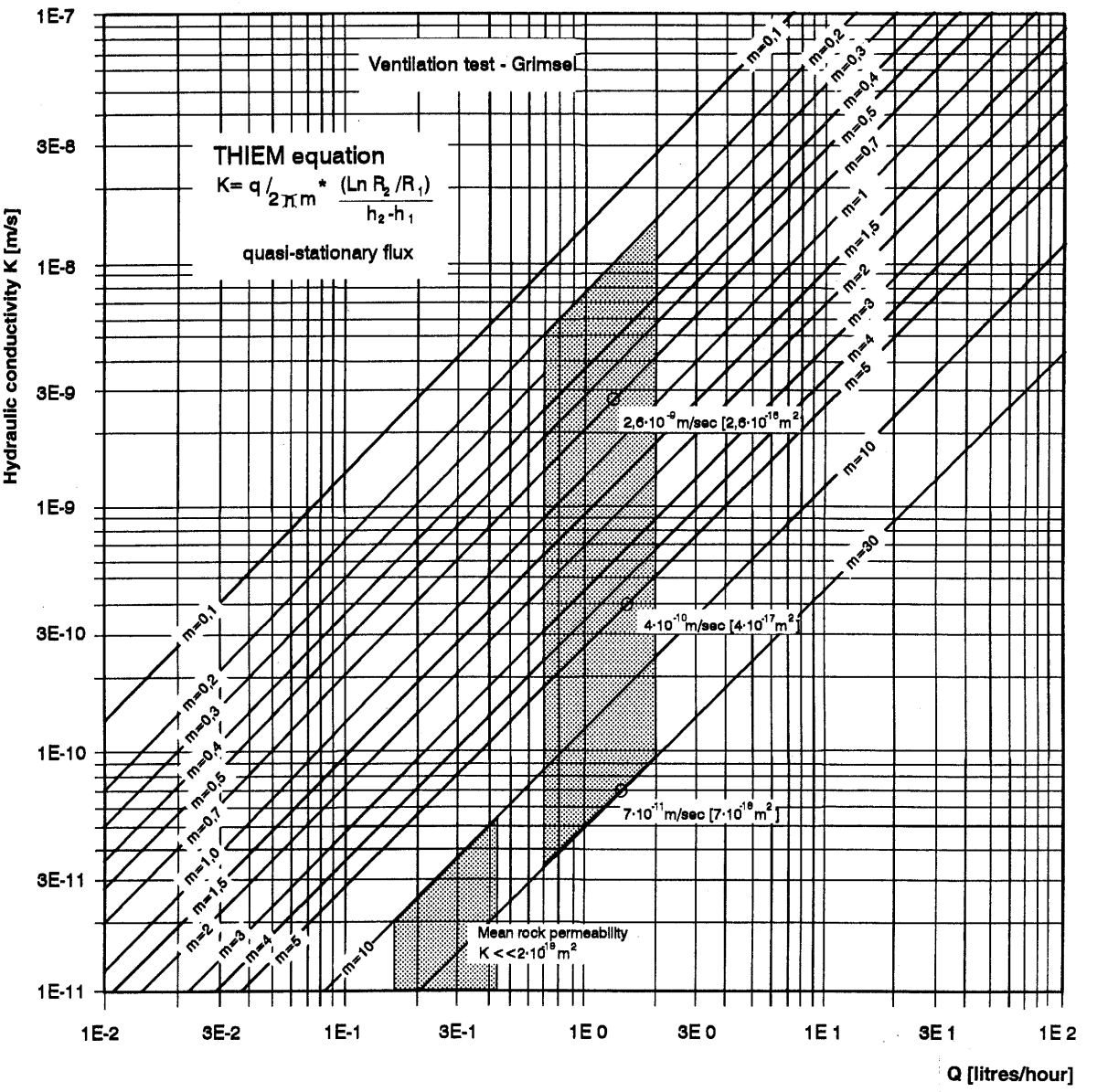

Fig. 22: Logarithmic representation of analytically determined mean hydraulic conductivities in the region of the ventilation test drift.

Hydraulic investigations (hydrotests) were carried out in boreholes BOVE 88.002, 88.003, 88.004 and SB 88.005 and the results are summarised in Fig. 23. The transmissivity (T) and storage coefficient (S) were determined for individual borehole measurement intervals. The hydraulic conductivities were then calculated from the transmissivity value and the length of the measurement interval. The areas targeted with the hydrotests were the less textured matrix zones and the intensively structured region of the shear zone (cf. chapter 3.3). The initial interval pressure (p_i) was determined from the pressure recovery curve after the tests had been completed. The hydraulic communication between different rock zones was determined from pressure resonances observed during the hydrotests (pseudo-interference tests).

The tested measurement intervals are divided into shear zone and matrix areas.

Depending on the evaluation procedure used, the individually calculated transmissivity values vary by an order of magnitude. Generally speaking, the transmissivities (from the constant head and constant flow tests) are smaller for non-stationary flow boundary conditions than for stationary conditions. There is a relatively good agreement between the results for the transmissivities calculated for non-stationary flow boundary conditions and the HORNER analysis.

The macropermeability (mean permeability) is between $7 \cdot 10^{-18}$ and $4 \cdot 10^{-17}$ m^2 for the shear zone and between $2 \cdot 10^{-19}$ and $2 \cdot 10^{-17}$ m^2 for the matrix. This information is based on the results for the non-stationary evaluation. According to these results, the mean hydraulic conductivity (macropermeability) for the shear zone can generally be assumed to be a factor of four higher than that for the matrix zones.

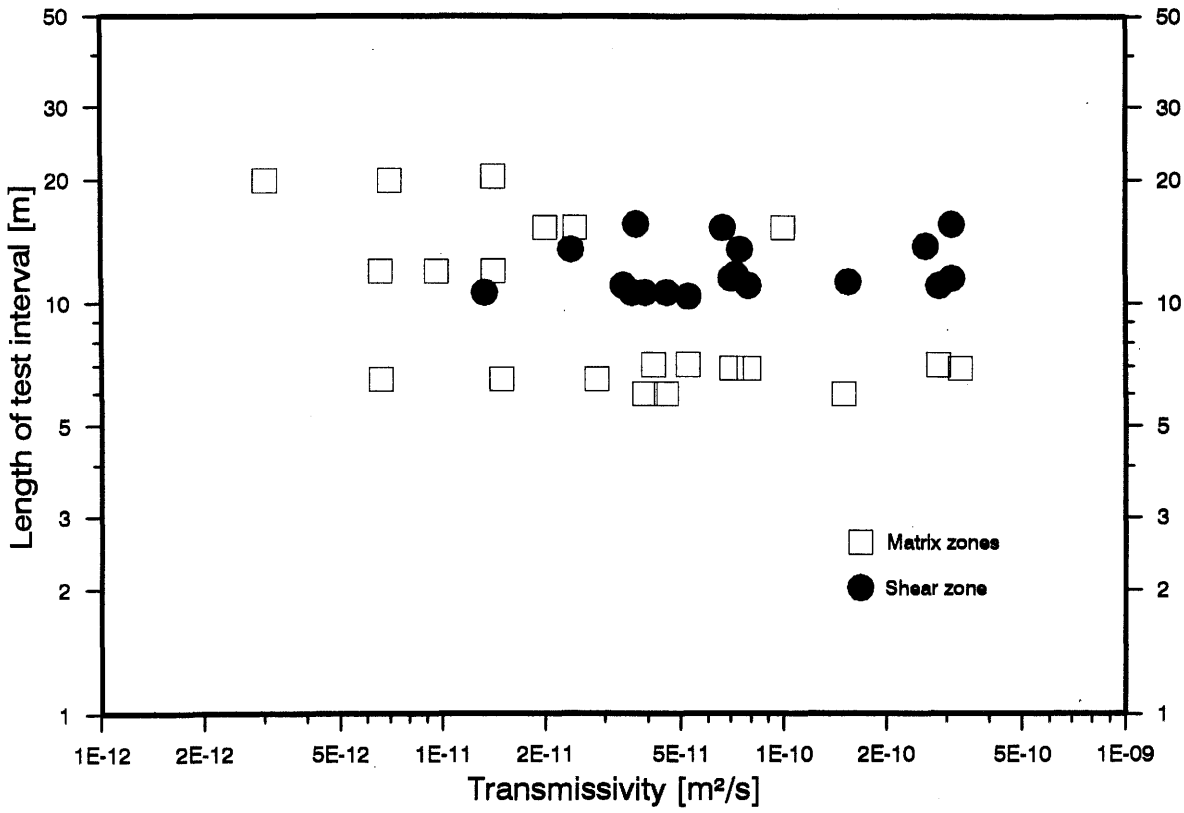

Fig. 23: Results of the hydrotests. The Figure shows the transmissivities determined for the matrix and shear zone areas as a function of the length of the test intervals (after HEINIGER, 1989).

According to HEINIGER (1989), the value calculated for the specific storage coefficient is influenced to a large extent by the test procedure, the flow boundary conditions and the structural geology of the test zone (e.g. open fractures). These factors should be taken into consideration when evaluating the orders of magnitude given for the specific storage coefficients for the shear zone ($3 \cdot 10^{-7} < Ss < 1 \cdot 10^{-3}$) and for the matrix ($1 \cdot 10^{-6} < Ss < 4 \cdot 10^{-4}$).

The pore water pressures measured in the borehole test intervals over a period of several months prior to the hydrotests, correlate well with the initial porewater pressures

derived according to HORNER (1951). As pressure observations in the parallel boreholes show (cf. chapter 4.4.2), quasi-stationary pressure conditions prevail in the pressure sink of the ventilation test drift. An approximation between the pore water pressures and the hydrostatic pressure of 4 MPa expected for this depth range was not detected.

The tests which generated a pressure response in a test interval of another borehole are listed in Table 7 (see also VOMVORIS & FRIEG, 1992).

Clear pressure responses between neighbouring boreholes were observed in the area of the shear zone, while pressure resonances between the test intervals of the matrix zones are very weakly expressed. One exception to this is a marked pressure response in the matrix zone between the two test intervals 5.3 (SB 80.005) and 3.3 (BOVE 88.003); this can be explained by the presence of a direct connection (open fracture). That intervals 5.3 and 3.3 are connected by a fracture is also confirmed by the measured pressure difference between the test intervals of 57 kPa, which corresponds exactly to the height difference of the test intervals of 5.7 m.

Table 7: Pressure resonances during hydrotesting (after HEINIGER, 1989).

Test interval	Test	Responding intervals	Pressure response dP [kPa]	Comments
2.1	QCH 2.1	-		
2.2	QCH 2.2	2.1	5.8	
2.3	QCH 2.3	2.1	2.5	
		2.2	5.3	
3.2	QCH 3.2	3.3	13.1	
		5.3	13.7	
		5.4	70.4	
3.3	QCH 3.3	5.3	1217.0	dP Interval 3.3 -> 5.3 = 56 k
Pa = 5.7 m				
4.1	QCH 4.1	-		
4.2	QCH 4.2	4.3	58.7	
4.3	QCH 4.31	4.2	24.1	
4.3	QCH 4.32	4.2	256.7	
		2.2	50.3	
		3.2	12.0	
5.1	QCH 5.1	-		
5.2	QCH 5.2	-		
5.3	QCH 5.3	3.3	1780.0	dP Interval 5.3 -> 3.3 = 46 kPa = 4.6 m
5.4	QCH 5.4	3.2	35.0	

4.6.4 Results of petrophysical laboratory investigations

Laboratory tests were carried out on 20 selected core samples from boreholes BOVE 84.011 and SB 83.001 in order to determine the matrix permeability and the effective porosity of the granodioritic gneisses and the lamprophyre. The results of the permeability tests, which were carried out using nitrogen, and the values for effective porosity and specific surface are presented in Table 8.

Without more detailed explanation, Table 8 also includes values for the rock conductivity, the formation factor and the conductivity of the formation water in the rocks under investigation.

Table 8: Results of petrophysical laboratory investigations.

Rock type	Grimsel Granodiorite	Lamprophyre
Mineral composition	Microcline/orthoclase Albite	Muscovite/biotite Quartz
(Principal components)	Muscovite/biotite Quartz	Epidot
Rock permeability for gas (m^2)	10^{-18} - 10^{-19}	10^{-19} - 10^{-20}
Porosity (%)	0.2 to 1.4	-
Density (g/cm^3)	2.706 ± 0.005	-
Specific surface(m^2/g)	0.05 ± 0.03	0.12 ± 0.01
Interface conductivity (S/m)	$1.5 \cdot 10^{-4}$	6 to 11 $\cdot 10^{-4}$
Formation factor (-)	200 < F < 650	
Conductivity of formation water (S/m)	ca. $1.1*10^{-2}$	

The permeability values determined using gas for the granodioritic gneisses are in the microdarcy range and lower, and are comparable with hydraulic conductivities between 10^{-18} and 10^{-19} m^2. High ambient pressures, which were simulated in the laboratory with mantle pressures of 19 MPa, generally reduce the rock permeabilities by a factor of 2.

The permeability values for the shear zone and the matrix zones vary in the same order of magnitude.

The permeability values for the lamprophyre are between 0.1 and 0.01 microdarcys, corresponding to hydraulic conductivities of 10^{-19} to 10^{-20} m^2. With high ambient pressures, there were isolated cases where the values measured were around two orders of magnitude lower.

The effective porosity of the granodioritic gneisses is generally between 0.2 and 1.4%.

The mean matrix density of the rocks is 2.706 g/cm^3.

With a value of 0.05 m^2/g, the specific surface of the Grimsel Granodiorite is significantly lower than that of the lamprophyre, which has a value of 0.12 m^2/g.

4.6.5 Overview of the results of the permeability calculations

The calculated (analytically) and weighted mean permeabilities (macropermeability) for the in situ ventilation test and the hydrotests show a good agreement.

The weighting applies in the first instance to the flow boundary conditions on which the evaluation procedure is based, and to the structural geology of the rock being investigated.

An equivalent porous medium was assumed for the flow model.

The shear zone does not differ significantly from the matrix in terms of calculated transmissivities and permeabilities. However, geological mapping of drill cores did indicate that there would be a significant difference.

Fig. 18 shows the formation pressures following pressure build-up as a function of radial distance between tunnel axis and measurement interval. A distinction was also drawn between shear zone and matrix intervals. In this representation, a logarithmic increase in pressure with increasing radial distance was expected. However, Fig. 18 shows that the increase appears rather to be linear. There are two possible explanations for this behaviour, which was also observed in other sections of the drift:

1) The rock in the near-drift zone is strongly inhomogeneous and anisotropic.

2) The presence of an unsaturated zone is simultaneously increasing the hydraulic gradients in the near-drift rock zone and lowering the formation water pressures.

5 MAPPING OF HOMOGENEOUS ZONES

The formation water in the saturated crystalline rock moves in zones which are classified as homogeneous matrix and in fracture systems (brittle structures). When considering a reduced section of rock, a further geometric differentiation of these water-bearing zones can often be made.

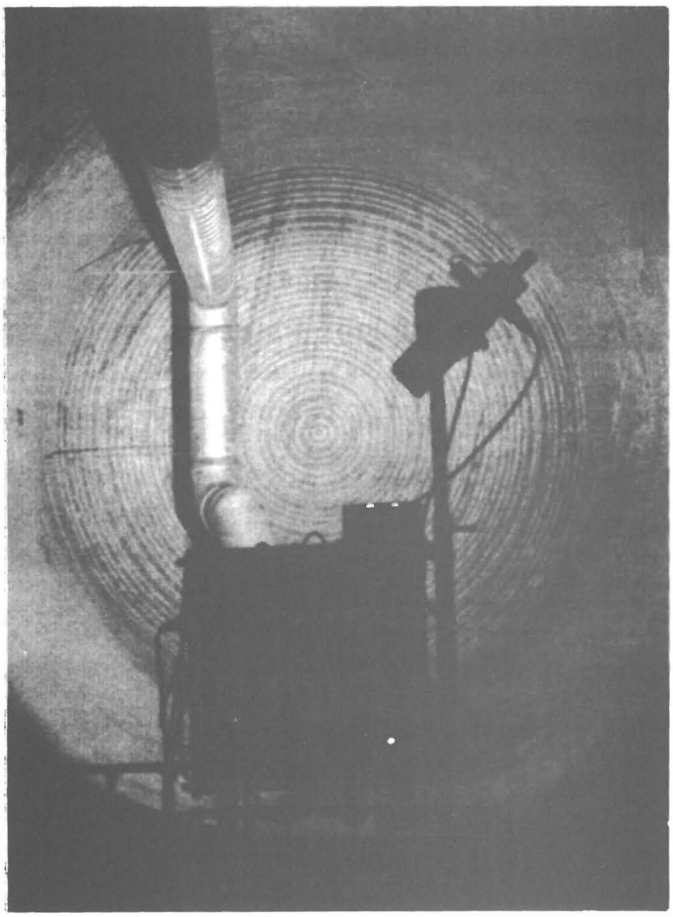

Fig. 24: Non-contact temperature measurements for identifying water-bearing zones. Photograph from rear chamber.

Given the same hydraulic boundary conditions (same pressure gradient) and the same structural geology, the explanation for differences in water flow in the matrix zones is

generally a change in the rock permeability. Compared with the effect which a water-bearing fracture system has on flow conditions, permeability changes of this type are not important for hydraulic characterisation of the homogeneous matrix zone as long as there is no disturbance of its large-scale hydraulic properties.

Isolated local fluctuations in matrix permeability can be identified in the drift from changes in surface temperatures (BRASSER & KULL, 1988a, c; 1989). A drop in temperature can generally be explained by cooling following evaporation at the drift surface. At fractures and other water-bearing brittle deformations in the drift, the lower temperature of the formation water, compared with the ambient temperature, causes a drop in surface temperature.

Measuring the temperature distribution at the drift surface allowed anomalies in the matrix zones and individual water-bearing structures to be identified; this makes it possible to delimit homogeneous rock zones.

5.1 Thermographic investigations in the ventilation test drift

In the ventilation test drift, surface temperature measurements were carried out in sections 450 to 475 m and 481 to 515 m.

During the ventilation phases, temperature distribution at the drift wall was measured using an infrared radiation thermometer (type HEIMANN KT4; Fig. 25). The aim of the measurements was to map temperature anomalies and to compare these results with structural geology mapping and with zones which are known to be hydraulically active. In a drift which is ventilated, only the larger water inflow points can be detected; smaller influx volumes tend to evaporate at the drift surface.

In both chambers of the ventilation drift, each measurement campaign consisted of eight temperature profiles with an

angular spacing of 45° which were recorded at the drift surface. The surface temperature distribution is presented by correlating the measured surface temperatures in isotherm charts.

In addition to this, surface temperature mapping was carried out in the rear chamber using a mobile line scanner equipped with a mercury-cadmium-telluride (HgCdTe) detector. Correlating the different segments together (the recording angle of the line scanner is 77°) allows accurate surface mapping of the water inflow points.

The design of the ventilation system and the air circulation in the measuring chambers causes a temperature stratification both parallel and perpendicular to the drift axis. This has a particularly marked influence on the surface temperature distribution in the vicinity of the air inlet and the floor of the two chambers. Taken over the whole chamber, temperature differences of up to 5°C are generated at the tunnel surface as a result of ventilation temperatures.

The influence of the temperature stratification is negligible since wet zones are distinguished from non-wet zones by significant temperature differences.

Without ventilation in the chambers, the temperature distribution at the drift surface more or less balances out and the temperature gradient between rock and air is close to zero. It is also impossible to detect relative temperature differences for these heat flux conditions.

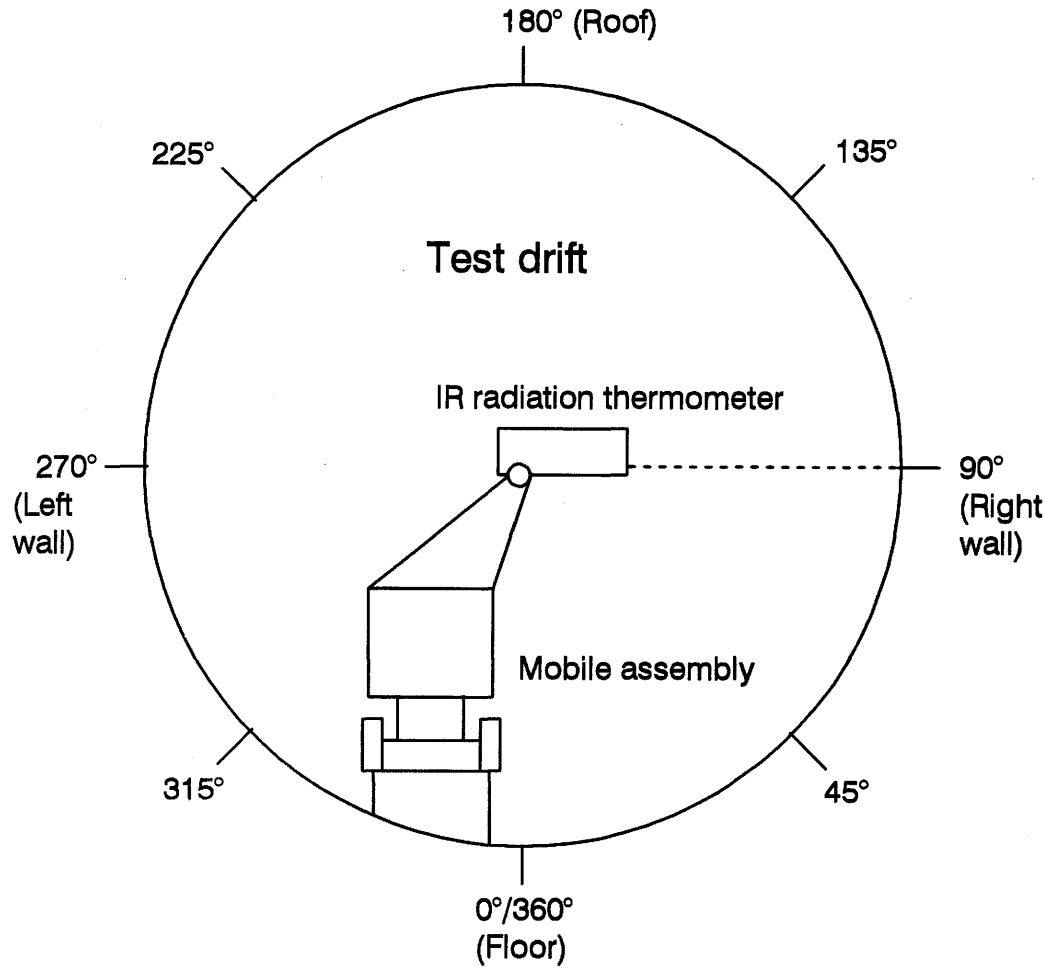

Fig. 25: Schematic test configuration for temperature mapping in the ventilation drift.

The rock in the rear chamber has a clearer parallel texture. Between L493 and L495 m and L500 and L504 m, disturbed lamprophyres pass through the rock. However, compared with the forward chamber, the rear chamber has relatively little structuring, with few drip points and low water flow. Without ventilation, the entire drift surface has an even temperature of 12.5°C.

5.2 Thermography technique

Non-contact measurement of surface temperatures is based on the radiation properties of a body. According to PLANCK'S law, the emitted radiation density is a function of the temperature of a body and this parameter can therefore be used indirectly to determine surface temperature. The concept of surface temperature is used because radiation density is proportional to the temperature at the surface of a body and not to the temperature distribution within the body itself.

The total radiation density of a body is made up of emission, transmission and reflection components.

$$E_{ges.} = E_E + E_T + E_R$$

E_E	= emission,	-
E_T	= transmission,	-
E_R	= reflection,	-

The following physical relationship applies for calculating the emitted radiation density:

$$\rho_{(\lambda,T)} d\lambda = (4\pi h\lambda^3 / c^3) \cdot (1 / (\exp(h\lambda/kT) - 1))\ d\lambda$$

ρ	= emitted radiation density,	$W\ m^{-1}$
λ	= frequency,	s^{-1}
h	= Planck's constant,	$J\ s$
k	= Boltzmann constant,	$J\ K^{-1}$
T	= temperature,	K
c	= velocity of light ,	$m\ s^{-1}$

In technical applications, the total emitted radiation intensity [W/m^2] is measured in a specified wavelength range

of 8 to 12 µm. For this purpose, the rock is assigned the radiation properties of a "black body".

The transmission and reflection radiation components and the influence of adsorption on the measurement results are ignored in the investigations carried out in the drift.

The radiation density is measured using detectors and is converted into surface temperatures. The equipment is calibrated via reference measurements on a body with a known surface temperature which has radiation characteristics corresponding to those of an "ideal black body".

5.2.1 Water flow paths in the ventilation test drift

The isotherm maps for the forward and rear chambers show "relative" temperature anomalies which were measured during the ventilation phases in the area of the shear zone (from L465 to L475 m) and at the lamprophyres (L492 to L496 m and L499 to L503 m); these correlate with water flow paths in the rock.

The **area of the shear zone** is characterised by marked cleavage and can be distinguished from the surrounding zone, which has less cleavage, by a clear jump in temperature.

The area with the (relatively) largest drop in temperature is located between L465 and L466.5 m. Depending on ventilation temperature, this relative drop can be up to 5°C. The negative temperature anomaly takes the form of a continuous radial band approximately one metre wide in the drift. The surface temperature also drops between L466 and L475 m. In this case, however, the drop in temperature is confined to individual decimetre-size zones ("cold spots") which are only partly interlinked. The relative drop in temperature in the vicinity of these anomalies is smaller than that in the neighbouring zone at L465 m (Fig. 26).

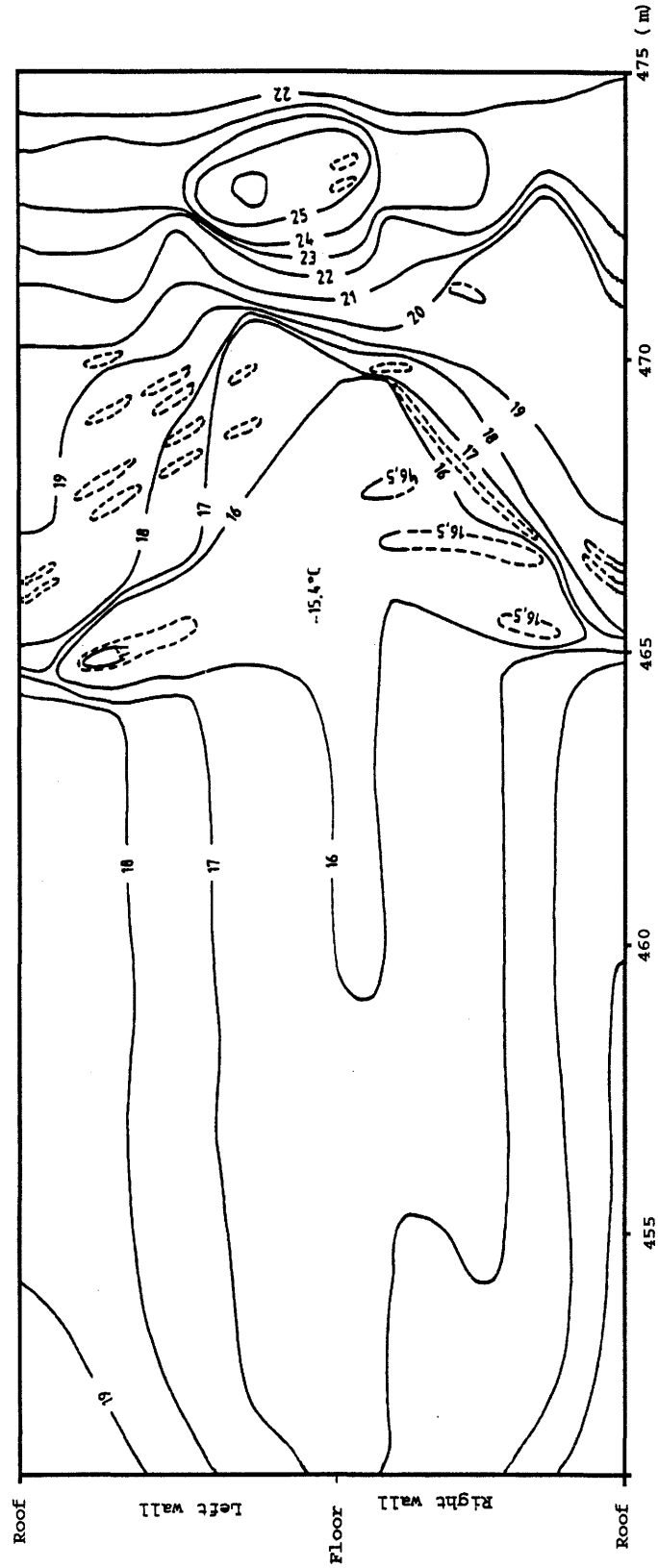

Fig. 26: Isotherm map (°C) for the forward chamber with an air temperature of approx. 17°C.

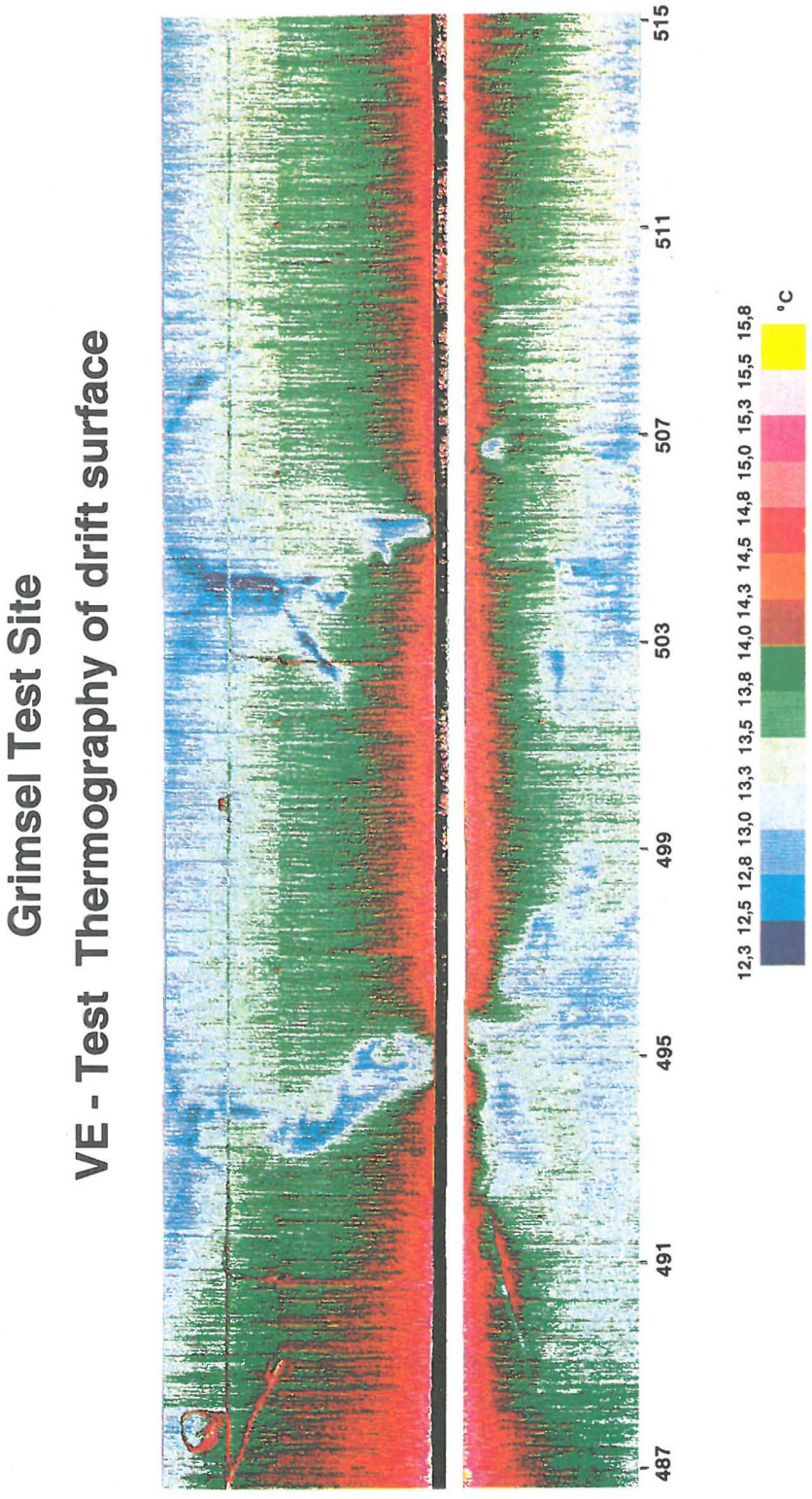

Fig. 27: Temperature distribution in the rear chamber. In the blue zones water is evaporating from the drift surface.

Within the shear zone, which is relatively cool, increasing air temperatures cause so-called "hot spots" to form; on the long-term these link up to form zones of equal temperature. These zones have surface temperatures similar to those of the matrix zones and are less permeable than the "cold spots".

Higher ventilation temperatures cause the negative temperature anomalies to break down until the temperature distribution at the drift surface is more or less completely homogeneous. Only the horizontal and vertical temperature stratification remains. This process also affects the area between L465 and L466.5 m where, with the exception of a few cold spots, no relative temperature differences remain.

The reason for the general evening out of temperature at the drift surface can be sought in the drying-out process occurring in the near-drift rock zone. The large volume of evaporation caused by high ventilation temperatures has the effect of gradually moving, that evaporation points away from the drift surface and into the rock itself. There is also a simultaneous equalisation between the air temperature and the temperature at the drift surface.

The negative temperature anomalies in the area of the shear zone, which could still be detected even with relatively high ventilation temperatures, can be considered as zones of enhanced permeability. Since these anomalies are locally restricted and not interconnected, it must be assumed that the permeability within the approximately ten metre-thick shear zone is locally higher than indicated by the hydraulic investigations. One possible explanation is that the rock drains via the shear zone and that, within the shear zone, water moves preferentially in individual zones which are particularly permeable. The calculation of the shear zone transmissivity has to take into account the extent of the temperature anomalies, particularly in the vicinity of L466 m. The extent of these zones is around one tenth of the true extent of the shear zone.

The rear chamber of the ventilation drift shows considerably more cleavage than the forward chamber; the isotherm charts for the rear chamber show negative temperature

anomalies almost exclusively in the vicinity of lamprophyres which are disturbed by fractures. The water fluxes in the lamprophyres and at the interfaces with the granodiorite can still be detected even at relatively high ventilation temperatures (Fig. 27).

The "relative" temperature anomalies at L493 m were recorded at high air temperatures and indicate that the rock drains along interfaces. Such interfaces can result from stress changes in the contact zones between materials with different elastic properties.

As in the case of the shear zone, the stringing together of the "cold spots" implies the existence of preferential water flow paths; these are restricted to the lamprophyre interfaces. No "cold spots" were detected in zones with very marked cleavage which are penetrated by brittle structures and are adjacent to the lamprophyres.

The lamprophyres at L461 m and the areas of the tension joints at L490 m, L505 m and L515 m, with their contact zones, show no notable temperature differences. The water flow in these structures can therefore be defined as low.

5.2.2 Matrix zones

In the low-cleavage zones of the ventilation test drift from L445 to L465 m, and in the average to strongly textured zones of the rear chamber (L481 to L521 m), a homogeneous temperature distribution is set up after short ventilation times.

Negative "relative" temperature anomalies ("cold spots") occur only at the beginning of the ventilation process, and only in isolated cases. They are generally associated with brittle deformations, e.g. the S2/S3 fracture at L454 m. The changes in temperature associated with the brittle deformation structures are short-term phenomena caused by the fracture running dry or by the neighbouring rock zones

draining via the fracture (dependent on the extent of drying-out of the drift region).

Large temperature differences at the drift surface which indicate inhomogeneities other than those mentioned above were not detected by line scanning. The sections of the ventilation drift which are considered to be homogeneous matrix zones are more readily identified on the basis of temperature distribution at the drift surface than by their cleavage intensity.

5.3 Summary of thermographic investigations

The thermographic temperature mapping of the drift surface confirmed the existence of the previously mentioned temperature anomalies and - at least from the point of view of temperature distribution - of the large-scale homogeneous zones in the rear chamber (Fig. 27).

The boundary zone between the compact granodiorite and the mylonitized shear zone is clearly indicated by low drift surface temperatures (Fig. 25). At some locations within these negative temperature anomalies, so-called "cold and hot spots" can be recognized. Their existence is dependent on the ventilation temperature and they indicate preferential water flow and areas of reduced water flow respectively. Negative temperature anomalies can also be identified in areas of the apparently compact granodiorite.

The ventilation process also revealed negative temperature anomalies in the contact zone of the lamprophyres; as observed in the forward chamber, continuous ventilation causes these anomalies to shrink and form so-called "cold spots". The temperature anomalies form radial bands at L494 and L502 m. The majority of the drift surface does, however, show a homogeneous temperature distribution during the different ventilation phases.

6 HYDRAULIC MODELLING OF THE VENTILATION TEST

During the course of the ventilation test, the methodology for interpreting a macropermeability test using models was further developed using the ECLIPSE/ECL program with a 3-D block model (BREWITZ et al., 1988; KULL et al., 1989).

A dual porosity system was assumed for modelling flow in the microfractured Grimsel crystalline.

The numerical model calculations used to analyse the flow regime were based on in situ results for a near-drift and an extended 3-D block model. The models were calibrated using the in situ measurement results.

In the near-drift model, the simulation calculations are dominated by the hydraulic activity of the shear zone. In the extended 3-D block model, the emphasis is on the influence of additional pressure sinks on the pressure distribution in the region of the ventilation test drift.

The plausibility and applicability of the hydraulic model evolved was tested by predictive calculation.

The ECLIPSE program and its mathematical solution algorithm were verified via comparison calculations for case example 2 of the HYDROCOIN project (GUNDFELT, 1985).

6.1 Theoretical basis of the ECLIPSE program

The ECLIPSE/INTERA/ECL program is a finite difference program for numerical simulation of multiphase flow in a dual porosity system.

The starting equation for the mathematical description of water flow in the fracture matrix system of the 3-D block model is the general diffusivity equation (cf. chapter 4.6.1).

The equation is derived from the continuity and DARCY equations and describes water flow through a porous medium (cf. MATTHEWS & RUSSEL, 1967); it takes the form of a partial parabolic 2nd order differential equation. The source terms (q_{mk}) and (q_e) on the left side of the equation describe the flow rate normalised to a defined block volume.

$$\frac{\partial}{\partial x}\left(\frac{k_x}{\mu_w \cdot B_w}\cdot\frac{\partial p}{\partial x}\right)+\frac{\partial}{\partial y}\left(\frac{k_y}{\mu_w \cdot B_w}\cdot\frac{\partial p}{\partial y}\right)+\frac{\partial}{\partial z}\left(\frac{k_z}{\mu_w \cdot B_w}\cdot\frac{\partial p}{\partial z}\right)-q_{mk}-q_e = \frac{\partial}{\partial t}\left(\frac{\Phi}{B_w}\right)$$

q_{mk}	= source term (fracture-matrix-block),	s^{-1}
q_e	= source term (removal block),	s^{-1}
k	= permeability,	m^2
Φ	= porosity,	-
μ_w	= viscosity,	Pa·s
B_w	= formation volume factor,	-
p	= pressure,	Pa

Indices

x,y,z	= cartesian coordinates,	-
mk	= matrix-fracture,	-
e	= removal,	-
w	= water,	-

A matrix-fracture-block of the 3-D block model consists of a fracture system and a matrix system (Fig. 28).

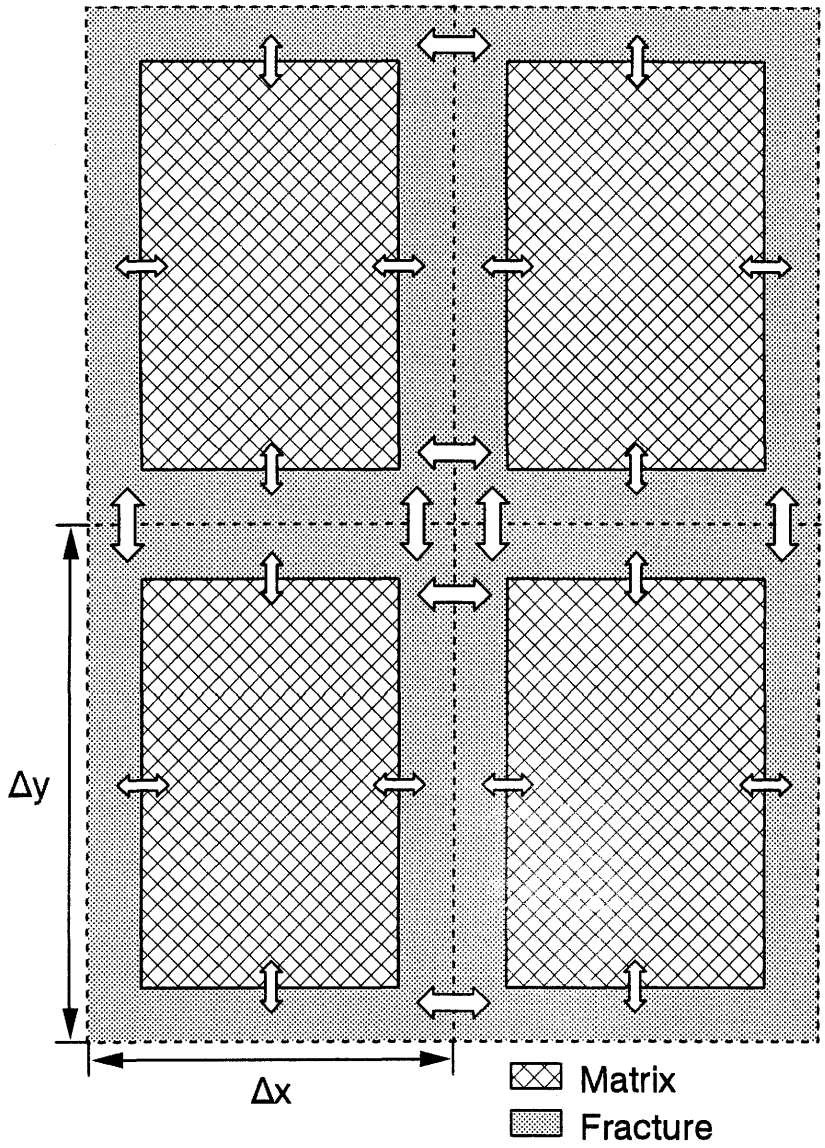

Fig. 28: Conceptual model of fluid exchange between matrix and fracture as simulated by ECLIPSE.

In a cartesian coordinate system, the flow equation for linear flow in the x-direction in a regular matrix-fracture block [i] at time [n+1] without material removal (q_e) is:

$$\frac{\left(\frac{k_x}{\mu_w \cdot B_w}\right)^n_{i-1/2} \cdot \left(\frac{p_{i-1}-p_i}{\Delta x_{i-1/2}}\right)^{n+1} - \left(\frac{k_x}{\mu_w \cdot B_w}\right)^n_{i+1/2} \cdot \left(\frac{p_i-p_{i+1}}{\Delta x_{i+1/2}}\right)^{n+1}}{x_i} = \frac{1}{\Delta t}\left[\left\{\frac{\phi}{B_w}\right\}^{n+1} - \left\{\frac{\phi}{B_w}\right\}^n\right]$$

In the case of a drop in pressure in the **fracture system**, the differential equation also describes **material flow** from block [i] into the neighbouring blocks [i+1] and [i-1] between times [n] and [n+1]. In the mass balance for the time step being considered [(n+1)-n], the outflow volume from the fracture system of block [i] (flow term and influx from the matrix) is equal to the fluid and rock expansion of the fracture-matrix block. The differential equation is extended if the cross-sectional surface ($\delta y \cdot \delta z$) of the fracture-matrix block being considered deviates from the cross-sectional surfaces of the neighbouring blocks.

$$T^{n}_{x,i-1/2}(p_{i-1}-p_i)^{n+1}-T^{n}_{x,i+1/2}(p_i-p_{i+1})^{n+1}+q_{mk}=\frac{\Delta x_i \Delta y_i \Delta z_i}{\Delta t}\left[\left\{\frac{\phi}{B_w}\right\}^{n+1}-\left\{\frac{\phi}{B_w}\right\}^{n}\right]$$

T = transmissibility, $m^3\ Pa^{-1}\ s^{-1}$

Indices

i = block number, -
n = time step, -

Different sizes of matrix-fracture blocks can be modelled using block-specific transmissibilities.

$$T_{x,i-1/2} = \left\{\frac{\Delta y \cdot \Delta z}{\Delta x}\right\}_{i-1} \cdot \frac{k_x}{\mu_w \cdot B_w}$$

The pressure-dependent fluid properties (μ_w), (B_w) and the porosity (Φ) are extrapolated to time [n+1] using the NEWTON-RAPHSON method.

$$\mu_w^{n+1} = \mu_w^n + \frac{\partial \mu_w}{\partial p} \cdot (p^{n+1} - p^n)$$

The flow from matrix to fracture system in block [i] is described by the equation

$$q_{mk} = T_{mk}(p_k - p_m)^{n+1} = \frac{V_m}{\Delta t} \cdot \left[\left\{ \frac{\phi_m}{B_w} \right\}^{n+1} - \left\{ \frac{\phi_m}{B_w} \right\}^{n} \right]$$

T	= block transmissibility,	$m^3\ s^{-1}$
p_k	= pressure in the fracture,	Pa
p_m	= pressure in the matrix,	Pa
Φ	= porosity,	-

Indices

k	= fracture,	-
m	= matrix,	-

This flow equation, which contains the two unknown pressures p_m and p_k at time [n+1] in the left term and ($p_m^{n+1} - p_m^n$)-dependent parameters in the right term, is solved simultaneously with the flow equation in the fracture system.

While the transmissibility in the fracture system T_k is dependent on the cross-section of the neighbouring fracture systems, T_{mk} is determined by the geometry of the block. In the 3-D block model, the cuboid form selected for the matrix blocks (L_x, L_y, L_z = side lengths in metres) with rock volume (V)

$$V = L_x \cdot L_y \cdot L_z$$

leads to a dynamic matrix-fracture transmissibility.

$$T_{mk} = T_{c_{mk}} \cdot \frac{1}{\mu_w \cdot B_w}$$

T_{cmk} = specific block transmissibility, m^3

The specific block transmissibility [T_{cmk}], which describes material flux between the matrix and fracture system, is constant within a block. The material flux in the x-, y- and z-direction is always via two sides (A_{xy}, A_{xz}, A_{yz}) of the matrix block. The direction-dependent specific block transmissibilities (T_{cmk})

$$T_{x_{c_{mk}}} = 2 \cdot \frac{A \cdot k_x}{L_x/2} = 4 \cdot L_y \cdot L_z \cdot \frac{k_x}{L_x}$$

$$T_{y_{c_{mk}}} = 2 \cdot \frac{A \cdot k_y}{L_y/2} = 4 \cdot L_x \cdot L_z \cdot \frac{k_y}{L_y}$$

$$T_{z_{c_{mk}}} = 2 \cdot \frac{A \cdot k_z}{L_z/2} = 4 \cdot L_x \cdot L_y \cdot \frac{k_z}{L_z}$$

give the total matrix-fracture transmissibility of the model block.

$$T_{c_{mk}} = 4 \cdot \left\{ \frac{k_x \cdot L_y \cdot L_z}{L_x} + \frac{k_y \cdot L_x \cdot L_z}{L_y} + \frac{k_z \cdot L_x \cdot L_y}{L_z} \right\}$$

If the rock volume (V_m) of the matrix block is included, this results in

$$T_{c_{mk}} = 4 \cdot L_x \cdot L_y \cdot L_z \left\{ \frac{k_x}{L_x^{\,2}} + \frac{k_y}{L_y^{\,2}} + \frac{k_z}{L_z^{\,2}} \right\}$$

The influence of the matrix geometry on the fluid exchange between the matrix and the fracture system is described by the matrix geometry factor (σ). If a constant permeability (k) is assumed in the matrix block, the matrix geometry factor can be estimated.

$$\sigma = 4 \cdot \left\{ \frac{1}{L_x^2} + \frac{1}{L_y^2} + \frac{1}{L_z^2} \right\}$$

The hydraulic pressures calculated in this way for the model blocks are presented as a pressure distribution for a given time step in horizontal and/or vertical sections. With a given water inflow volume into the drift, the approximation of calculated pressure values to measured values is done by adjusting the extent of the shear zone and its anisotropy as so-called match parameters.

Band matrices are used to solve the partial differential equation which describes the flow between the matrix-fracture blocks; for each time step, these band matrices calculate the hydraulic pressure in the blocks according to the conjugate gradient method. Solution of this matrix, which is made up from the differential representation

$$A \cdot x = R$$

A = JACOBI matrix
x = solution vector
R = non-linear remainder

is performed with an approximated equation

$$B \cdot y = R.$$

Using the solution vector (y), the material balance error (r)

$$r = R - A \cdot y = (B - A) \cdot y$$

can be determined. The size of the material balance error depends inter alia on how accurately the water volume measurement can be performed. In the present case, a material balance error of $10^{-7}m^3$, related to the modelled rock block, was considered acceptable.

6.2 Dual porosity model

BARENBLATT et al. (1960) define a dual porosity system as a matrix continuum surrounded by a fracture continuum.

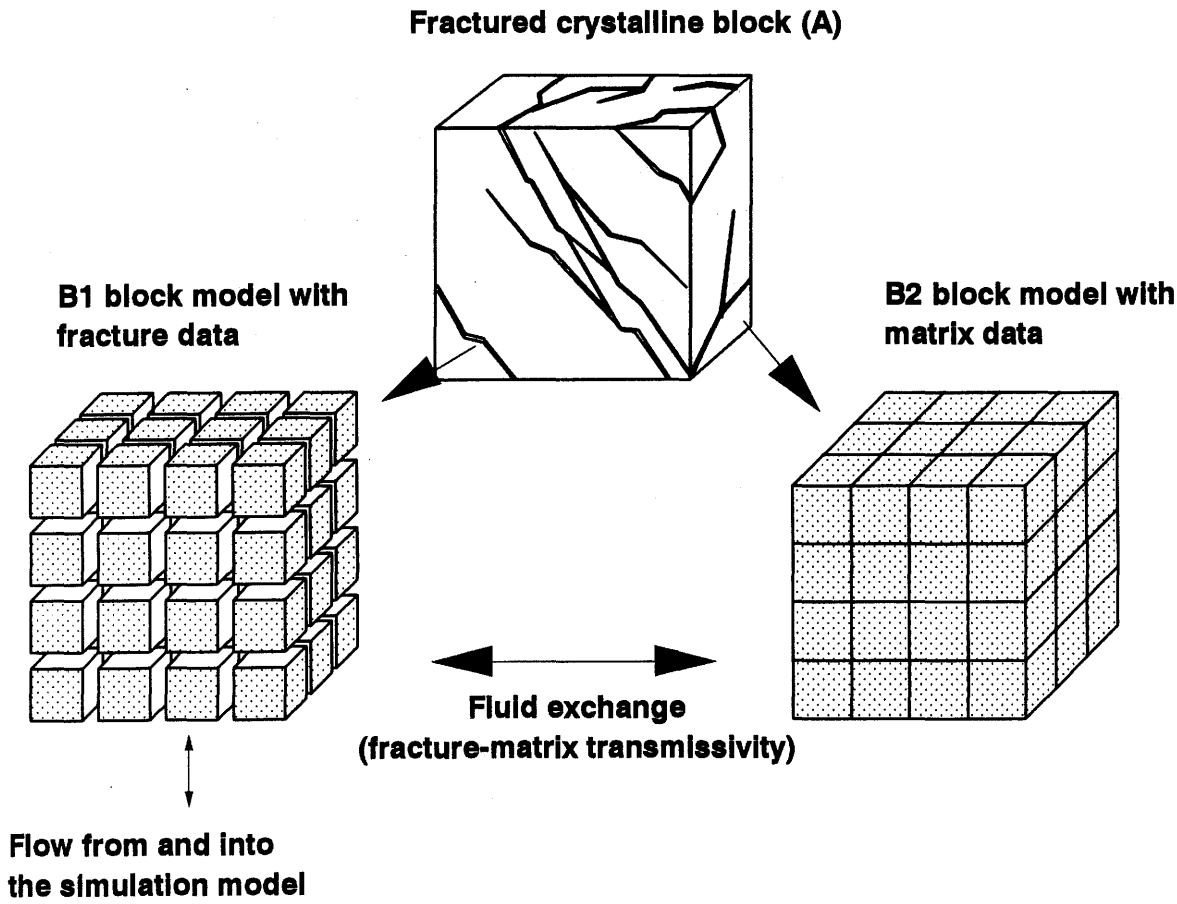

Fig. 29: Example of modelling a dual porosity medium (after WARREN & ROOT, 1963).

This concept was adapted for the numerical modelling of the hydrological conditions in the vicinity of the ventilation test drift. In this special model, a dual layer (shear zone) with a higher microfracture density and higher permeability, but a low storativity, is surrounded by a matrix system with a low permeability and a large storativity.

In the numerical definition, the modelled shear zone is therefore also a matrix zone with increased microfracture density.

The actual matrix zones can be considered as reservoirs which, depending on the pressure differences during single-phase flow, either supply water to, or remove it from, the microfracture system of the shear zone.

The main component of water movement occurs via the shear zone. Fig. 29 shows the model of a real dual porosity system (A) and the schematic model (B1+B2) adapted for the three-dimensional numerical modelling.

6.2 Development of a 3-D block model

A spatially restricted and an extended hydrogeological block model were developed for numerical simulation of the hydraulic flow conditions in a completely water-saturated, homogeneous granodiorite matrix and in the shear zone in the vicinity of the ventilation test drift.

Compared with the near-drift model, the geometry of the extended block model also takes account of the KWO main access tunnel and the migration drift.

Fixed input parameters for both block models include the geometry of the ventilation test drift, the orientation of the shear zone and the water inflow rates in the forward chamber and the pressure distribution in the observation boreholes. The orientation and width of the shear zone and the S1/S2/S3 structures was varied. Only single-phase flow (water) in the saturated rock was considered.

The model geometry (3-D block model) is based on the data from geological mapping, the dimensions and orientation of the ventilation test drift and core logging results for the boreholes running parallel and perpendicular to the drift.

The **actual near-drift 3-D block model** has the dimensions x = 60 m, y = 265 m and z = 450 m, and consists of 1,400 model blocks.

In the extended block model with outer dimensions x = 325.5 m, y = 325.5 m and z = 450 m, the simulated rock zone is discretised into 7,700 model blocks.

The vertical and horizontal grid of the extended model is shown in Figs. 30 and 31. The block size (cuboid form) in each case is adapted to take account of the level of information available. The smallest blocks have an edge length of one metre.

The shear zone in the forward section of the ventilation test drift was incorporated into the modelling concept as a significant discontinuity in an otherwise homogeneous, isotropic and anisotropic matrix.

The measured water inflow rate and hydraulic pressures were used to calibrate the model (Figs. 13 and 16). The average water influxes in the ventilation test drift come from longer-duration ventilation phases. In the simulation calculations, the water inflow rate was assumed to be constant and equivalent to the infiltration rate at ground surface. Water inflow through the rock to the ventilation drift was assumed to be radially symmetric.

The quasi-stationary hydraulic pressures were measured in intervals of the observation boreholes BOVE 84.011, 84.018, 80.005 and 83.001.

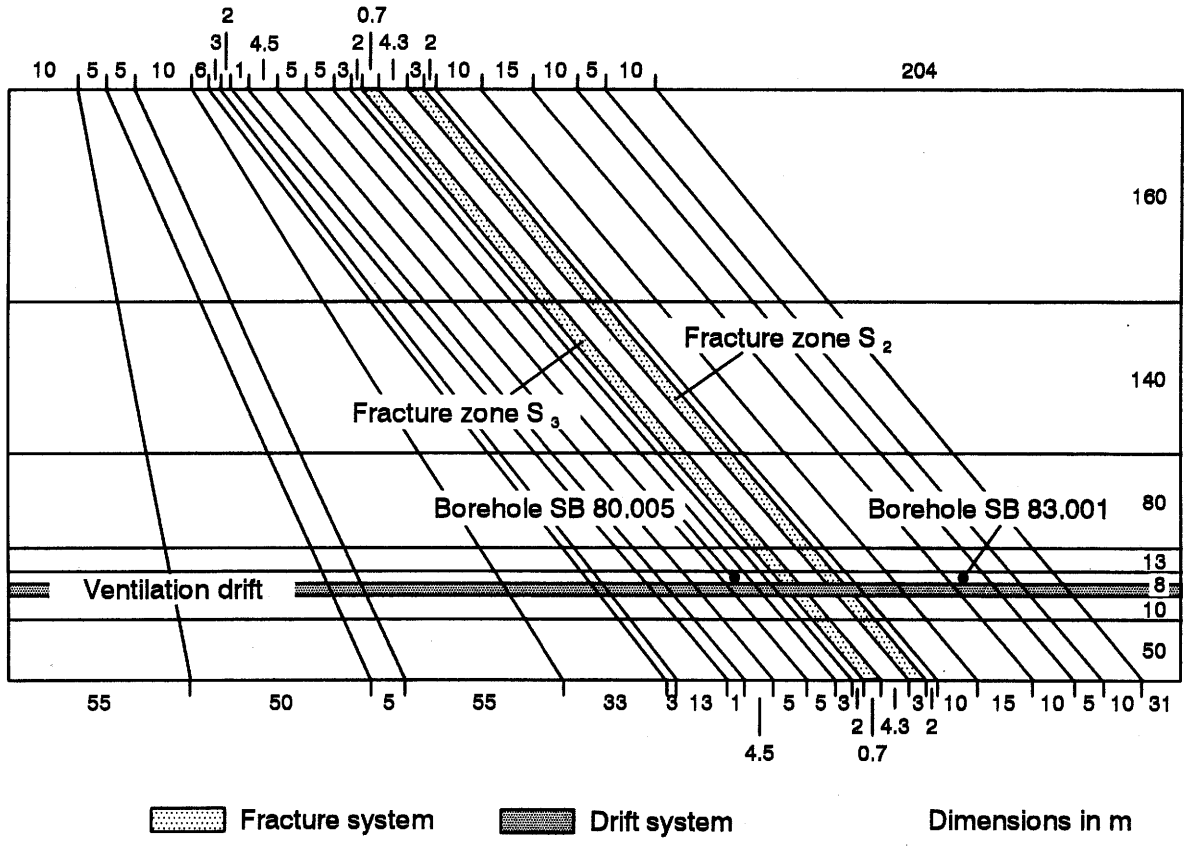

Fig. 30: Grid of the extended simulation model (vertical section through the plane of the ventilation test drift).

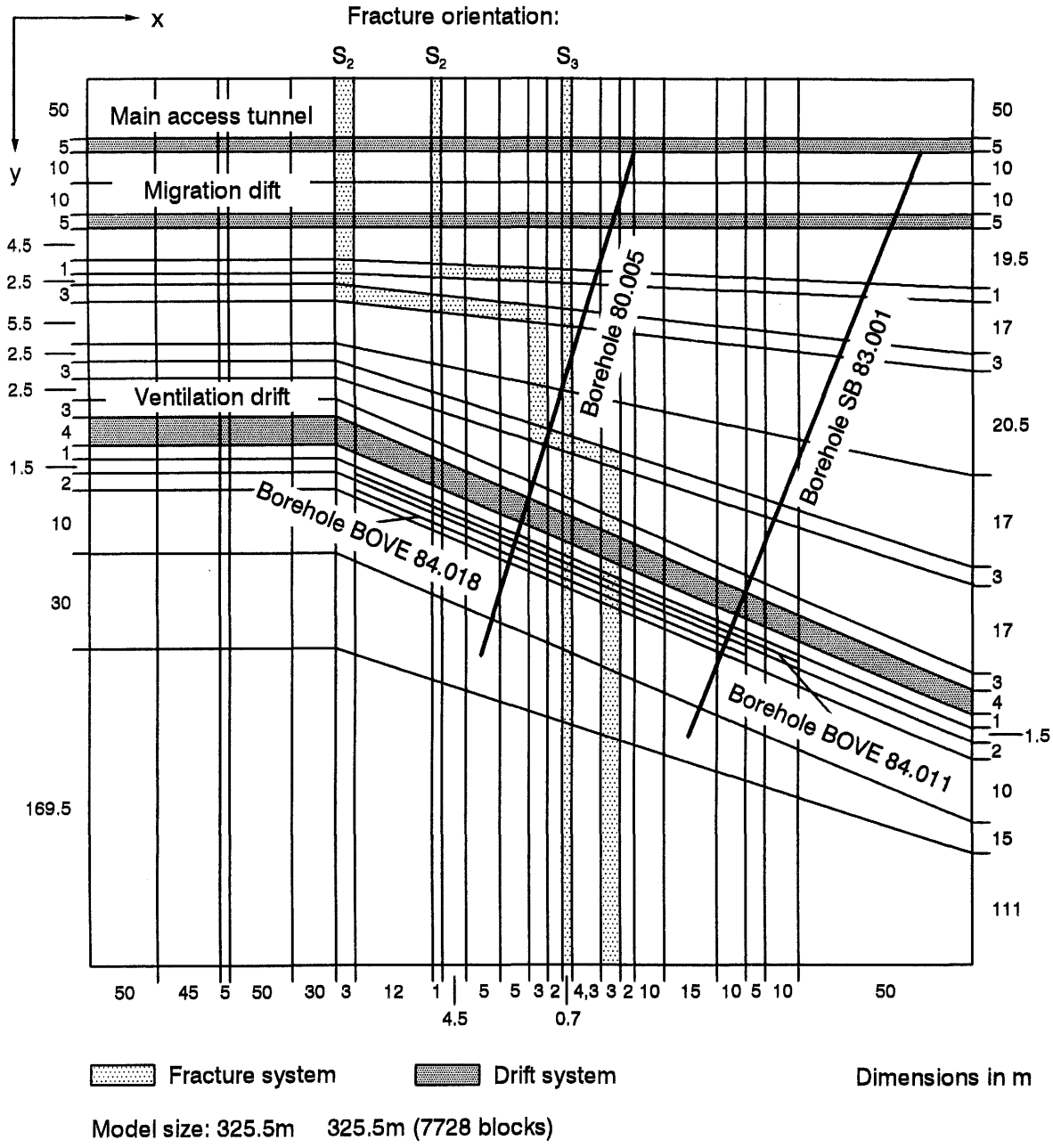

Fig. 31: Grid of the extended simulation model (horizontal section through the plane of the drift system).

Table 9: Petrophysical model input data.

		Near-drift model		Extended model		
Parameter		Shear zone	Matrix	Matrix	Shear zone S2	Shear zone S3
Matrix porosity	Φ_m=...%	1	1	1	1	1
Matrix permeability	k_m=..*$10^{-18}m^2$	0.5	0.5	0.1 - 1	0.5	0.5
Fracture porosity	Φ_{kl}=..%	0.0001	0.0001	0.001	0.001	0.001
Fracture permeability	k_{kl}=..*$10^{-18}m^2$	17 - 600	0.5	0.1 - 1	30 - 100	150 - 600
Compressibility (pore space)	$c_{gest.}$=..Pa^{-1}	$2*10^{-11}$				
Rock temperature	$T_{gest.}$=..°C	12				
Compressibility (water)	c_w=..Pa^{-1}	$4.4*10^{-10}$				
Density (water)	p_w=..g/cm^3	1				
Viscosity (water)	μ_w=..Pa·s	$1.1*10^{-3}$				

The petrophysical input data for the model are given in Table 9. They describe the different model domains, whereby domains S2 and S3 take into account the high microfracture component in the shear zone.

Initially the model was assigned a hydrostatic pressure distribution which would give a starting pressure of 4 MPa for the level of the drift system. An atmospheric pressure of 0.1 MPa was assumed for the ventilation test drift (internal pressure boundary conditions). The external boundary conditions included flow boundary (flow barriers) and pressure boundary conditions (pressure continuum).

A pressure boundary condition of 1 bar was assumed for the upper edge of the extended model. The pressure boundary condition was varied at the sides of the block model down to a depth of 300 m (Fig. 32). Removal of water was exclusively via the pressure sinks (drift systems). The fluid exchange between the blocks of the rock matrix and the

fracture matrix was via the microfracture structures, which agrees with the dual porosity model.

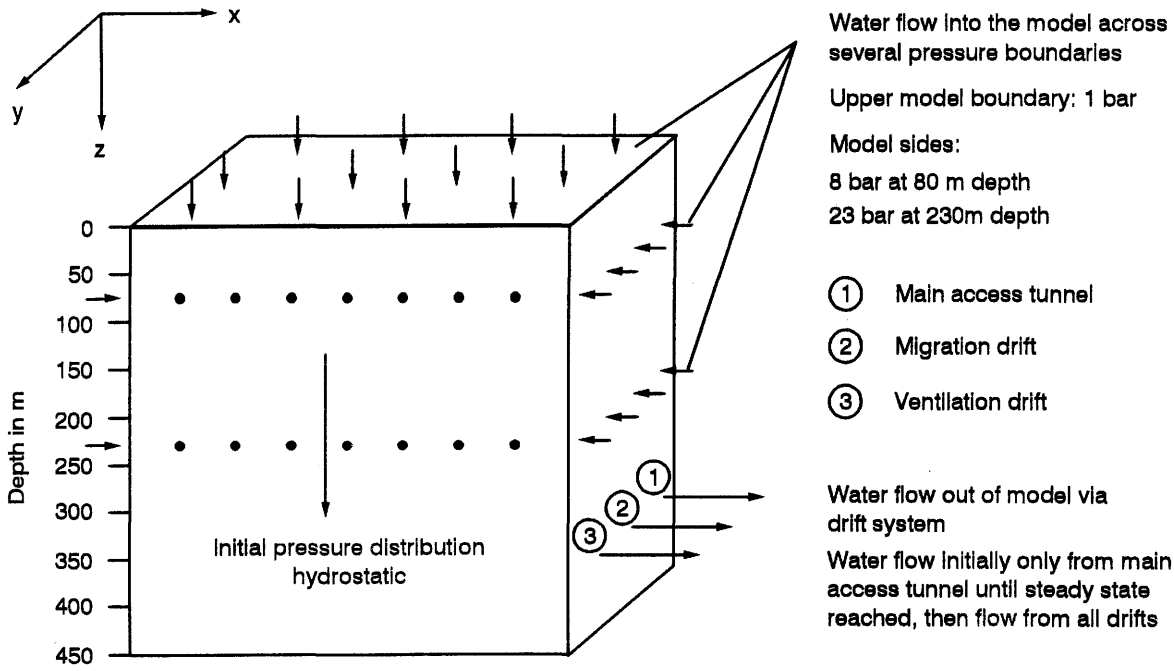

Fig. 32: Boundary conditions for the extended 3-D block model.

In order to approximate the measured hydraulic potentials and the constant water flow rate, the extent and the permeability of the shear zone were varied in the simulation calculations.

The simulation calculations were carried out until equilibrium conditions were reached, for durations of several hundred days up to 10 years.

6.3.1 Modelling a hydraulically active shear zone

Within the context of the near-drift modelling, the emphasis was on analysing the hydraulic activity of the shear zone as a function of its spatial extent in the rock structure; this was done in two simulation runs.

The shear zone was modelled as a section 5 m or 0.7 m thick with a dip of 53° and a length (vertical degree of penetration) of 265 m; it has a high permeability compared to the microfractured granodiorite. The extent in the strike direction (lateral degree of penetration) was varied according to the horizontal model width of 60 m.

In the first simulation calculation, the influence of the extent of the shear zone on water inflow into the ventilation drift was investigated, assuming that the shear zone is supplied exclusively from the rock matrix. The thickness of the hydraulically active section of the shear zone was taken as 5 m and 0.7 m in two separate modelling runs.

The hydraulic anisotropy between the hydraulically more active dip direction and the strike direction of the shear zone was taken into account in the modelling with an anisotropy factor of 2.5 to 1.

The influence of the fracture porosity was investigated together with the simulation of the 5 m thick shear zone.

The influence of a pressure continuum and the sensitivity of lateral extent were determined for the 0.7 m-thick shear zone. The model was extended to 2100 blocks and the width of the shear zone was increased from 60 m to 230 m.

In the second simulation calculation, a 0.7 m thick section of the shear zone was assumed to outcrop at ground surface. In contrast with the first simulation calculation, water infiltration is thus directly into the shear zone from above ground.

The influence of the longitudinal extent of the shear zone section (lateral degree of penetration) on the hydraulic

properties was investigated by varying the model size in the boundaries 40 m, 60 m and 100 m. In this case, a lateral pressure boundary condition (pressure continuum) rather than a lateral flow boundary was assumed by extending the model boundaries with additional matrix blocks.

Using the "match procedure", the pressures measured in situ in P12 and P28 (130 and 300 kPa respectively) were compared with pressures calculated on the basis of parameter variations for permeability, porosity and extent of the shear zone. The plausibility of the different values for hydraulic pressure was checked with reference to the hydrogeological modelling assumptions for hydraulically active sections of the shear zone.

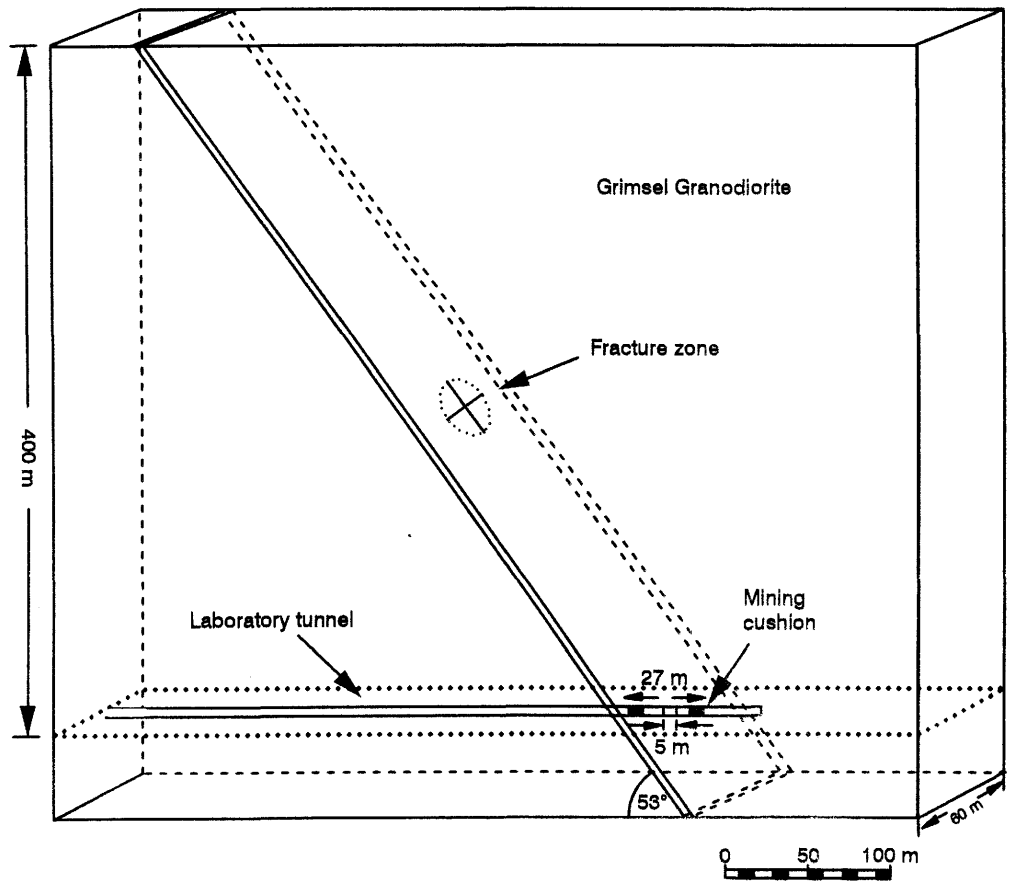

Fig. 33: Simplified hydraulic 3-D block model (near-drift).

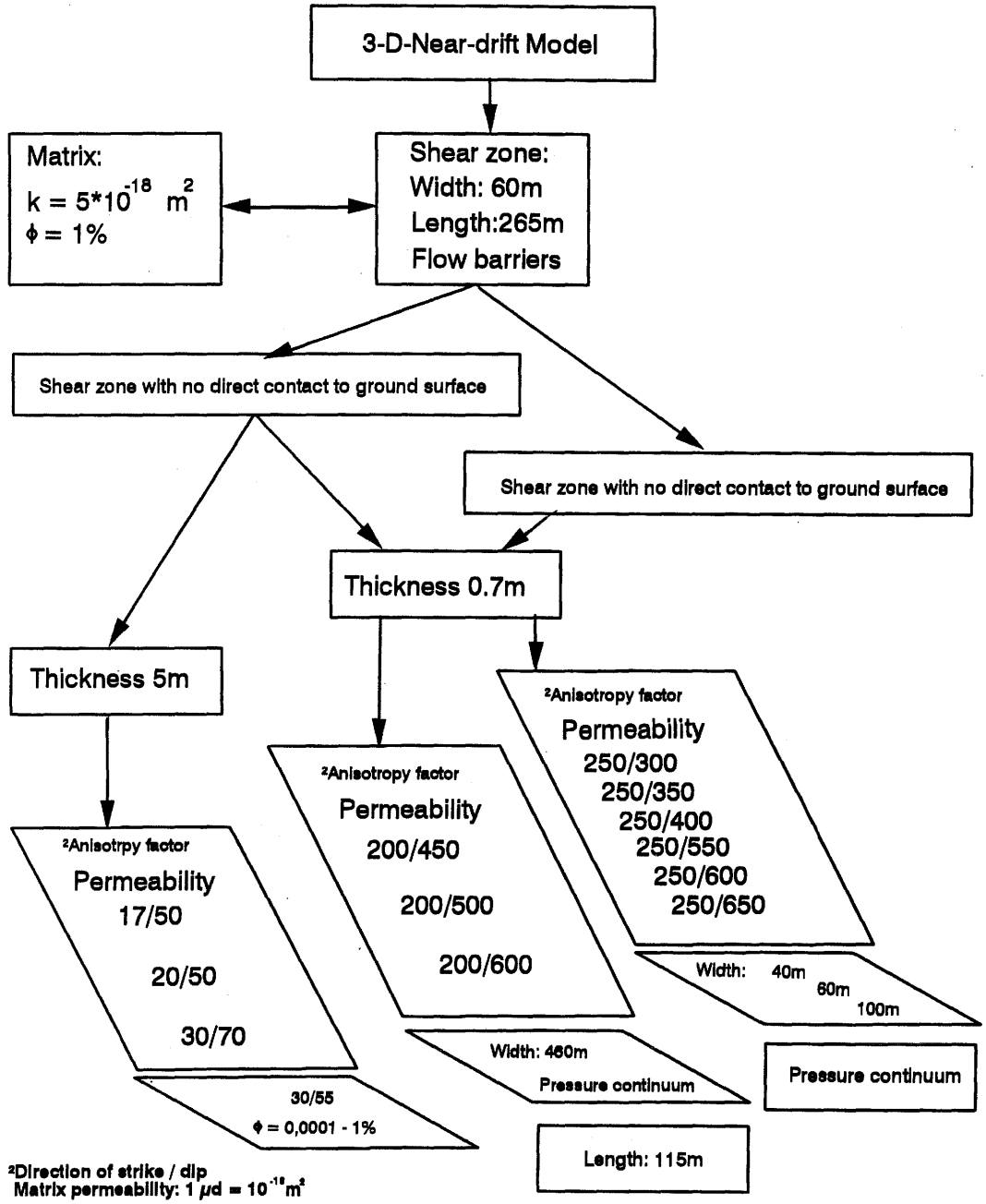

Fig. 34: System for modelling the near-field of the ventilation test.

6.3.1.1 Results of the near-drift modelling

Based on the hydrogeological rock properties and the simulation calculations performed for the near-drift zone (Fig. 34), the following conclusions can be derived:

- assuming that the shear zone is supplied exclusively from the surrounding rock matrix, the measured pressures and flow rates are reached within 8 years

- the permeability of the shear zone decreases by around an order of magnitude from approx. $4 \cdot 10^{-16}$ m^2 to $5 \cdot 10^{-17}$ m^2 if the thickness of the hy-draulically active section is increased from 0.7 m to 5 m

- if the shear zone is shortened from 265 m to 115 m in the vertical direction, the pressures in the measurement intervals used for calibration decrease and the water influx drops below the measured 1.6 l/h

- if the shear zone has a greater lateral extent (>> 60 m), even after 8 years the calculated pressures will be higher than the calibration pressures

- increasing the fracture porosity in the shear zone (influence of storage capacity) by four orders of magnitude from 0.0001 to 1% has the effect of increasing the pressure level in the measurement intervals only very slightly.

The following conclusions can be derived if it is assumed in the model that water influx is directly from above ground through the shear zone:

- with an assumed permeability of $3 \cdot 10^{-16}$ m^2 for a 0.7 m-thick shear zone section, the pressures in the calibration measurement intervals and the water influx rates can be simulated numerically

- for the measurement intervals, an increase in the permeability values means a higher pressure level than measured, with a time delay in pressure equalisation

- the model boundary condition selected (flow barrier or pressure continuum) has a considerable influence on the modelling results

- the pressure continuum has the opposite effect to the flow barrier on the pressure evolution in the measurement intervals. If the shear zone is assumed to be 40 m wide, the pressure level drops below the calibration pressure **without** lateral pressure extension - **with** lateral extension the calibration pressure is reached. The increase of the width of the shear zone up to 100 m causes a calculated pressure level higher as measured.

6.3.2 Modelling additional pressure sinks

In the extended 3-D block model, which includes the migration drift and the KWO main access tunnel, the influence of additional pressure sinks on pressure distribution and water influx was analysed (cf. Fig. 35).

Figs. 30 and 31 show the discretisation of the extended model with the hydraulically active structures of the shear zone (S1/S2 and S3) in a horizontal and a vertical section.

The sensitivity of the anisotropy factor was investigated using direction-dependent matrix permeabilities (Table 10).

Table 10: Parameter variation in the extended 3-D block model.

Model boundary condition	Pressure continuum	Flow barriers		
Factor	Matrix permeability			
Matrix anisotropy (k_{xy} : k_z)	Shear zone shortened laterally by 150 m	Shear zone up to model boundary	Shear zone shortened laterally by 150 m	Shear zone shortened - S3 interrupted
	[$*10^{-18} m^2$]	[$*10^{-18} m^2$]	[$*10^{-18} m^2$]	[$*10^{-18} m^2$]
1 : 1	0.5 : 0.5			
1 : 2	0.25 : 0.5	0.25 : 0.5	0.25 : 0.5	0.25 : 0.5
1 : 5	0.1 : 0.5	0.1 : 0.5	0.1 : 0.5	0.1 : 0.5
1 : 10	0.1 : 1.0			

The pressures measured in the intervals of the parallel boreholes BOVE 84.011 and BOVE 84.018 and in BOSB 80.005 and BOSB 83.001 were used to calibrate the model calculations.

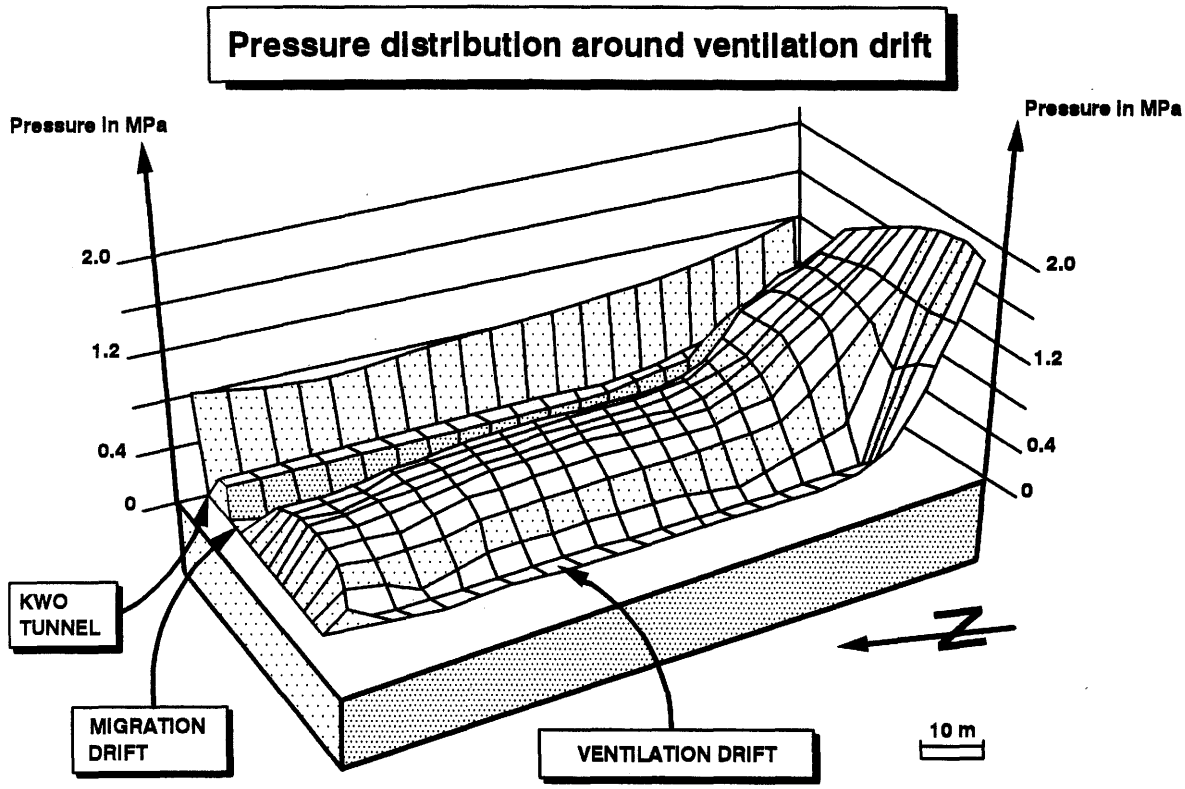

Fig. 35: The spatial pressure distribution between the KWO tunnel and the ventilation test drift.

6.3.2.1 Results of the extended modelling

The modelling results for the extended area of rock, which includes additional pressure sinks, allow the following conclusions to be drawn regarding the sensitivity of a matrix anisotropy and the influence of a shear zone of varying extent:

- the measured pressures and water inflow rates can also be simulated numerically when additional pressure sinks are taken into account, based on the modelling assumptions described previously

- the approximation between the calculated pressure values and the measured values can be improved if a lateral volume extension (pressure continuum) is taken into consideration

- high anisotropy factors in the matrix enhance the formation of pressure sinks and, at the same time, increase the general pressure level

- the best approximation of the calculated pressure values with the pressure evolution in the observation boreholes was achieved with an anisotropy factor of 1:5 ($k_{x/y} = 1 \cdot 10^{-19}$ m^2 and $k_z = 5 \cdot 10^{-19}$ m^2)

- a lateral decrease in the shear zone sections improves the approximation of the match parameters, while vertical shortening has the opposite effect.

6.4 Predictive modelling

Prior to drilling the observation boreholes BOVE 88.001, 88.002, 88.003 and 88.004, numerical calculations were carried out to predict the pressure evolution anticipated in these boreholes. The predictive calculations were based on the extended 3-D block model.

The aim of the predictive calculations was to check the 3-D block model by making a direct comparison between predicted formation water pressures and the water pressures measured in the newly drilled observation boreholes.

The observation boreholes are between 30 and 55 m long and penetrate through both shear zone and matrix areas. The radial distance between the measurement intervals (5 to 15 m long) and the drift is between 5 and ca. 40 m. Pressure measurements were carried out in the floor of the drift (BOVE 88.001), in the roof zone (BOVE 88.003) and in the undisturbed rock zone (BOVE 88.002 and BOVE 88.004) to the west of the test location.

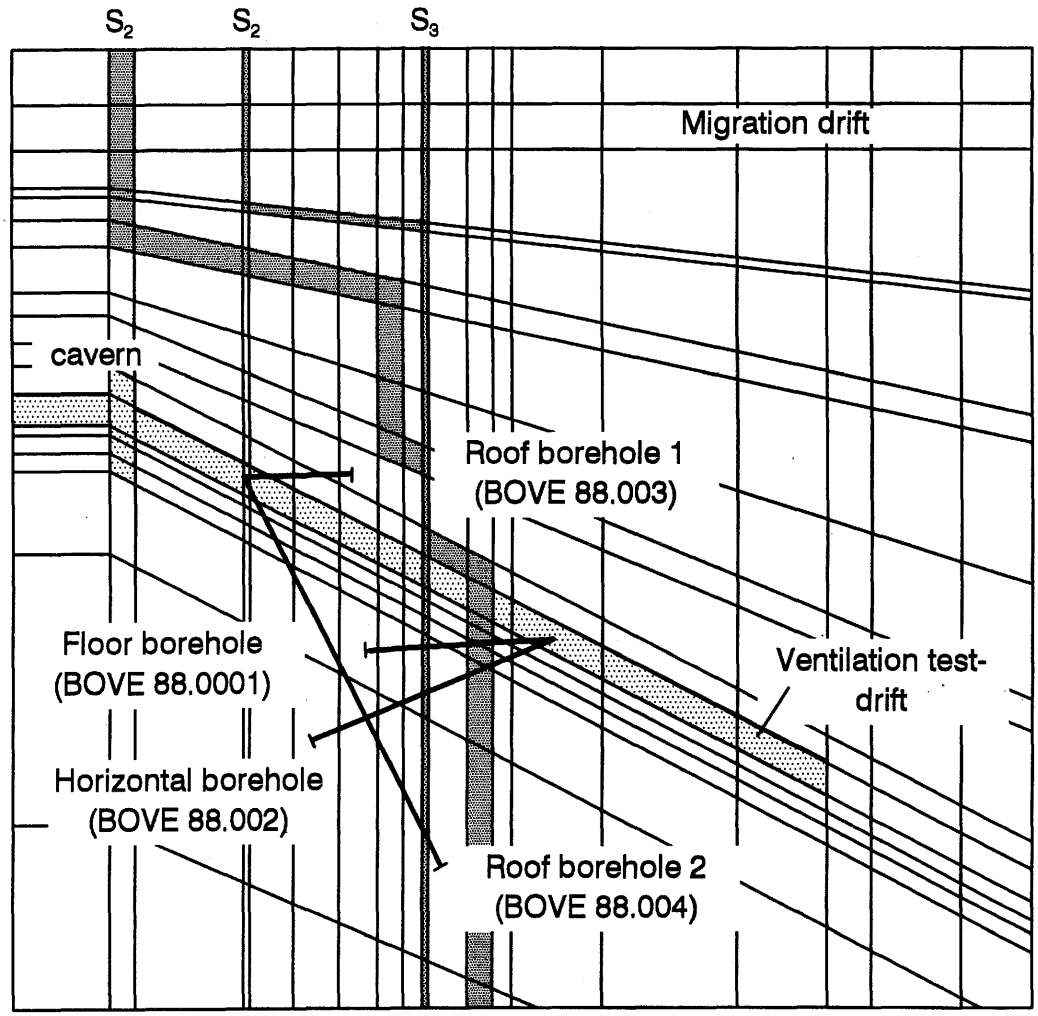

Fig. 36: Horizontal grid of the predictive model showing the locations of the measurement boreholes.

Fig. 36 shows the horizontal grid at the level of the ventilation test drift, with the locations of the observation boreholes and the modelled shear zone. With this grid, deviations result between the predicted location of the shear zone in the model and its in situ extent as indicated by the boreholes.

The boundary conditions for the predictive model are identical to those for the extended 3-D block model.

The water pressures predicted with the ECLIPSE program for a time one year after drilling and equipping of the boreholes are shown in Fig. 37 as pressure values as a function of borehole length. The pressures measured in the borehole intervals are also given.

According to the results of the predictive calculations, the formation water pressure in the boreholes initially increases steadily with distance from the ventilation test drift. After an initial value of 0.1 MPa (atmospheric pressure) in the drift, the pressure rises, up to a distance of 5 m away, to 0.4 MPa in boreholes BOVE 88.002 and BOVE 88.004 and to 0.3 MPa in boreholes BOVE 88.001 and BOVE 88.003. The pressure evolution is thus influenced by the distance of the model blocks from the ventilation drift and the extent of the pressure sink dominating at the time of the calculation.

In the continued trend of pressure increase in the boreholes, the sharp drop in the pressure curve reflects the influence of the shear zone. In boreholes BOVE 88.002 and 88.004, a pressure plateau forms between around 0.5 and 0.7 MPa in the area of the shear zone. The rise in pressure after the shear zone is once again relatively steep.

The pressures predicted for the end of the boreholes are between 0.7 and 0.8 MPa for the 30 m-long boreholes (BOVE 88.001, 88.002 and 88.003) and around 1.6 MPa for the 55 m-long borehole (BOVE 88.004).

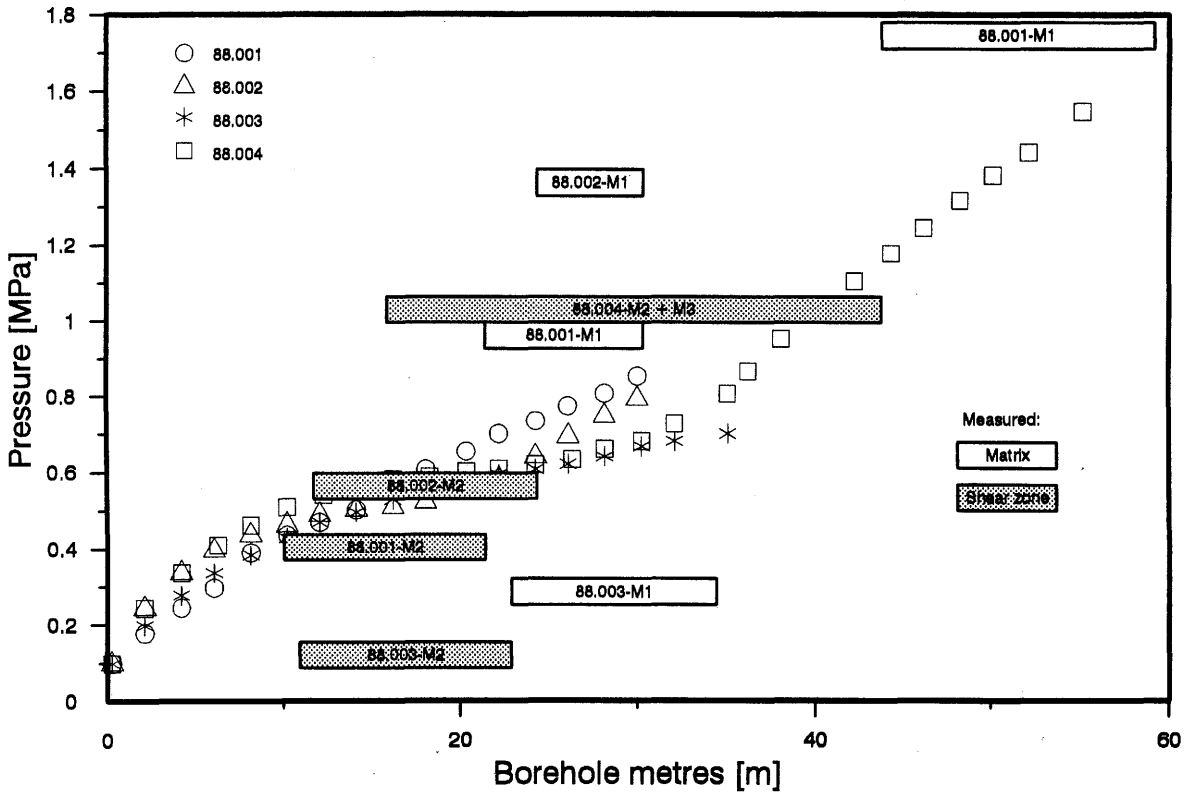

Fig. 37: Comparison of predicted pressure evolution with measured pressures (boreholes BOVE 88.001/2/3/4).

Comparison with the pressures measured in situ shows that the predicted pressure evolution corresponds to the in situ conditions, but that the comparison pressures from the predictive model are generally lower. One exception is the higher pressure in borehole BOVE 88.003 (roof borehole). An explanation for the fact that the pressures measured in this case do not tie in with the depth range could be the presence of a fracture network which is open to the migration drift, which is not taken into account in the model grid.

Taking into account the varying influence on pressure evolution of the different lengths of the measurement intervals, there is a relatively good agreement between predicted and in situ results.

6.5 Verification of the ECLIPSE program

The ECLIPSE program was verified for case example 2 of stage I of the HYDROCOIN project.

In stage I of the HYDROCOIN project, the effect of different mathematical solution algorithms on the calculation of formation water fluxes was investigated.

In the test to date, the calculation potential for solving different case examples has been compared for a total of 19 finite element and 2 finite difference programs. The accuracy of the numerical model solution is demonstrated by a comparison with analytical solutions or, as in the case example described here, by intercomparison of the model solutions. Particular attention was paid to the degree of discretisation of the models.

The objective in case example 2 of the HYDROCOIN project is to model a stationary formation water flux in a two-dimensional vertical section through a fractured rock body with widely ranging permeabilities. This example was computed with ECLIPSE since the model parameters are very similar to the flow conditions in the ventilation test zone.

The two-dimensional model describes an idealised rock body which extends 1600 m in a horizontal direction and approx. 1150 m in a vertical direction. The upper edge of the model is represented by two symmetrically arranged valleys. Two fracture zones of differing lateral extent extend out from the valleys and intersect at a given depth. Both fracture zones are assumed to be homogeneous and isotropic. The model boundaries are defined by flow barriers so that any water inflow or outflow must be via the topography, which simultaneously represents the free water table.

Other model boundary conditions include complete water saturation of the rock body and the applicability of DARCY's law. The hydraulic conductivity of the matrix zones was taken as $k_m = 10^{-8}$ m/s, and that of the fracture zones as $k_{kl} = 10^{-6}$ m/s. The porosity of the rock body was assumed to be $\Phi = 3\%$.

The potential distributions determined for the matrix and fracture zones were given for five different depths (0 m, 200 m, 400 m, 600 m and 800 m) and compared with one another. The influence on the results of the differing degree of discretisation of the two-dimensional models was also considered.

The hydraulic pressures obtained using ECLIPSE were converted to corresponding hydraulic potentials using

$$p = \rho_w \cdot g \cdot h.$$

p	= block pressure,	Pa
h	= half block thickness,	m
ρ	= water density,	kg m^{-3}
g	= earth acceleration,	m s^{-2}

Case example 2 was calculated using ECLIPSE with a fine-meshed rectangular block model (model 1) and a coarse-meshed block model with oblique-angled blocks (CORNER-POINT model 2a). The latter was more finely discretised in the x-

direction (model 2b) and in the z-direction (model 2c), as well as being replaced with a coarse-meshed, oblique-angled model (model 3) with uninterrupted coordinate lines and approximately rectangular blocks.

Fig. 38 shows the results of the ECLIPSE modelling together with the results from other programs. The calculated potential distribution at the 200 m level is compared. In principle, the comparison of results which follows also applies for other depths.

For the 200 m depth level, the potential distribution calculated with fine-meshed model 1 shows the best agreement with the results of other computer programs which have provided comparable results within the framework of the HYDROCOIN project.

The results for the coarse-meshed corner-point model 2a deviate from the other results, but are still within their range of accuracy. Refining the block grid does not improve the correlation (models 2b and 2c).

A good agreement is achieved with the coarse-meshed corner-point model 3, where the oblique-angled model blocks largely retain their rectangular form.

When verifying a computer program by comparing its results with the numerical modelling results of other programs, it should be noted that there is no guarantee of the absolute accuracy of the programs in the HYDROCOIN study.

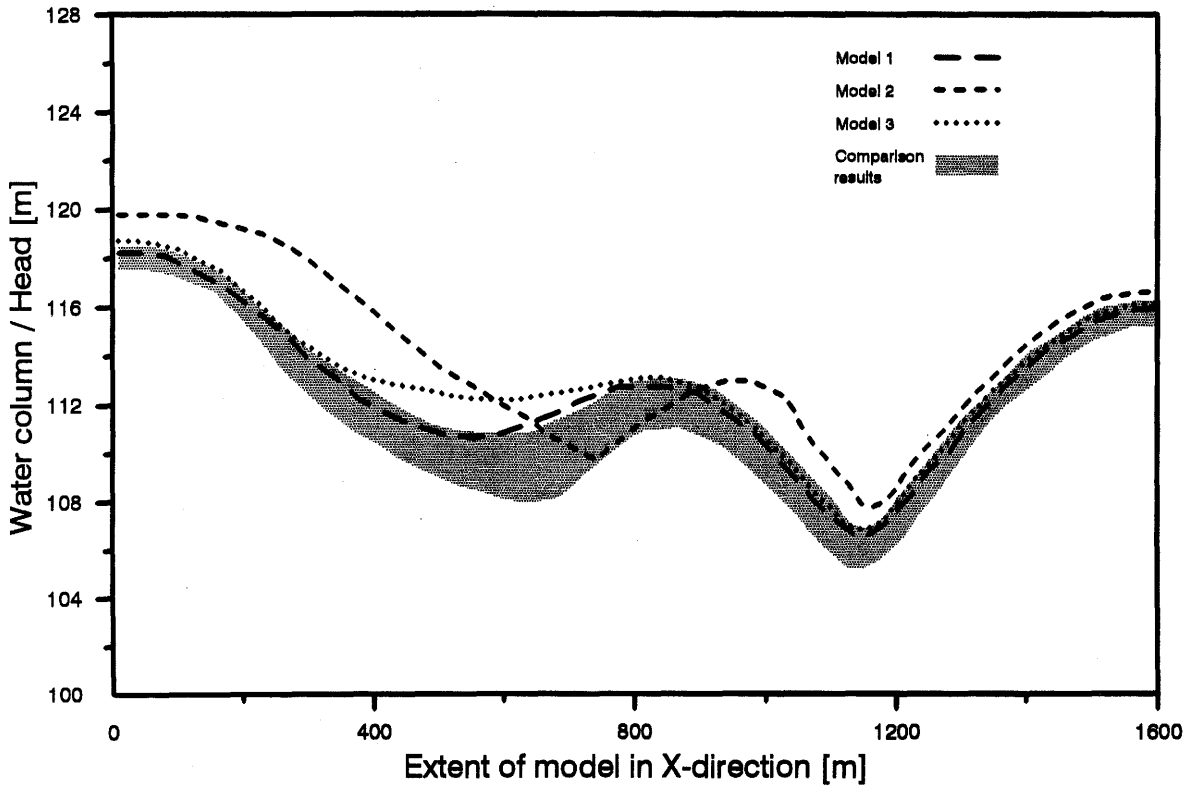

Fig. 38: Results of verification calculations with the ECLIPSE program (for 200 m depth). Comparison with the results of other programs.

6.6 Overview of modelling results

The aim of the numerical modelling which accompanied the ventilation experiments was to provide a three-dimensional flow model which could be used to determine the rock parameters which cannot be measured in situ. The flow model should also be capable of reproducing the measured rock parameters.

Based on structural geological mapping of the ventilation test drift, the working hypothesis was that the water-bearing shear zone in the drift is the most important hydraulic element.

Different sensitivity studies investigated the influence of the spatial extent and hydraulic anisotropy of the shear zone.

The water outflow and the measured pressures in the parallel boreholes were used as so-called "match parameters".

The calculations were carried out with the ECLIPSE finite difference program (Darcy flow, continuous porous medium); a modified dual porosity system with a matrix continuum surrounded by a fracture continuum was assumed.

Plausible solutions were found for different modelling assumptions. The permeability value obtained for the shear zone ranges in the cases considered between $4.5 \cdot 10^{-16}$ m^2 and $2 \cdot 10^{-17}$ m^2. However, the thickness of the hydraulically active shear zone has to be less than that observed from underground investigations of structural geology. The matrix permeability of the homogeneous Grimsel Granodiorite is in order of $5 \cdot 10^{-19}$ m^2.

The in situ measured values can be modelled successfully if the extent of the shear zone is assumed to be restricted. However, surface outcropping of part of the shear zone cannot be ruled out. Supply of water to the shear zone can be from above ground and exclusively from the homogeneous matrix zones. The selected model boundary condition (pressure

continuum or flow barrier) has a significant effect on determining the extent of the shear zone.

The assumption of enhanced permeability in the vertical direction in the matrix and shear zones improves the correlation with comparison data from different model calculations.

The solution algorithm of the ECLIPSE program and the selected flow model can be considered suitable for the numerical modelling of hydraulic conditions.

7 DISCUSSION OF THE ANALYTICAL AND NUMERICAL PERMEABILITY CALCULATIONS

The results of the transmissivity and permeability calculations are presented in Figs. 22 and 23. They provide an overview of the order of magnitude of the permeability of the rock and a hydraulically active shear zone opened up in the area of the ventilation test drift.

The analytical and numerical procedures used for calculating the rock permeabilities assume an equivalent Darcy flow. While the analytical flow model is based on an equivalent porous medium, the numerical flow model assumes a dual porosity medium.

Compared with the macropermeability values determined by numerical and analytical calculation, the permeability values obtained in the laboratory are too low. This is particularly true for the vicinity of the shear zone. One possible explanation could be that the volume of the samples investigated is too small to include all hydraulically active microfractures.

The permeabilities derived from the analytical transmissivity calculations assume homogeneous surfaces and rock zones with the same hydraulic properties; these were found to exist for some sections of the surface of the ventilation drift. An element of uncertainty attaches to the determination of the large-scale hydraulic properties of the rock at a greater distance from the drift, and to the extent of homogeneous zones.

As they proceed on the basis of the same measured hydraulic values, the numerical model calculations can make a significant contribution in this respect. The extent of homogeneous zones can be determined by means of parameter variation and comparison with the underlying hydrogeological model concepts.

The model boundary conditions have a significant influence on the results of numerical modelling. The selection of the boundary condition thus determines whether a hydraulically

active discontinuity such as the shear zone is to be treated as an independent structure which extends to the ground surface or simply as a spatially restricted zone which represents part of the rock matrix.

Taking into account the limitations of both the analytical and numerical calculations, the correlation of the results is in fact relatively good. The flow properties of the microfractured rock can be represented with an equivalent porous and a dual porosity flow model.

8 ASSESSING THE MACROPERMEABILITY

The macropermeability of the Grimsel Granodiorite in the vicinity of the ventilation test drift is in the order of $k = 10^{-18}$ m^2 or $K = 10^{-11}$ m/s.

Hydraulic inhomogeneities located within the section of rock being considered have significantly higher permeabilities, which can be explained by the presence of microfractures and additional textural elements. Depending on the thickness of these zones (cf. Fig. 22), their permeabilities may be up to two orders of magnitude greater than the macropermeability. The permeabilities determined for the shear zone in the ventilation test are in the range 10^{-16} to 10^{-17} m^2.

When determining macropermeability, the significance of such zones lies in their extent. The results of the in situ investigations and the hydraulic modelling indicate both a restricted local extent and a large-scale regional extent for the shear zone.

The influence of individual lamprophyre dykes and/or brittle deformation structures (fractures) on the macropermeability of the rock is considered to be small. The reason for this is the spatially restricted extent of these geological features. Because they are interrupted or integrated into homogeneous matrix zones, their hydraulic properties have only a local influence.

The in situ measured data which formed the basis for calculating the macropermeability can be determined with a sufficient degree of accuracy, given the technical limitations of the experiments.

When determining water inflow rates, these limitations relate mainly to measuring water volumes. The additional volumes of water released by drying-out processes lead, in the permeability calculation, to higher, conservative values.

The location of water inflow points can be determined relatively accurately by means of thermographic mapping, which means that the influence of inaccurate geometric base data on the permeability calculation can be considered as small.

As investigations have shown, the values for hydraulic gradient contain the greatest element of uncertainty. The reasons for this are the influence of the drift and the lengths of measurement intervals on the pressures measured in the boreholes. Particularly in the near-drift zone, changes in saturation and decompression phenomena can affect pressure values. The non-equipped boreholes also represent additional pressure sinks which can have a disturbing effect on measurement of normal pressure distribution.

A comparison of the analytically determined macropermeability with the results of the model calculations does, nevertheless, allow the conclusion that the macropermeability of a large-scale area of crystalline rock can be determined sufficiently accurately using the selected investigation methods.

GLOSSARY OF ABBREVIATION

b	=	Klinkenberg coefficient	Pa
c	=	velocity of light	$m \cdot s^{-1}$
g	=	earth acceleration	$m \cdot s^{-2}$
h	=	Planck's constant	$6.6262\ 10^{-34}$ J·s
h	=	hydraulic head	m
k	=	Boltzmann constant	$1.38\ 10^{-23}$ $J \cdot K^{-1}$
k	=	permeability	m^2
l	=	length	m
p	=	pressure	Pa
q	=	flow rate	$m^3 \cdot s^{-1}$
q_{mk}	=	source term, normative flow rate	s^{-1}
q_e	=	source term, normative flow rate	s^{-1}
t	=	time	s
v	=	velocity	$m \cdot s^{-1}$
A	=	area	m^2
B	=	formation volume factor	-
C	=	compressibility	Pa^{-1}
K	=	hydraulic conductivity	$m \cdot s^{-1}$
L	=	length	m
Q	=	flow volume	m^3
S	=	storage coefficient	-
T	=	temperature	K
T	=	transmissibility	$m^3 \cdot Pa^{-1} s^{-1}$
T_{mk}	=	block transmissibility	$m^3 \cdot s^{-1}$
T_{cmk}	=	specific block transmissibility	m^3
T	=	transmissivity	$m^2 \cdot s^{-1}$
V	=	volumene	m^3
λ	=	frequency	s^{-1}
μ	=	viscosity	Pa·s
ρ	=	density	$kg \cdot m^{-3}$
q	=	radiation density	$W \cdot m^{-2}$
r	=	specific weight	$Pa \cdot m^{-1}$
Φ	=	porosity	-

Indices

e	=	removal block
eff.	=	effective
gest.	=	rock
i	=	block number
mk	=	matrix-fracture block
n	=	time step
w	=	water
x,y,z	=	cartesian coordinates, directions

REFERENCES

BERTHE, D., CHOUKRONE, P. & JEGOUZO, P. (1979): Orthogneiss, mylonite and non coaxial deformation of granites: the example of the South American Shear Zone. - Journ. Struct. Geol. Vol. I, 31-42.

BARENBLATT, G.J., ZHELTOV, I.P. & KOGHINA, I.N. (1960): Basic Concepts in the Theory of Seepage of homogeneous Liquids in Fissured Rocks. - J. Appl. Math. Mech, vol. 24, no. 5.

BOSSART, P. & MARTEL, S. (1990): Hydrogeological Implications of Ductile and Brittle Deformation in the Grimsel Crystalline, upper Aare Valley, Switzerland. - Nagra Internal Report (unpublished); Baden (Switzerland).

BOSSART, P. & HUFSCHMIED, P. (1989): FLG Ermittlung von Kluftzuflüssen durch Folienabdeckung, Ventilationsstollen, FLG - Nagra Internal Report (unpublished), Baden (Switzerland).

BRASSER, TH. (1986): Erfahrungen mit dem Ventilationstest - einem untertägigen Großversuch zur Ermittlung der Gebirgspermeabilität. - Tagung der Fachsektion Hydrogeologie der Deutschen Geologischen Gesellschaft; 25. - 29. May 1987; Regensburg.

BRASSER, TH. & KULL, H. (1988a): Subsurface Application of an Infrared Thermometer to Determine Zones of prefered Water Pathways. - Int. Symp. "Detection of Subsurface Flow Phenomena by Self-Potential, Geoelectrical and Thermomechanical Methods"; 14 - 18 March 1988 Karlsruhe.

BRASSER, TH. & KULL H. (1988b): The Ventilation Test in an Underground Laboratory, Results from Konrad Mine (FRG) and Grimsel Test Site (CH). - Symp. Hydrogeologie et Sureté des Dépots de Déchets Radioactifs et industriels toxiques, Vol. 1: Communications, pp. 199-200. - Documents du B.G.R.M. No. 160; Orléans (France).

BRASSER, TH. & KULL, H. (1988c): Untertägiger Einsatz eines Infrarot-Strahlungsthermometers zur Identifizierung und Abgrenzung wasserführender Kluftzonen. - Felsbau 6 (2), S. 72-74; Essen.

BRASSER, TH. & KULL, H. (1989): Einsatz thermographischer Verfahren bei der untertägigen Erkundung von Hohlräumen zur Reststoffablagerung. - Tagungsband, 9. Jahrestagung der Gesellschaft für Photogrammetrie und Fernerkundung, Freiburg i.Br., 25.-27.10.1989.

BRASSER, TH., KULL, H. & SCHNEEFUSS, J. (1988): Stress and Temperature Effects on the Permeability in Granitic Rock around a Gallery Excavated by Continuous Mining. - OECO/AECL Workshop on Excavation Response in Deep Radioactive Waste Repositories - Implications for Engineering Design and Safety Performance; Winnipeg, (Canada).

BREWITZ, W., BRASSER, TH., HUFSCHMIED, P. & KULL, H. (1988): Ventilationstest. - In: Nagra informiert" 1 + 2/88, p. 46-49; Baden (Switzerland).

BREWITZ, W., KULL, H. & TEBBE, W. (1984): In situ Experiments for the Determination of Macro-Permeability and RN-Migration in Faulted Rock Formations. - Proc. Design and Instrumentation of Experiments in Underground Laboratories. CEC, OECO/NEA, 15.-17. Mai 1984; Brussels.

BREWITZ, W. & PAHL, A. (1986): The German Participation in the Underground Laboratory Grimsel (Switzerland). Targets and Methods of in situ Experiments in Granite for Radioactive Waste Disposal. - Int. Symp. on Siting, Design and Construction of Underground Repositories for Radioactive Waste, 3.-7. March 1986 (IAEA-SM-289/24); Hannover.

CHOUKROUNE, P. & GAPAIS, D. (1983): Strain pattern in the Aar Granite (Central Alps): orthogneiss developed by bulk inhomogeneous flattening. - Jour. Struct. Geol. 5, p. 411-418.

COOPER, H.H. & JACOB. C.E. (1946): A generalized graphical method for evaluating formation constants and summarizing well field history. - Trans. Amer. Geophys. Union, 27, pp. 526-534.

DE MARSILY, G. (1986): Quantitative Hydrogeology. - Academic Press; New York.

DARCY, H. (1856): Les foutaines publiques de la ville de Dijon.- VII + 647 S., zahlr. nicht nummerierte Tab., Atlas mit zahlreichen Abb. auf 28 Tafeln; Paris (Victor Dalmont).

DUPUIT, J. (1863): Etudes théoriques et pratiques sur le mouvement des eaux dans les canaux découverts et à travers les terrains perméables. - 2. Aufl. XXVIII + 304 S., 77 Abb. auf 6 Tafelbeilagen; Paris (Dunod).

FLACH, D. & NOELL U. (1989): Neigungsmessungen zur Ermittlung Neotektonischer Vorgänge. - Nagra Technical Report 89-11, Baden (Switzerland).

GUNDFELT, B. (1985): The International HYDROCOIN-Project, Level 1: Code Verification, Proposal for case 2. Stockholm.

HEINIGER, P. (1989): FLG-Ventilationstest - Hydrogeologische Untersuchungen in den Bohrungen BOVE 88.001, 88.002, 88.003, 88.004 und in der Bohrung BOSB 80.005. - Nagra Internal Report (unpublished); Baden (Switzerland).

HORNER, D.R. (1951): Pressure build-up in wells. - Proc. Third World Pet. Cong., the Hague (1951) Sec. II, 503-523. Reprint Series, No. 9 - Pressure Analysis Methods, Society of Petroleum Engineers of AIME; (1967) pp. 25-43; Dallas.

IROUSCHEK A. & BOSSART P. (1989): FLG-Ventilationstest Geologischer Bericht der 4 Validierungsbohrungen BOVE 88.001, 88.002, 88.003 und 88.004. - Nagra Internal Report (unpublished); Baden (Switzerland).

JACOB, C.E. & LOHMAN, S.W. (1952): Nonsteady flow to a well of constant drawdown in an extensive aquifer. - Amer. Geophys. Union Trans., Nr. 33 (4), pp. 559-569.

KEUSEN, H.R., GANGUIN, I., SCHULER, P. & BULLETTI, M. (1989): Felslabor Grimsel - Geologie.- Nagra Technical Report Bericht, NTB 87-14; Baden (Switzerland).

KULL, H., LEITENBAUER, J., SIEBERT, R. & WEBER, R. (1989): Simulation of Groundwater Flow in Crystalline Formations with the Use of Three-Dimensional, Dual-Porosity-Modell. - Proc. ENVIROTECH Vienna 1989, Vienna 20. - 23.2.1989; Vienna.

LABHART, T.P. (1977): Aarmassiv und Gotthardmassiv. Sammlung geologischer Führer, Band 63.

LANGGUTH, H.-R. & VOIGT, R. (1980): Hydrogeologische Methoden.- Springerverlag; Berlin.

LUNDSTRÖM, L. & STILLE, H. (1978): Large Scale Permeability Test of the Granite in the Stripa Mine and Thermal Conductivity Test. - Lawrence Berkeley Laboratory LBL-7052; Berkeley.

MATTHEWS, C.S. & RUSSEL, D.G. (1967): Pressure Buildup and Flow Tests in Wells. - Society of Petroleum Engineers of AIME; p. 6; Dallas (USA).

MOYE, D.G. (1967): Diamond Drilling for Foundation Exploration. - Civil Eng. Trans., Inst. Eng. Australia, Apr. 1967, pp 95-100.

NAGRA, (1985): Grimsel Test Site - Overview and Test Programms. - Nagra Technical Report, NTB 85-46; Baden (Switzerland).

THEIS, C.V. (1935): Relation between the lowering of the piezometric surface and the rate and duration of discharge of a well using ground-water storage. - Trans. Am. Geophys. Union, 16, (2); Richmond, Va.

THIEM, A. (1870): Die Ergiebigkeit artesischer Bohrlöcher, Schachtbrunnen und Filtergalerien - Jour. f. Gasbeleuchtung und Wasserversorgung 14; S. 450-467; München.

THIEM, G. (1906): Hydrogeologische Methoden. - Leipzig (Gebhard).

VOBORNY, O., ADANK, P., HÜRLIMANN, W., VOMVORIS, S. & MISHRA, S. (1991): Modeling of groundwater flow in the rock body surrounding the underground laboratory - Nagra Technical Report, NTB 91-03; Baden (Switzerland).

VOMVORIS, S. & FRIEG, B. (1992): Overview of Nagra field and modeling activities in the ventilation drift (1988 - 1990). - Nagra Technical Report, NTB 91-34; Wettingen (Switzerland).

WARREN, J.E. & ROOT, P.J.(1963): The behaviour of naturally fractured reservoirs. - Soc. Pet. Eng. J. (Sept. 1963), 245-255; Trans., AIME, 228.

WILSON, C.R.; LONG, J.C.S.; GALBRAITH, R.M.; KARASAKI, K.; ENDO, H.K.; DU BOIS, H.O.; MC PHERSON & RAMQUIST, G. (1981): Geohydrological Data from the Macro-permeability Experiment at Stripa, Sweden. - Lawrence Berkeley Laboratory, LBL-12520, Berkeley.